

การยึดจับและพลศาสตร์ของเอ็นเอส3/4เอเซอร์โนโปรทีเอสจากเชื้อไวรัสตับอักเสบบีและนิเวศวิทยา
เดสจากเชื้อไวรัสไข้หวัดใหญ่ชนิดเอในการเกิดสารเชิงซ้อนกับสารยับยั้งด้วยการจำลองแบบเอ็ม
เอ็มและคิวเอ็ม/เอ็มเอ็ม



นางสาวอาทิตยา มีประเสริฐ

จุฬาลงกรณ์มหาวิทยาลัย

CHULALONGKORN UNIVERSITY

วิทยานิพนธ์นี้เป็นส่วนหนึ่งของการศึกษาตามหลักสูตรปริญญาวิทยาศาสตรดุษฎีบัณฑิต

สาขาวิชาเคมี ภาควิชาเคมี

คณะวิทยาศาสตร์ จุฬาลงกรณ์มหาวิทยาลัย

ปีการศึกษา 2556

ลิขสิทธิ์ของจุฬาลงกรณ์มหาวิทยาลัย

บทคัดย่อและแฟ้มข้อมูลฉบับเต็มของวิทยานิพนธ์ตั้งแต่ปีการศึกษา 2554 ที่ให้บริการในคลังปัญญาจุฬาฯ (CUIR)

เป็นแฟ้มข้อมูลของนิสิตเจ้าของวิทยานิพนธ์ ที่ส่งผ่านทางบัณฑิตวิทยาลัย

The abstract and full text of theses from the academic year 2011 in Chulalongkorn University Intellectual Repository (CUIR) are the thesis authors' files submitted through the University Graduate School.

BINDING AND DYNAMICS OF HEPATITIS C VIRUS NS3/4A SERINE PROTEASE AND
INFLUENZA A NEURAMINIDASE IN COMPLEXATION WITH INHIBITORS BY MM AND
QM/MM SIMULATIONS



Miss Arthitaya Meeprasert

จุฬาลงกรณ์มหาวิทยาลัย
CHULALONGKORN UNIVERSITY

A Dissertation Submitted in Partial Fulfillment of the Requirements

for the Degree of Doctor of Philosophy Program in Chemistry

Department of Chemistry

Faculty of Science

Chulalongkorn University

Academic Year 2013

Copyright of Chulalongkorn University

Thesis Title	BINDING AND DYNAMICS OF HEPATITIS C VIRUS NS3/4A SERINE PROTEASE AND INFLUENZA A NEURAMINIDASE IN COMPLEXATION WITH INHIBITORS BY MM AND QM/MM SIMULATIONS
By	Miss Arthitaya Meeprasert
Field of Study	Chemistry
Thesis Advisor	Professor Supot Hannongbua, Dr.rer.nat.
Thesis Co-Advisor	Thanyada Rungrotmongkol, Ph.D.

Accepted by the Faculty of Science, Chulalongkorn University in Partial
Fulfillment of the Requirements for the Doctoral Degree

.....Dean of the Faculty of Science
(Professor Supot Hannongbua, Dr.rer.nat.)

THESIS COMMITTEE

.....Chairman
(Assistant Professor Warinthorn Chavasiri, Ph.D.)

.....Thesis Advisor
(Professor Supot Hannongbua, Dr.rer.nat.)

.....Thesis Co-Advisor
(Thanyada Rungrotmongkol, Ph.D.)

.....Examiner
(Associate Professor Pornthep Sompornpisut, Ph.D.)

.....Examiner
(Associate Professor Polkit Sangvanich, Ph.D.)

.....External Examiner
(Ornjira Aruksakunwong, Ph.D.)

.....External Examiner
(Professor Adrian J. Mulholland, Ph.D.)

อาทิทยา มีประเสริฐ : การยึดจับและพลศาสตร์ของเอ็นเอส3/4เอเซอร์อินโปรทีเอสจากเชื้อไวรัสตับอักเสบบีและนิวรามินิเดสจากเชื้อไวรัสไข้หวัดใหญ่ชนิดเอในการเกิดสารเชิงซ้อนกับสารยับยั้งด้วยการจำลองแบบเอ็มเอ็มและคิวเอ็ม/เอ็มเอ็ม. (BINDING AND DYNAMICS OF HEPATITIS C VIRUS NS3/4A SERINE PROTEASE AND INFLUENZA A NEURAMINIDASE IN COMPLEXATION WITH INHIBITORS BY MM AND QM/MM SIMULATIONS) อ.ที่ปรึกษาวิทยานิพนธ์หลัก: ศ. ดร. สุพจน์ หารหนองบัว, อ.ที่ปรึกษาวิทยานิพนธ์ร่วม: อ. ดร. ธัญญา รุ่งโรจน์มงคล, 132 หน้า.

เอนไซม์เอ็นเอส3/4เอ โปรทีเอสและนิวรามินิเดสมีบทบาทสำคัญในการตัดพันธะเปปไทด์และพันธะไกลโคไซด์ระหว่างการจำลองตัวของเชื้อไวรัสตับอักเสบบีและไข้หวัดใหญ่ตามลำดับ ดังนั้นเอนไซม์เอ็นเอส3/4เอและนิวรามินิเดสทั้งชนิดดั้งเดิมและชนิดกลายพันธุ์ H274Y ของเชื้อไข้หวัดสายพันธุ์ H5N1 และ pH1N1 จึงเป็นที่สนใจ โดยในขั้นต้นได้อาศัยเทคนิคการจำลองพลวัตเชิงโมเลกุลแบบดั้งเดิมเพื่อศึกษารูปแบบการยึดจับ อันตรกิริยาการเข้าจับและประสิทธิภาพการยึดจับระหว่างเอนไซม์เอ็นเอส3/4เอกับสารยับยั้ง (โบเซพรีเวียร์ เทลาพรีเวียร์ ดาโนพรีเวียร์ และปีโอ201335) และเอนไซม์นิวรามินิเดสทั้ง 4 สายพันธุ์กับลานินามิเวียร์ จากการคำนวณพลังงานเสรีแบบแยกของแต่ละกรดอะมิโนโดยอาศัยวิธีการแก้สมการกลศาสตร์เชิงโมเลกุลแบบโมเดลทั่วไปของบอร์น (Generalized Born model) พบว่ากรดอะมิโนที่ตำแหน่ง 41-43 57 81 136-139 155-159 และ 168 ของเอนไซม์เอ็นเอส3/4เอ และ 118-119 151-152 178 224 227 276 292 and 371 ของเอนไซม์นิวรามินิเดสทั้ง 4 สายพันธุ์ มีความสำคัญต่อการยึดจับระหว่างเอนไซม์และสารยับยั้ง นอกจากนี้ยังพบว่าแรงแวนเดอร์วาลส์เป็นแรงกระทำหลักที่ช่วยให้การยึดจับของสารยับยั้งการทำงานของเอนไซม์เอ็นเอส3/4เอมีเสถียรภาพ ขณะที่แรงกระทำหลักที่ช่วยรักษาเสถียรภาพของการยึดจับระหว่างเอนไซม์นิวรามินิเดสกับสารยับยั้งคือแรงระหว่างประจุ อย่างไรก็ตามมีการตรวจพบว่ายาที่ใช้รักษาส่งผลข้างเคียงผู้ป่วยไวรัสตับอักเสบบี การทำงานของเอนไซม์เอ็นเอส3/4เอจึงยังคงเป็นที่ต้องการ ดังนั้นงานวิจัยนี้จึงได้ค้นหายาที่มีประสิทธิภาพจากสารประกอบในฐานข้อมูล ZINC ทั้งหมด 40 ลิแกนด์ โดยอาศัยเทคนิคการจำลองพลวัตเชิงโมเลกุลแบบสเตียร์บนข้อสมมติฐานที่ว่าลิแกนด์ที่ใช้แรงฉีกมากแสดงว่าที่ประสิทธิภาพในการยึดจับกับเอนไซม์ได้ดี ซึ่งจากการศึกษาพบว่าที่สารประกอบ 9 ตัวที่น่าจะดีเทียบเท่าหรือดีกว่าสารยับยั้งทั้ง 4 ตัว บนพื้นฐานเทคนิคการจำลองพลวัตเชิงโมเลกุลที่ผสมผสานกลศาสตร์ควอนตัมและกลศาสตร์โมเลกุล (QM/MM MD) โดยใช้ระเบียบวิธี SCC-DFTB สำหรับการคำนวณกลศาสตร์ควอนตัม พบว่ากลไกการเกิดปฏิกิริยาเอซิลเลชันของเอนไซม์เอ็นเอส3/4เอกับโบเซพรีเวียร์และเทลาพรีเวียร์นั้นเกิดผ่านกลไกแบบคอนเซิตเตดเช่นเดียวกับสารตั้งต้นตามธรรมชาติ โดยค่าพลังงานก่อกัมมันต์สำหรับการเกิดปฏิกิริยาแบบย้อนกลับของทั้งสองระบบมีค่าประมาณ 19-23 kcal/mol ซึ่งค่าพลังงานดังกล่าวใกล้เคียงกับผลที่ได้จากการทดลอง

ภาควิชา	เคมี	ลายมือชื่อนิสิต
สาขาวิชา	เคมี	ลายมือชื่อ อ.ที่ปรึกษาวิทยานิพนธ์หลัก
ปีการศึกษา	2556	ลายมือชื่อ อ.ที่ปรึกษาวิทยานิพนธ์ร่วม

5173880423 : MAJOR CHEMISTRY

KEYWORDS: HEPATITIS C VIRUS / INFLUENZA A VIRUS / NS3/4A PROTEASE /
NEURAMINIDASE / MD SIMULATION / STEERED MD SIMULATION / QM/MM MD
SIMULATION

ARTHITAYA MEEPASERT: BINDING AND DYNAMICS OF HEPATITIS C VIRUS
NS3/4A SERINE PROTEASE AND INFLUENZA A NEURAMINIDASE IN
COMPLEXATION WITH INHIBITORS BY MM AND QM/MM SIMULATIONS.
ADVISOR: PROF. SUPOT HANNONGBUA, Dr.rer.nat., CO-ADVISOR: THANYADA
RUNGROTMONGKOL, Ph.D., 132 pp.

NS3/4A protease and neuraminidase (NA) enzymes play a crucial role to cleave the peptide bond and glycosidic bond during the replication process of hepatitis C and influenza viruses, respectively. Thus, NS3/4A and both wild-type (WT) and H274Y mutant of NA subtypes H5N1 and pH1N1 were focused. Initially, NS3/4A binding to the current inhibitors (boceprevir, telaprevir, danoprevir as well as NA bound with laninamivir were studied in order to investigate their binding pattern and ligand-target interactions as well as the binding efficiency using the conventional molecular dynamics (MD) simulation. The per-residue decomposition energy was calculated by molecular mechanics (MM)/generalized Born surface area (GBSA) indicating that the residues 41-43, 57, 81, 136-139, 155-159 and 168 of NS3/4A and 118-119, 151-152, 178, 224, 227, 276, 292 and 371 of all 4 NAs are the key binding residues. Van der Waals interaction is the main contribution to NS3/4A protease inhibitors binding, whereas the main contribution stabilized laninamivir binding is electrostatic interaction. Since some side effects have been observed in patients who treated by approved anti-HCV drugs, the new potent NS3/4A inhibitors have been needed. Therefore the potent inhibitors against NS3/4A were searched from the collected 40 ZINC ligands using steered MD technique based on the hypothesis that the high rupture force is needed for the high efficiency ligand. It was found that 9 top-hit compounds were probably good as or better than the 4 current NS3/4A inhibitors. Based on the SCC-DFTB/MM MD simulation, the acylation step of NS3/4A binding to beceprevir and telaprevir was occurred in the concerted manner as same as the native substrates which their energy barriers for the backward reaction of both systems were 19-23 kcal/mol approximately. This result is somewhat similar to the experimental data.

Department: Chemistry

Student's Signature

Field of Study: Chemistry

Advisor's Signature

Academic Year: 2013

Co-Advisor's Signature

ACKNOWLEDGEMENTS

Firstly, I would like to express my very great appreciation to my advisor, Prof. Dr. Supot Hannongbua, who always supports and encourages during my Ph.D. study and also gave me the valuable opportunity to study under the Royal Golden Jubilee Ph.D. program since 2008. He has not only given the constructive guidance but also motivated me to conduct this research. I would also like to greatly thank my co-advisor, Dr. Thanyada Rungrotmongkol for her untiring mentorship and very useful commentary of this dissertation. Special thanks given to Prof. Dr. Adrian J. Mulholland and Prof. Dr. Mai Suan Li for their encouragement, extremely helpful suggestions and wonderful experience in their laboratories during my stay in Bristol in 2013-2014 and Warsaw in 2012. My grateful thanks are extended to Dr. Marc W. Van der Kamp for his scientific advice and sacrificing his time to help me to learn the knowledge of QM/MM and do the QM/MM MD calculations. Additionally, I would like to express my sincere gratitude to all committee members: Assist. Prof. Dr. Warinthorn Chavasiri, Assoc. Prof. Dr. Pornthep Sompornpisut, Assoc. Prof. Dr. Polkit Sangvanich and Dr. Ornjira Aruksakunwong and Prof. Dr. Adrian J. Mulholland for their advice and very useful suggestions. I personally would like to thank all comrades and members in the Computational Chemistry Unit Cell who have supported and fulfilled me as well as shared valuable experiences during my Ph.D. course.

Finally, I would like to thank the Royal Golden Jubilee Ph.D. Program for providing financial support, the Computational Chemistry Unit Cell at Chulalongkorn University and the Centre for Computational Chemistry at University of Bristol for providing computer facilities and software.

CONTENTS

	Page
THAI ABSTRACT	iv
ENGLISH ABSTRACT	v
ACKNOWLEDGEMENTS	vi
CONTENTS	vii
LIST OF TABLES	xii
LIST OF FIGURES	xiii
LIST OF ABBREVIATIONS	xviii
CHAPTER 1 INTRODUCTION	1
1.1 RESEARCH RATIONALES AND THEORIES.....	2
1.1.1 Hepatitis C virus (HCV)	2
1.1.2 Influenza A virus.....	6
1.1.3 Steered molecular dynamics approach	10
1.1.4 Combined quantum mechanics and molecular mechanics (QM/MM) molecular dynamics (MD) simulation.....	11
1.2 RESEARCH METHODOLOGY	13
1.2.1 The structure and dynamics of proteins were calculated using the conventional MD simulation.	13
1.2.1.1 The per-residue decomposition energy was computed by molecular mechanics/generalized Born surface area (MM/GBSA).	13
1.2.1.2 The binding free energy and its components were calculated over 100 snapshots of each simulation using MM/GBSA and/or molecular mechanics/Poisson-Boltzmann surface area (MM/PBSA), whilst the entropic term was calculated by nmode analysis.	13
1.2.2 The SMD simulation was employed to pull ligands out from the binding pocket of the protein along a pathway, then the pulling forces were ranked in order to compare the binding affinity.....	13

1.2.3 The reaction mechanism of the enzyme with the current drugs has been investigated by means of the QM/MM MD approach.....	14
1.3 OBJECTIVES.....	14
1.3.1 To explore the structural properties and binding affinity of NS3/4A protease of HCV complexed with boceprevir, telaprevir, danoprevir and BI201335	14
1.3.2 To screen the potent inhibitor against NS3/4A protease	14
1.3.3 To investigate the reaction mechanism of NS3/4A protease with boceprevir and telaprevir bound	14
1.3.4 To compare the structural properties and binding pattern of H5N1 and pH1N1 NA for both WT and H274Y mutant binding to laninamivir	14
1.4 SCOPE OF THIS DISSERTATION	14
1.5 EXPECTED BENEFICIAL OUTCOMES	16
1.5.1 Fundamental information of the structural properties, ligand-target interactions and the key binding residues involved in the binding of boceprevir, telaprevir, danoprevir and BI201335 to NS3/4A protease	16
1.5.2 Discovery of the potent inhibitors that higher susceptibility than or similar to the current inhibitors	16
1.5.3 Information of the reaction mechanism of NS3/4A protease with boceprevir and telaprevir bound	16
1.5.4 Comparative information of the structural properties, ligand-target interactions and the key binding residues involved in the binding of laninamivir to the NA for both WT and H274Y mutation of H5N1 and pH1N1 strains.....	16
CHAPTER 2 PROTEIN STRUCTURE, DYNAMICAL PROPERTIES AND LIGAND-TARGET INTERACTIONS OF THE HCV NS3/4A PROTEASE IN COMPLEXATION WITH ITS INHIBITORS.....	17
2.1 ABSTRACT	18
2.2 INTRODUCTION	18
2.3 MATERIALS AND METHODS	22
2.3.1 Starting models and system preparation.....	22

	Page
2.2.3 Molecular Dynamics (MD) simulations	24
2.2.4 Binding free energy.....	25
2.2.5 Decomposition free energy	26
2.4 RESULTS AND DISCUSSION.....	28
2.4.1 Stability of global structures	28
2.4.2 Key residues for ligand binding.....	29
2.4.3 Hydrogen bond (H-bond) interactions.....	33
2.4.4 Binding affinity predictions.....	37
2.5 CONCLUSION.....	38
CHAPTER 3 SEARCHING FOR POTENT NS3/4A PROTEASE INHIBITORS.....	40
3.1 ABSTRACT	41
3.2 INTRODUCTION	41
3.3 MATERIALS AND METHODS	52
3.3.2 NS3/4A protease and inhibitor complexes preparation	52
3.3.3 Steered Molecular Dynamics (SMD) simulations.....	53
3.4 RESULTS AND DISCUSSION.....	55
3.4.1 Choice of pulling path.....	55
3.4.2 Validity of the SMD approach	58
3.4.3 Ranking of binding affinity of ligands	61
3.5 CONCLUSION.....	71
CHAPTER 4 THE REACTION MECHANISM OF NS3/4A PROTEASE OF HCV WITH BOCEPREVIR AND TELAPREVIR.....	72
4.1 INTRODUCTION	73
4.2 MATERIALS AND METHODS	76
4.3 RESULTS AND DISCUSSION.....	79
4.4 CONCLUSIONS	85
CHAPTER 5 PROTEIN STRUCTURE AND LIGAND-TARGET INTERACTIONS OF THE NEURAMINIDASE SUBTYPES A/H5N1 AND A/pH1N1 COMPLEXED LANINAMIVIR.....	86

	Page
5.1 ABSTRACT	87
5.2 INTRODUCTION	87
5.3 METHODOLOGY	91
5.3.1 System preparation	91
5.3.2 Partial Charge and Force Field Development for laninamivir	92
5.3.3 Molecular Dynamics (MD) simulations	93
5.4 RESULTS AND DISCUSSION.....	94
5.4.1 Stability of the global structure.....	94
5.4.2 Laninamivir binding patterns	95
5.4.3 Hydrogen bonding interactions.....	95
5.4.4 Key residues for drug binding.....	99
5.5 CONCLUSIONS	102
CHAPTER 6 CONCLUSIONS.....	104
REFERENCES	107
APPENDIX.....	127
VITA.....	132

LIST OF TABLES

	Page
Table 1.1 Currently reported drug resistance mutations in HCV NS3 protease	6
Table 2.1 Comparison of the averaged binding free energy and energetic components (kcal/mol) calculated using 100×3 MD trajectories from the three independent simulations and experimental IC_{50} and K_i (nM) values of the four inhibitors binding to NS3/4A protease of HCV	38
Table 3.1 The biological activities of NS3/4A substrates and their cleaved products. 45	
Table 3.2 Drug resistance profile of the four currently available NS3 protease HCV inhibitors.....	47
Table 5.1 The 50% inhibitory concentration (IC_{50}) values of laninamivir for neuraminidase (NA) from various influenza strains.	91

LIST OF FIGURES

	Page
Figure 1.1 The HCV ssRNA genome (top) and the polyprotein translational processing produced the 4 structural and 6 non-structural proteins (bottom) [7]	2
Figure 1.2 (a) Molecular surface of the NS3 and NS4A cofactor bound with its inhibitor (vdW sphere). (b) The catalytic triad residues His57, Asp81 and Ser139 (white ball and sticks) and the other residues in the binding site (green ball and sticks).....	4
Figure 1.3 The chemical structures of the neuraminidase inhibitors, OTV, ZNV, PRV and LNV [29]	6
Figure 1.4 (a) The total usage of oseltamivir in comparison with zanamivir and (b) oseltamivir usage each year in Japan, US and the rest of the world [36].....	7
Figure 1.5 (a) The action of neuraminidase in the influenza life cycle and (b) the mechanism of neuraminidase inhibitor activity [41]	8
Figure 1.6 A scheme of protein-ligand complex during the SMD, which a ligand is pulled out from the binding pocket using the harmonic potential [51]	11
Figure 1.7 The QM region locating in the active site is calculated with QM method as shown in ball and stick and the rest system including solvent is treated with MM method [53]	12
Figure 2.1 (A) The four current inhibitors (boceprevir, telaprevir, danoprevir and BI201335 shown by ball and stick model) binding to the active site of the HCV protease where the most hydrophilic and hydrophobic surface shaded by blue and orange red, respectively.....	20
Figure 2.2 Chemical structures of the four NS3/4A protease inhibitors boceprevir (SCH 503034), telaprevir (VX-950), danoprevir (ITMN-191) and BI201335. The P1', P1, P2, P3 and P4 substituents are colored by black, red, blue, green and purple, respectively.	22
Figure 2.3 Root-mean square displacements (RMSDs) for all atoms of the four NS3/4A-inhibitor complexes compared to their initial structures from the three independent simulations (MD1-MD3).....	28
Figure 2.4 Per-residue decomposition free energy of NS3 protease for the four studied inhibitors from the three independent simulations	29

Figure 2.5 (Left) Averaged energy contributions over the three independent simulations from the residue backbone and side chain for the four studied complexes of the NS3/4A protease with (A) boceprevir, (B) telaprevir, (C) danoprevir and (D) BI201335. (Right) Aver aged electrostatic and vdW energy contributions from each residue. Note the standard deviation among the three simulations is shown as error bar.....	31
Figure 2.6 The averaged percentage of H-bond occupation of the NS3/4A residues contributed to (A) boceprevir, (B) telaprevir, (C) danoprevir and (D) BI201335 over the three MD simulations where the standard deviation is given as error bar.....	33
Figure 2.7 The binding pattern of (A) boceprevir, (B) telaprevir, (C) danoprevir and (D) BI201335 in the NS3/4A active site demonstrated from the last snapshot from MD1 simulation. Note that residue H57 is in the HIE type and D81 is in neutral form for the NS3/4A--BI201335 complex, whilst in the other complexes they are the HID type and negatively charged form, respectively.	35
Figure 3.1 (A) Polyprotein of hepatitis C virus (HCV), where the green and blue present structural and non-structural proteins, respectively. (B) (Left) Structure of the NS3/NS4A cofactor complex with the inhibitor bound (vdW sphere), and (right) the catalytic triad residues (H57, D81 and S139 in white ball and sticks) and the other residues (violet ball and sticks) at the binding site.	43
Figure 3.2 Chemical structures of the four NS3/4A protease inhibitors: boceprevir, telaprevir, danoprevir (ITMN-191) and BI201335	46
Figure 3.3 The structure of the narlaprevir derivative scaffold [109]	49
Figure 3.4 (A) Three possible pathways shown with their average radius and depth for ligand unbinding path constructed by pulling boceprevir from the NS3/4A binding site. (B) The force-time and (C) force-displacement profiles of boceprevir along the three pathways shown in (A).....	57
Figure 3.5 (A) The force-time and (B) the force-displacement profiles of the four inhibitors pulled from the NS3/4A protease binding site through the selected tunnel (pathway 1 in Fig. 3.4A), where in (A) the x-axis refers to the extended distance from the reference position of the ligand (at $t = 0$).....	59

Figure 3.6 The correlation between the rupture force (F_{max}) and the calculated binding free energies obtained from the experimental values, based on $\Delta G = -RT \ln(K_i)$ where $R = 1.987 \times 10^{-3}$ kcal/mol, $T = 298$ K, K_i is inhibition constant and IC_{50} is the half maximal inhibitory concentration.....	60
Figure 3.7 Ranking of the binding affinity to the NS3/4A protease of the top 40 ligands from the ZINC database and the four currently used HCV inhibitors (shown in grey) for comparison	61
Figure 3.8 (A) Superimposition of the last snapshots for NS3/4A in complex with the best nine screened compounds from the ZINC database: 59500093 (black), 59784724 (red), 13527817 (green), 26660256 (blue), 29482733 (cyan), 25977181 (pink), 28005928 (yellow), 13527826 (olive green) and 13471529 (navy blue). The (B) and (C) force-time profiles, and (D) and (E) force-displacement profiles were obtained from the representative trajectories.	63
Figure 3.9 Time dependencies of the hydrogen binding number of top 13 ligands, the arrow pointed at F_{max}	65
Figure 3.10 Electrostatic (E _{ele}) and van der Waals (E _{vdW}) energies (shown in grey and black line, respectively) as the ligand is withdrawn at a constant force per unit time for the top thirteen ligands	68
Figure 3.11 Close up of the NS3/4A protease in complex with danoprevir (green ball and stick model) at (A) the equilibrium state (before pulling), (B) the maximum point (F_{max} at $t = 385$ ps in Fig. 3.4), and (C) the independent state (after passing the maximum point at $t = 450$ ps). The blue and orange colors represent hydrophilic and hydrophobic surfaces, respectively	69
Figure 3.12 Hydrogen bond formation between danoprevir and its binding residues in HCV NS3/4A protease at (A) the equilibrium state, (B) the maximum pulling force in correspondence to Fig. 3.11	70
Figure 4.1 The catalytic mechanism of the peptide cleavage reaction by the HCV NS3/4A protease	74
Figure 4.2 Fragments of the NS3 catalytic residues and telaprevir (left) and boceprevir (right) included in the QM region, where the QM and MM parts are partitioned by the red line.....	77

Figure 4.3 Proposed reaction mechanism of NS3/4A protease with the keto-amide inhibitor.....	78
Figure 4.4 The root mean-square displacements (RMSDs) relative to the initial structures of NS3/4A protease with boceprevir (BOC) and telaprevir (TVR) bound as shown in the red and black lines, respectively.	80
Figure 4.5 Free energy profile (FEP) obtained from WHAM of 3 umbrella sampling calculations for the proton transfer between H57 and the hemiketal oxygen of (A) BOC-NS3/4A and (B) TVR-NS3/4A	81
Figure 4.6 The three individual SCC-DFTB/MM free energy surfaces (FESs) for the acylation mechanism of NS3/4A protease binding to (A-C) boceprevir and (D-E) telaprevir with different initial structures	82
Figure 4.7 Structures and distances of the tetrahedral intermediate, transition state and reactant of NS3/4A-boceprevir complex in the acylation reaction	83
Figure 4.8 Structures and distances of the tetrahedral intermediate, transition state and reactant of NS3/4A-telaprevir complex in the acylation reaction	84
Figure 5.1 The chemical structures of four NA inhibitors (NAIs) in the active metabolite form: oseltamivir, zanamivir, peramivir and laninamivir.....	88
Figure 5.2 (Left) Close up of laninamivir binding to the catalytic pocket of the pH1N1 NA (cyan) obtained from the 3TI3 crystal structure[170] with a superimposition of the H5N1 NA (2HU4 [42], green). (Right) From the X-ray structure of the laninamivir-NA complex, the hydrogen bond formations through the backbone and side chain of the surrounding residues are represented by blue and green arrows, respectively.	90
Figure 5.3 Root mean-square displacements (RMSDs) relative to the starting structure for all atoms of the laninamivir binding to the WT and H274Y NAs of the influenza H5N1 and pH1N1 viruses.....	94
Figure 5.4 Percent occupation pattern of hydrogen bonds formed from the dihydropyran ring and the four side chains of laninamivir to the binding residues (label given along y-axis) in the active site of the four NAs: (a) H5N1 WT, (b) H5N1 H274Y, (c) pH1N1 WT and (d) pH1N1 H274Y.	97

Figure 5.5 The (Left) decomposition of the binding free energy in pairwise per-residue basis, and its energy contributions from the backbone and side chain atoms, and (Right) the electrostatic and vdW energy 101



LIST OF ABBREVIATIONS

AIDS	=	Acquired immunodeficiency syndrome
AMBER	=	Assisted model building with energy refinement
BOC	=	Boceprevir
CCDC	=	Cambridge crystallographic data center
CG	=	Conjugated gradient
CoMFA	=	Comparative molecular field analysis
CoMSIA	=	Comparative molecular indices analysis
DFT	=	Density functional theory
ER	=	Endoplasmic reticulum
ESP	=	Electrostatic potential
FDA	=	Food and Drug Administration
FEP	=	Free energy perturbation
FES	=	Free energy surface
GA	=	Genetic algorithm
GAFF	=	General AMBER force field
GOLD	=	Genetic optimization for ligand docking
GROMACS	=	GRONingen MACHine for Chemical Simulations
GBSA	=	Generalized Born surface area
HCV	=	Hepatitis C virus
HF	=	Hartree-Fock
HFMD	=	Hand, foot and mouth disease
HIV	=	Human immunodeficiency virus
LIE	=	Linear interaction energy
LINC	=	Linear constraint solver
LNV	=	Laninamivir
MD	=	Molecular dynamics

MM	=	Molecular mechanics
NA	=	Neuraminidase
NAI	=	Neuraminidase inhibitor
NCIDS	=	NC Office of Indigent Defense Services
PBSA	=	Poisson-Boltzmann surface area
PDB	=	Protein Data Bank
PEG-IFN	=	Peg-interferon
PLP	=	Piecewise linear potential
PME	=	Particle mesh Ewald
PMF	=	Potential mean force
QM	=	Quantum mechanics
QSAR	=	Quantitative structure-activity relationship
RC	=	Reaction coordinate
RdRp	=	RNA-dependent RNA-polymerase
RESP	=	Restrained electrostatic potential
RMSD	=	Root-mean square displacement
SASA	=	solvent accessible surface area
SCC-DFTB	=	self-consistent charge density functional tight-binding
SD	=	Steepest descents
SMD	=	Steered molecular dynamics
ssRNA	=	Single-stranded ribonucleic acid
TI	=	Tetrahedral intermediate
TS	=	Transition state
TVR	=	Telaprevir
vdW	=	van der Waals
WT	=	Wild-type
X-ray	=	Crystallographic spectroscopy

CHAPTER 1

INTRODUCTION

Virus is the most important factor that leads to several human diseases for both infectious and non-infectious such as hepatitis C, influenza (flu), acquired immunodeficiency syndrome (AIDS), dengue fever and hand, foot and mouth disease (HFMD) etc. However, hepatitis C and influenza are only focused in this work according to it is well known that the influenza widely emerged and spread out all over the world, especially the avian flu (H5N1) and 2009 pandemic H1N1 (pH1N1). While over 170 million people in worldwide have been infected with the hepatitis C virus (HCV) that is the cause of several liver diseases including liver cancer and the number of infected people tends to increase every year. Lately, the novel anti-influenza drug, laninamivir (LNV) was developed to inhibit the neuraminidase (NA) for both wild-type (WT) and oseltamivir resistant mutants which its binding pattern with WT and the H274Y mutant of both H5N1 and pH1N1 have not been published yet. For the HCV treatment, boceprevir and telaprevir were newly approved and marketed. Unfortunately, some side effects have been found in the HCV patients who have taken either boceprevir or telaprevir. Hence, the main goal of this work was to provide a comparative understanding of the drug-target interactions, binding pattern and binding affinity of laninamivir binding to both WT and H274Y mutant neuraminidases of H5N1 and pH1N1 as well as the HCV inhibitors (boceprevir, telaprevir, danoprevir and BI201335) binding to NS3/4A protease. The catalytic mechanisms of boceprevir and telaprevir have been additionally established as well. These molecular-level studies may give very useful information for designing and developing of the higher potential inhibitors in the future.

1.1 RESEARCH RATIONALES AND THEORIES

1.1.1 Hepatitis C virus (HCV)

HCV is the cause of chronic liver disease, liver inflammation, cirrhosis that possibly develops to be hepatocellular carcinoma. Recently, the Food and Drug Administration (FDA) have recently approved the four anti-HCV drugs (ribavirin, peg-interferon, telaprevir and beceprevir). Unfortunately, some side effects have been found in the patients and approximately 40-50% of the genotype 1 patients medicated with ribavirin and peg-interferon combination have failed in the HCV treatment. Even though adding either boceprevir or telaprevir result in an increase in succeeded rate, it also increases the adverse side effects [1-4]. This is therefore it comes to be one of global health issues [5, 6]. In addition, the novel potent HCV inhibitors with less toxicity are still needed.

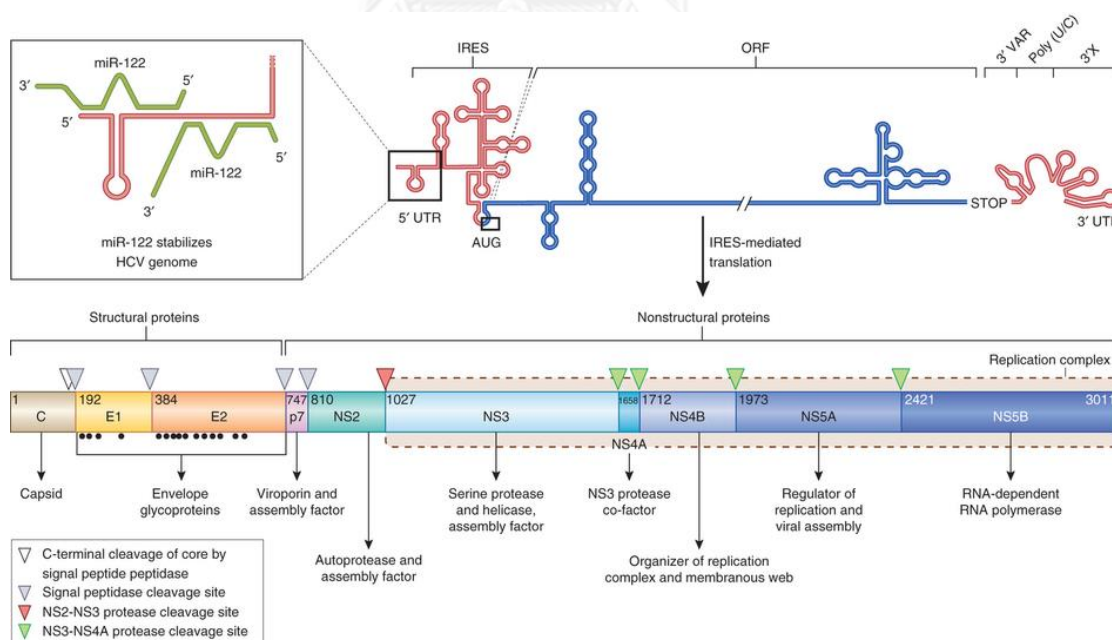


Figure 1.1 The HCV ssRNA genome (top) and the polyprotein translational processing produced the 4 structural and 6 non-structural proteins (bottom) [7]

HCV is an enveloped virus of *hepacivirus* genus under the *Flaviviridae* family containing about ~9,600 nucleotide of positive single-stranded RNA (ssRNA) genome [8]. After the gene encoding, a polyprotein precursor has been produced, and then it is proceeded by host and viral proteases in order to generate 4 structural proteins (C, E1, E2 and p7) and 6 non-structural proteins (NS2, NS3, NS4A, NS4B, NS5A and NS5B) that are important for the viral replication as shown in Fig. 1.1. Among these individual proteins, the NS3/4A that is responsible for cleavage of the scissile peptide bond between P1' and P1 sites of NS3/NS4A, NS4A/NS4B, NS4B/NS5A and NS5A/NS5B substrates is one of the major drug-targets. To function as a serine protease enzyme, the required minimal number of residues is 180 amino acids counting from the N-terminus of NS3 protein and 14 amino acids of the NS4A protein, which are embedded in NS3 protease domain [8]. Absence of the NS4A cofactor significantly decreased a proteolytic activity of NS3 protease owing to the His57 and Asp81 conformations are unaligned and, then the NS3 protease is unable to cleave the peptide bond [9, 10]. It implies the presence of the NS4A cofactor is needed to adjust the three catalytic residues (His57, Asp81 and Ser139 as shown in Fig. 1.2) into the active conformation that is suitable for the Michaelis addition. The NS3/4A belongs to the trypsin/chymotrypsin-like serine protease family, but its binding pocket is rather solvent exposed and shallow (as displayed in Fig. 1.2) than the others, such as thrombin and elastase [11]. This leads to the drug design and development against the NS3/4A protease of HCV is somewhat more challenging. Thus, there is several researches both experimental and computational studies that focused on the NS3/4A.

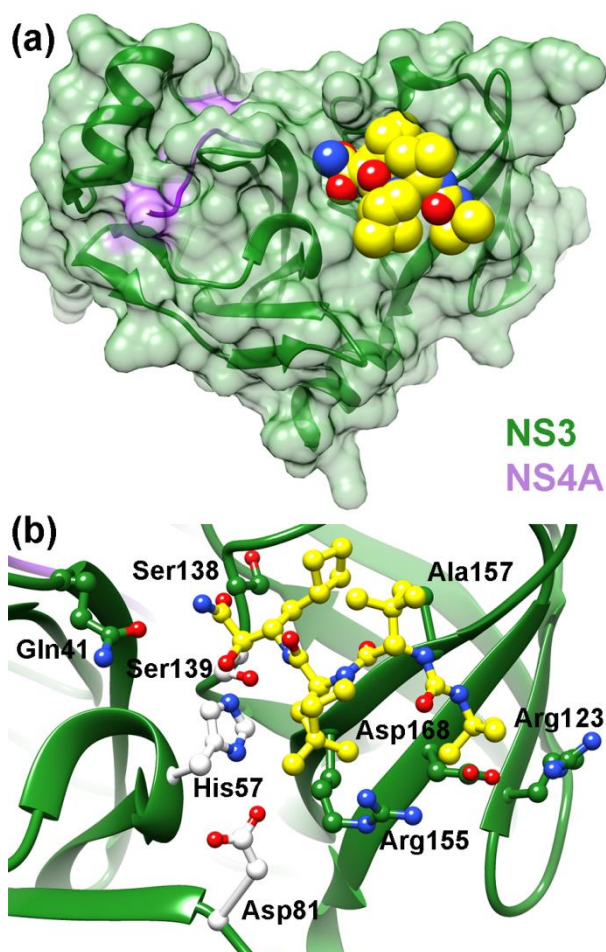


Figure 1.2 (a) Molecular surface of the NS3 and NS4A cofactor bound with its inhibitor (vdW sphere). (b) The catalytic triad residues His57, Asp81 and Ser139 (white ball and sticks) and the other residues in the binding site (green ball and sticks).

According to the experimental study, different N-terminal hexamer products were able to effectively inhibit the NS3/4A protease activity towards the different target sites [12]. Substrate-like inhibitors have been continuously developed [13-15]. However, their pharmacokinetic properties are quite poor. These cleaved products were then consequently optimized or modified to the substrate mimic inhibitors by modifying the scissile peptide bond to an aldehyde, α -ketoamide and boronate groups etc. Generally, the NS3/4A protease inhibitor can be divided into 2 types;

covalent and non-covalent inhibitors. For the covalent inhibitor, the covalent bond is formed between an inhibitor and Ser139 which is similar to the HCV natural substrates, but the NS3/4A is incompetent to break this covalent bond resulting in an inactivation of the enzyme. This is because the P site of an inhibitor has been replaced with an electrophile warhead, such as α -ketoamide, aldehyde, trifluoromethyl ketone, α -ketoester, etc. Meanwhile, the non-covalent inhibitor, such as danoprevir, BI201335, and simeprevir commonly contains a carboxylic or sulfonamide groups instead of an electrophile warhead on the P-site and so an electrostatic interaction is mainly formed with Ser139.

Even though several anti-HCV drugs were designed, the drug resistance has been detected. This is due to the virus has no proofreading and so the error rates (and thus mutation rates) during replication are relatively high. The currently prevalent resistant mutations in the HCV NS3 protease are summarized in Table 1. For example, the broad drug resistance due to the R155K mutation is the most frequently found mutation in infected HCV genotype 1 patients [16-18]. The mutations at Val36 and Thr54 residues show low and medium resistant levels towards keto-amide based inhibitors [16, 19, 20]. Apart from those drug resistances, the A156T mutation resulted in a high level of resistance to both boceprevir and telaprevir with a 400- and 390-fold increase in the K_i compared to that for the wild-type, respectively [21]. Since it has a very high resistant fold, Guo and co-workers used the free energy perturbation (FEP) method in order to investigate the effects of the A156T or D168V/Q mutations towards boceprevir and telaprevir [22]. Then it was suggested that a decrease of their binding affinities might be due to the steric effect

obtained from the side chain of Thr156 resulting to a reorientation of the P2 and P3 moieties of boceprevir and a repulsion of the P4 moiety of telaprevir.

Table 1.1 Currently reported drug resistance mutations in HCV NS3 protease

Residue	Mutation	Inhibitors
Val36 [19, 20, 23-25]	Ala, Met, Gly	Boceprevir, Telaprevir
Gln41 [24]	Arg	Boceprevir, Danoprevir
Phe43 [24]	Ser, Cys, Val, Ile	Boceprevir, Telaprevir, Danoprevir, TMC435
Thr54 [19, 20, 23-26]	Ala, Ser	Boceprevir, Telaprevir, BI201335
Val55 [27]	Ala	Boceprevir, Telaprevir
Gln80 [28]	Lys, Arg, His, Gly, Leu	TMC435
Arg155 [19, 20, 23, 24, 26, 28]	Lys, Thr, Gln, Gly	Boceprevir, Telaprevir, BI201335, Danoprevir, TMC435
Ala156 [19, 20, 23, 24, 26, 28]	Ser, Thr, Val, Gly	Boceprevir, Telaprevir, BI201335, Danoprevir, TMC435
Asp168 [23, 26, 28]	Ala, Val, Gly, Asn, Glu, Thr, Tyr, His, Ile	BI201335, Danoprevir, TMC435
Val170 [23, 24]	Ala	Boceprevir, Telaprevir

1.1.2 Influenza A virus

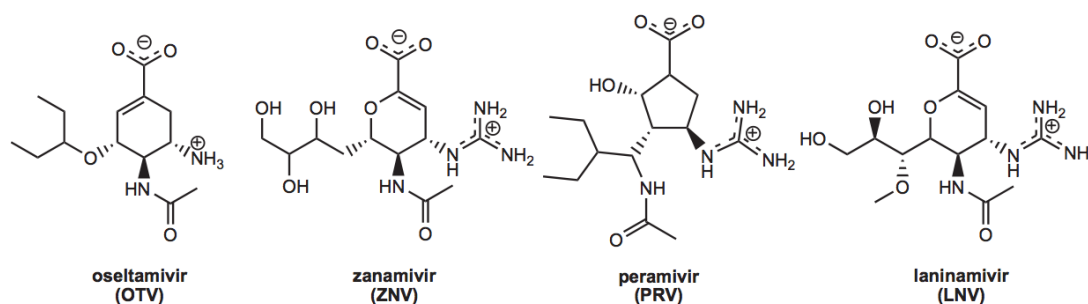


Figure 1.3 The chemical structures of the neuraminidase inhibitors, OTV, ZNV, PRV and LNV [29]

Influenza A virus is widely spread out in worldwide causing a lot of human and poultry deaths, especially subtypes H5N1 (avian flu or bird flu) and 2009 pandemic H1N1 (pH1N1) [30-32]. To date, there are 2 classes of anti-influenza drugs targeting on neuraminidase (NA) such as oseltamivir (Tamiflu) and zanamivir (Relenza)

as depicted in Fig. 1.3 and (ii) targeting on M2 channel such as amantadine (Symmetrel) and rimantadine (Flumadine). However, amantadine and rimantadine are resistance to seasonal H3N2 and pH1N1. They are not recommended to use for an influenza treatment whereas oseltamivir is the most usage and the most common drug taken (Fig. 1.4) as a capsule or suspension [33]. But it was found that several strains are resistant to oseltamivir [34-37]. Laninamivir (LNV) is highly effective against the NA of both influenza A and B viruses as well as the oseltamivir-resistant strains with a long-term of action which lately approved to market in Japan [38-40]. Nevertheless, understanding the drug-target interactions of laninamivir bound with the WT and H274Y of N1 strains may provide fundamental information that could be useful for a therapeutic application.

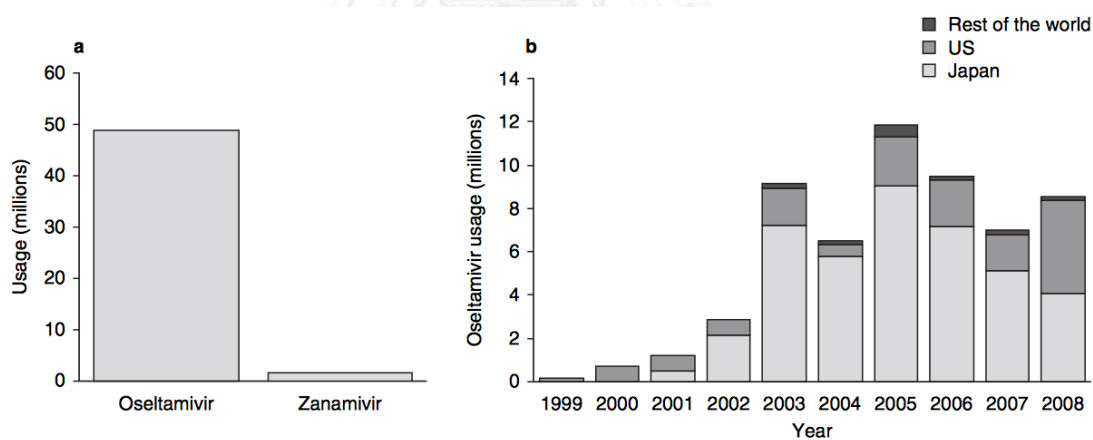


Figure 1.4 (a) The total usage of oseltamivir in comparison with zanamivir and (b) oseltamivir usage each year in Japan, US and the rest of the world [36]

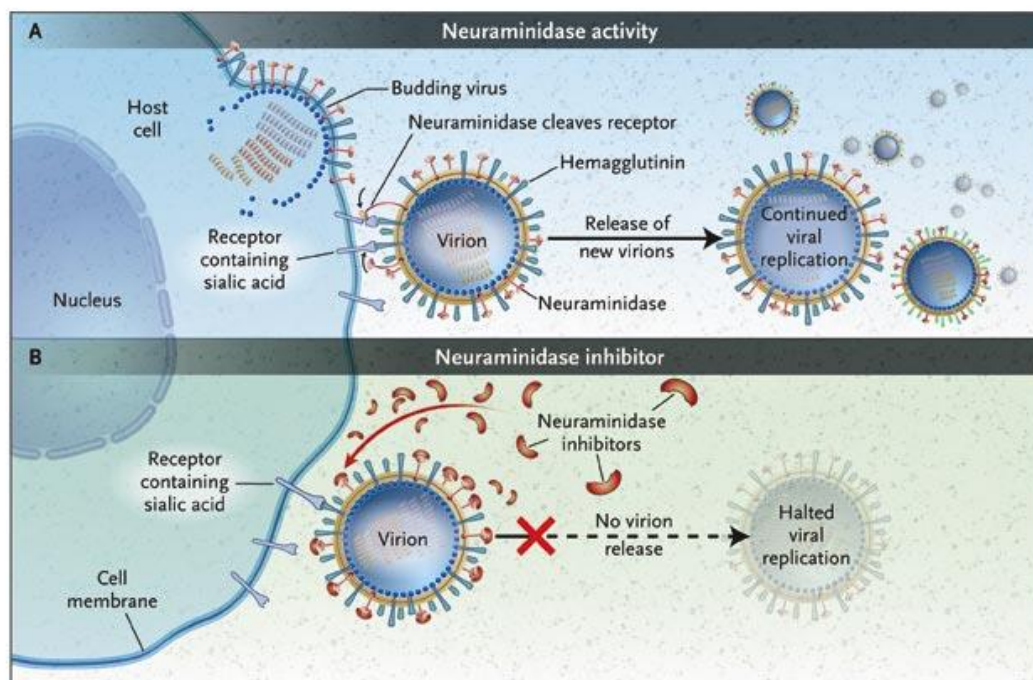


Figure 1.5 (a) The action of neuraminidase in the influenza life cycle and (b) the mechanism of neuraminidase inhibitor activity [41]

The influenza NA is a glycoprotein locating on the viral surface and is responsible for the cleavage of the glycosidic linkage at the terminal sialic acid of host receptor in order to release the new viral progeny. Therefore, the inhibition of neuraminidase activity could block influenza transmission as represented in Fig 1.5. Based on the genetic and crystal structures, NA is divided into group-1 consists of N1, N4, N5 and N8 and group-2 contains N2, N3, N6, N7 and N9 [42]. These 2 groups differ in a cavity size on the 150-loop. However, the active site of all neuraminidases conservatively contains an arginine triad (Arg118, Arg292 and Arg371), Asp151, Arg152, Arg224, Glu276 and Y406, while the framework site normally contains Glu119, Arg156, Trp178, Ser179, Asp198, Ile222, Glu227, His274, Glu277, Asn294 and Glu245. According to its role, NA has become a main target for anti-influenza drugs

improvement that generally is designed based on a transition state of sialic acid including both oseltamivir and zanamivir [43-46]. However, the lack of proofreading capacity as found in the other RNA virus leads to increase the mutation rate of NA. That is also the cause of drug-resistant especially oseltamivir, hence the oseltamivir-resistant has been more seriously concerned. The high-level resistance has been continuously reported. For example, the H274Y, R292K and R152K mutations in the NA of H1N1 increased the inhibition activity of oseltamivir up to 400-, 9,400- and 190-fold compared to the wild-type, whilst the low-level resistance to zanamivir were observed for all variants excepting the H274Y mutant that is still sensitive [47]. Additionally, the H274Y NA of pH1N1 significantly reduced a susceptibility to oseltamivir, approximately 250-fold. The highly resistant of H274Y variant of subtype H5N1 to oseltamivir has been reported as well, with the 300- to 7,000-fold decreased affinity [48].

In 2009, peramivir was authorized by FDA for an emergency use to treat the patient who infected with pH1N1. Yamashita and co-workers subsequently synthesized the second generation of neuraminidase inhibitor, laninamivir (Fig. 1.3) [49] and then launched by Daiichi Sankyo Co. Ltd. in Japan and Biota. Besides it is able to inhibit both influenza A and B viruses, it provides a long-acting activity according to a gradual elimination from the respiratory tract. Therefore, laninamivir is a high efficiency NA inhibitor that might be accomplished with a single treatment [38].

In this work, understanding the drug-target interactions, binding pattern and binding efficiency of NS3/4A protease and neuraminidase inhibitors were investigated

by means of molecular dynamics (MD) simulation, while combined quantum mechanics and molecular mechanics (QM/MM) MD simulation was applied to examine the catalytic mechanism of NS3/4A protease with the current drugs. In addition, searching the potent inhibitor against NS3/4A was performed using the steered molecular dynamics (SMD) approach. These studies might provide useful information for further drug design and development and might lead to discover the potent inhibitors against the HCV protease.

1.1.3 Steered molecular dynamics approach

Steered molecular dynamics (SMD) method is a computational technique imitated the developed atomic force microscope (AFM) that determines a force required to take out a ligand from protein as displayed in Fig. 1.6 [50]. Hence SMD is a tool for prediction of the ligand-protein interactions, binding as well as unbinding processes. Based on a classical MD simulation, a coulombic and Lennard-Jones potentials are also used for electrostatic and van der Waals (vdW) interactions. Differently, the external force is applied in term of a harmonic potential. A ligand is connected to a harmonic spring with spring constant (k), where the pulling force (F) and external potential (U) can be calculated as following.

$$F(x, t) = K(x(t_0) - x(t)) \quad (1.1)$$

$$U = \frac{K}{2}(x(t) - x(t_0))^2 \quad (1.2)$$

$x(t)_0$ and $x(t)$ are an initial position and reaction coordinate at time, t , respectively. For the constant velocity SMD, the fluctuation of the force represents the interactions between protein and ligand along pulling pathway, in which the

higher force indicates the higher interaction strength. To perform the SMD simulation, it requires a pulling direction for applying an external force. However, the pulling direction is quite sensitive due to the binding pocket may be distorted during the simulation.

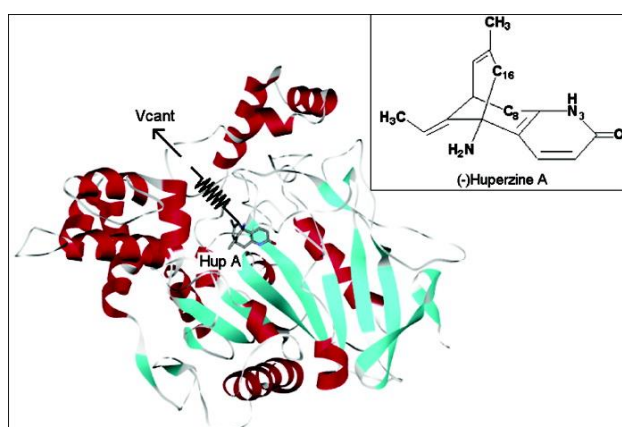
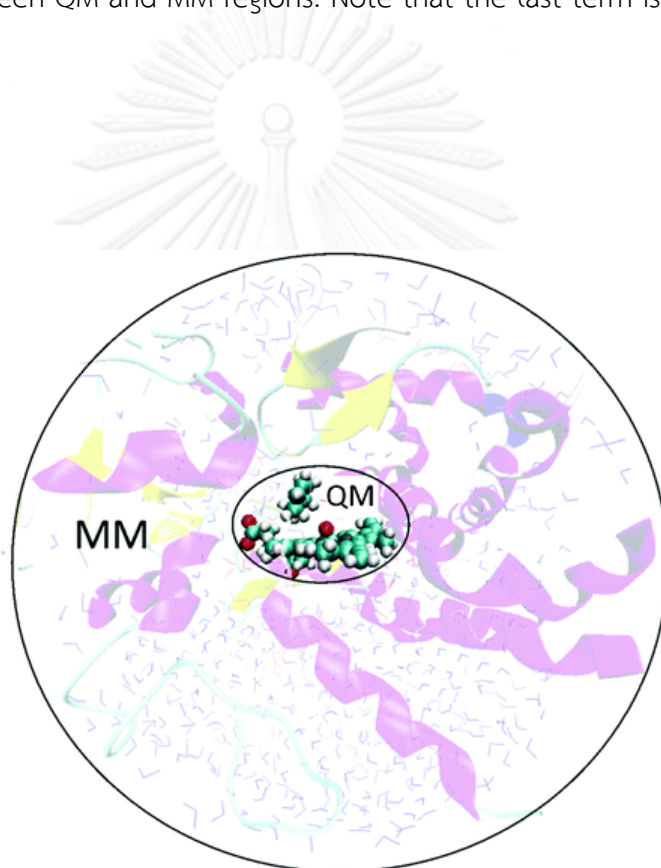


Figure 1.6 A scheme of protein-ligand complex during the SMD, which a ligand is pulled out from the binding pocket using the harmonic potential [51]

1.1.4 Combined quantum mechanics and molecular mechanics (QM/MM) molecular dynamics (MD) simulation

Recently, the QM/MM methods are widely used to investigate the reaction mechanism of numerous enzymes and the other biomolecular systems since it was firstly revealed by Warshel and Levitt in 1976 [52]. According to the conventional MD approach, this method cannot model the chemical reaction such as proton transfer, bond breaking and forming due to the harmonic term in the force fields. Thus, the QM methods have been combined with the MM to solve this problem. For the QM/MM MD approach, the system is generally separated into 2 regions; the region involved in the reaction is calculated by a QM method, whilst MM is employed to

treat the rest of system as represented in Fig. 1.7. To calculate the total energy (E_{total}) of the QM/MM system in the additive approach, the energy of QM region (E_{QM}) in absence of perturbation from MM is combined together with the MM energy (E_{MM}) and the QM/MM energy ($E_{\text{QM/MM}}$) that represented the interactions between QM and MM regions. Note that the last term is calculated using MM force field.



$$E_{\text{total}} = E_{\text{QM}} + E_{\text{MM}} + E_{\text{QM/MM}} \quad (1.3)$$

Figure 1.7 The QM region locating in the active site is calculated with QM method as shown in ball and stick and the rest system including solvent is treated with MM method [53]

The easy way to calculate the $E_{\text{QM/MM}}$ is to ignore an electrostatic coupling between QM and MM and treat the vdW and electrostatic interaction with MM

method. However, this may lead to a problem, if the reaction is related to a charge transfer due to the parameters and charges are constant along the simulation. Therefore, the point charges of the QM region are taken from the electronic structure of each step. The $E_{\text{QM/MM}}$ can be computed as below.

$$E_{\text{QM/MM}} = \sum_{\mathbf{k}}^{N_{\text{MM}}} \int dr \frac{\rho_{\text{QM}}(r) Q_{\mathbf{k}}}{|r - R_{\mathbf{k}}|} + \sum_{\mathbf{A}}^{N_{\text{QM}}} \sum_{\mathbf{k}}^{N_{\text{MM}}} \varepsilon_{\mathbf{A}\mathbf{k}} \left[\left(\frac{\sigma_{\mathbf{A}\mathbf{k}}}{R_{\mathbf{A}\mathbf{k}}} \right)^{12} - \left(\frac{\sigma_{\mathbf{A}\mathbf{k}}}{R_{\mathbf{A}\mathbf{k}}} \right)^6 \right] \quad (1.4)$$

N_{MM} and N_{QM} are the number of atoms in the MM and QM regions, respectively. From the Eq. 1.4, the coulombic interaction between the total charge density of the QM region (ρ_{QM}) and the fixed MM point charge ($Q_{\mathbf{k}}$) is represented in the first term, while the vdW interaction between the atoms in the QM and MM regions is denoted in the second term. The bonded term is additionally included for the system that the covalent bond is located at the QM/MM boundary.

1.2 RESEARCH METHODOLOGY

1.2.1 The structure and dynamics of proteins were calculated using the conventional MD simulation.

1.2.1.1 The per-residue decomposition energy was computed by molecular mechanics/generalized Born surface area (MM/GBSA).

1.2.1.2 The binding free energy and its components were calculated over 100 snapshots of each simulation using MM/GBSA and/or molecular mechanics/Poisson-Boltzmann surface area (MM/PBSA), whilst the entropic term was calculated by nmode analysis.

1.2.2 The SMD simulation was employed to pull ligands out from the binding pocket of the protein along a pathway, then the pulling forces were ranked in order to compare the binding affinity.

1.2.3 The reaction mechanism of the enzyme with the current drugs has been investigated by means of the QM/MM MD approach.

1.3 OBJECTIVES

1.3.1 To explore the structural properties and binding affinity of NS3/4A protease of HCV complexed with boceprevir, telaprevir, danoprevir and BI201335

1.3.2 To screen the potent inhibitor against NS3/4A protease

1.3.3 To investigate the reaction mechanism of NS3/4A protease with boceprevir and telaprevir bound

1.3.4 To compare the structural properties and binding pattern of H5N1 and pH1N1 NA for both WT and H274Y mutant binding to laninamivir

1.4 SCOPE OF THIS DISSERTATION

In this thesis, the binding interactions of protease inhibitors (boceprevir, telaprevir, danoprevir and BI201335) binding to NS3/4A protease of HCV including the structural and dynamical properties were investigated using classical molecular dynamics (MD) simulations. From the result, it was found that the key residues stabilized the ligand binding are residues 41-43, 57, 81, 136-139, 155-159 and 168 in the NS3 domain. Even though the binding pattern of all ligands were somewhat different, the P3 site was likely to be recognized by A157 residue. Additionally, the binding affinity that was predicted by both MM/GBSA and MM/PBSA over 100 snapshots of each MD, exhibits a similar trend to the experimental data. More details were discussed in Chapter 2. Consequently, the 40 ligands obtained from ZINC database were screened to search for the high potent inhibitors against HCV protease by means of SMD approach. There are top 9 compounds that showed the binding affinity higher or similar to the current inhibitors as discussed in Chapter 3. However,

the reaction mechanisms of NS3/4A protease with boceprevir and telaprevir have not been provided yet, therefore, their mechanisms have been explored using SCC-DFTB/MM MD simulations with the umbrella sampling method. To study the reaction mechanisms of HCV protease with the 2 drugs, we presumed that their reactions are similar to the native substrates but the NS3/4A cannot cleave the keto-amide group of the ligand. Then there are consisted of 2 steps; the acylation (rate limiting step) and the proton transfer between His57 and hemiketal oxygen of the ligand. The free energy profiles along the reaction coordinates were plotted and discussed in Chapter 4.

The comparative study of the ligand-target interactions of laninamivir binding to the NA of both WT and H274Y mutant of H5N1 and pH1N1 strains was revealed in Chapter 5. In this chapter, the hydrogen bonding interaction and the per-residue decomposition energy of the surrounding residues were analyzed. In addition, the hydrogen bonds between laninamivir and the NA are conserved, even though the H274 residue is mutated to tyrosine. Therefore, laninamivir is able to inhibit both WT and oseltamivir-resistant strains.

1.5 EXPECTED BENEFICIAL OUTCOMES

1.5.1 Fundamental information of the structural properties, ligand-target interactions and the key binding residues involved in the binding of boceprevir, telaprevir, danoprevir and BI201335 to NS3/4A protease

1.5.2 Discovery of the potent inhibitors that higher susceptibility than or similar to the current inhibitors

1.5.3 Information of the reaction mechanism of NS3/4A protease with boceprevir and telaprevir bound

1.5.4 Comparative information of the structural properties, ligand-target interactions and the key binding residues involved in the binding of laninamivir to the NA for both WT and H274Y mutation of H5N1 and pH1N1 strains

From this thesis, it is anticipated that these results could be useful for a better understanding in the ligand-protein interactions of either NS3/4A protease or neuraminidase. Additionally, it may be used as a basic knowledge for a further drug design and development in the future.

CHAPTER 2
PROTEIN STRUCTURE, DYNAMICAL PROPERTIES AND LIGAND-TARGET
INTERACTIONS OF THE HCV NS3/4A PROTEASE IN COMPLEXATION WITH ITS
INHIBITORS

Key Binding and Susceptibility of NS3/4A Serine Protease Inhibitors against
Hepatitis C Virus

Arthitaya Meeprasert¹, Supot Hannongbua¹ and Thanyada Rungrotmongkol²

¹*Department of Chemistry, Faculty of Science, Chulalongkorn University, 254
Phayathai Road, Patumwan, Bangkok 10330, Thailand*

²*Department of Biochemistry, Faculty of Science, Chulalongkorn University, 254
Phayathai Road, Bangkok 10330, Thailand*

จุฬาลงกรณ์มหาวิทยาลัย
CHULALONGKORN UNIVERSITY

This article has been accepted in journal: Journal of Chemical Information and
Modeling Year: 2014

2.1 ABSTRACT

Hepatitis C virus (HCV) causes an infectious disease that manifests itself as liver inflammation, cirrhosis and can lead to the development of liver cancer. Its NS3/4A serine protease is a potent target for drug design and development since it is responsible to cleave the scissile peptide bonds in the polyprotein important for the HCV life cycle. Herein, the ligand-target interactions and the binding free energy of the four current NS3/4A inhibitors (boceprevir, telaprevir, danoprevir and BI201335) were investigated by all-atom molecular dynamics simulations with three different initial atomic velocities. The per-residue free energy decomposition suggests that the key residues involved in inhibitor binding were residues 41-43, 57, 81, 136-139, 155-159 and 168 in the NS3 domain. Van der Waals interactions yielded the main driving force for inhibitor binding at the protease active site for the cleavage reaction. In addition, the highest number of hydrogen bonds was formed at the reactive P1 site of the four studied inhibitors. Although the hydrogen bond patterns of these inhibitors were different, their P3 site was most likely to be recognized by the A157 backbone. Molecular mechanics (MM)/Poisson-Boltzmann surface area and MM/generalized Born surface area approaches predicted the relative binding affinities of the four inhibitors in somewhat similar trend to their experimentally-derived biological activities.

2.2 INTRODUCTION

Over 170 million people worldwide are infected with hepatitis C virus (HCV) and this is increasing at about 3–4 million new people every year [6]. Importantly, HCV is one of the major causes of liver inflammation which can eventually lead to cirrhosis, and in some cases might develop to hepatocellular carcinoma or liver

cancer [5, 6]. Regrettably, the approved anti-HCV drugs (ribavirin, peg-interferon, boceprevir and telaprevir) require a long duration of treatment with a very high cost as well as inducing some side effects, such as flu-like symptoms, anemia and hemolysis in HCV patients [54, 55]. Treatment with ribavirin in combination with peg-interferon (PEG-IFN) shows only about a 40-50% success rate in HCV genotype 1 treatment [1, 4]. This combination is used for inhibiting the polymerase and/or inosine monophosphate dehydrogenase, whereas the α -ketoamide inhibitors, boceprevir and telaprevir, target the NS3/4A protease. Consequently, the new and potentially promising high potent and selective non-covalent inhibitors, danoprevir (ITMN-191) and BI201335, were designed against the HCV protease. These two inhibitors are currently in phase 2 and phase 3 clinical trials, respectively [26]. In preclinical profiles, danoprevir presented a very high inhibition of all six HCV genotypes [56], while BI201335 displayed a high level of efficacy in inhibiting HCV protease genotypes 1 and 4-6, but was dramatically less effective against the other genotypes [57]. The NS3/4A protease in complex with each of the four aligned inhibitors is shown in Fig. 2.1. Up to date, a comparative understanding of drug-target interactions of the α -ketoamide and non-covalent inhibitors binding to NS3/4A protease of HCV has not been provided yet. In this study conventional molecular dynamics (MD) simulations were performed to achieve this goal.

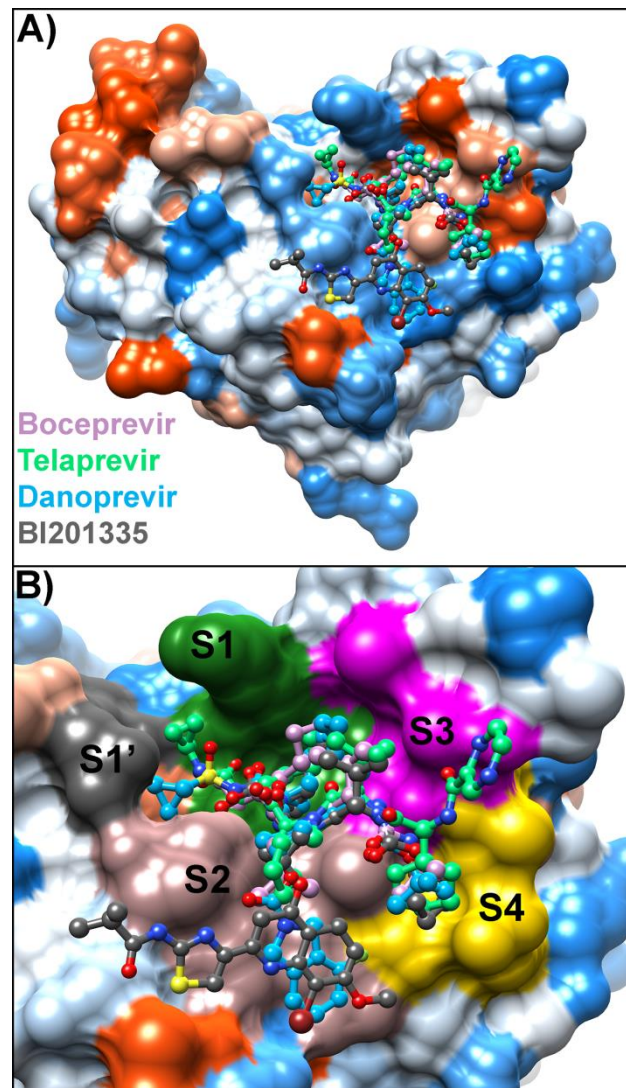


Figure 2.1 (A) The four current inhibitors (boceprevir, telaprevir, danoprevir and BI201335 shown by ball and stick model) binding to the active site of the HCV protease where the most hydrophilic and hydrophobic surface shaded by blue and orange red, respectively

HCV is a positive-sense single-stranded (ss)RNA virus in the *Hepacivirus* genus (*Flaviviridae* family) encoding for approximately 3000 amino acids. After ssRNA translation, the polyprotein encodes for four structural proteins (C, E1, E2 and p7) and six non-structural proteins (NS2, NS3, NS4A, NS4B, NS5A and NS5B) that are

subsequently produced by cleavage by protease enzymes of host cell and HCV origin. Among the non-structural proteins, the NS3 serine protease complexed with the NS4A cofactor and NS5B polymerase play an essential role in the viral replication process and so become one of the most attractive targets for anti-HCV drug design and development [58-61]. The NS3/4A cleaves the scissile peptide bond between the non-structural proteins, NS3/NS4A (self-cleavage), NS4A/NS4B, NS4B/NS5A and NS5A/NS5B, recognizing the D/EXXXC/T-S/A amino acid sequence [8, 62]. The 180 amino acids at the N-terminus of NS3 protein and 14 amino acids of NS4A cofactor have been shown to be essential for NS3/4A activity [6, 8, 63]. Without the NS4A cofactor, the HCV protease activity and cleavage rate acceleration are dramatically reduced due to the conformational change of the catalytic residues in the NS3 active site [8, 64].

Based on the reported crystal structures of HCV NS3/4A protease [65-68], the active site located on a solvent exposable surface has a rather shallow pocket (Fig. 2.1A) in comparison with the other chymotrypsin-like proteases [11, 69, 70]. This leads to a more challenging drug design and development. The designed protease inhibitors have generally been modified from the decapeptide (P6-P4') substrate and its cleaved products [13-15, 71]. For example, the scissile peptide bond has been substituted with α -ketoamide for boceprevir and telaprevir, sulfonate for danoprevir or carboxylate for BI201335 (Fig. 2.2).

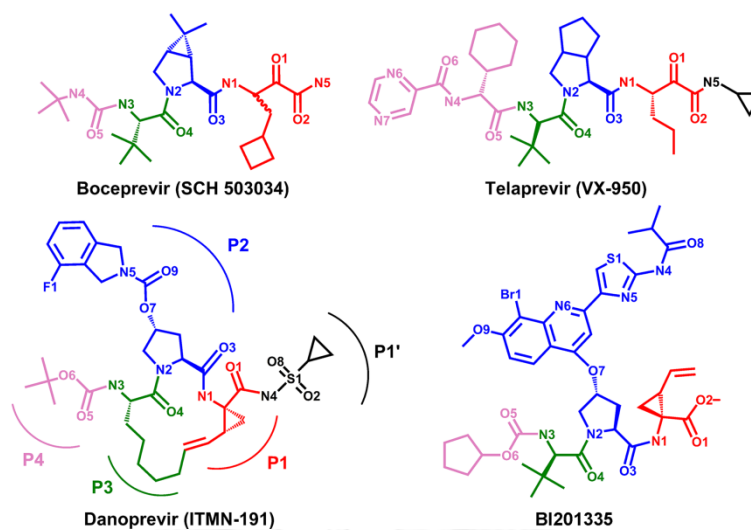


Figure 2.2 Chemical structures of the four NS3/4A protease inhibitors boceprevir (SCH 503034), telaprevir (VX-950), danoprevir (ITMN-191) and BI201335. The P1', P1, P2, P3 and P4 substituents are colored by black, red, blue, green and purple, respectively.

In this work, the all atomistic MD simulations in conjunction with binding free energy calculations were applied on the HCV NS3/4A protease in complex with its four inhibitors (boceprevir, telaprevir, danoprevir and BI201335) in order to investigate the key binding pattern, drug-target interactions and drug susceptibility. The theoretical information on drug specificity and targeted inhibition should be useful for HCV anti-viral drug design and development.

2.3 MATERIALS AND METHODS

2.3.1 Starting models and system preparation

The structure of the NS3/4A protease of HCV genotype 1a with boceprevir, tetra-peptide inhibitor (similar to telaprevir), danoprevir (ITMN-191), and BI201335 (the last one is found in genotype 1b) bound were obtained from the respective crystal

structures (Protein Data Bank (PDB) entry codes 2OC8 [67], 2P59 [66], 3M5L [68] and 3P8N [65]) and were then separately prepared as follows. To build the NS3/4A-telaprevir complex, the P4 moiety of the tetra-peptide inhibitor was only modified to the cyclohexyl-2-pyrazin-2-ylcarbonyl of telaprevir. From the crystallization process, the catalytic S139 residue in the danoprevir complex was mutated to alanine using the site-directed mutagenesis [68] and so in this study the A139 residue was changed back to S139. The co-crystal structure of BI201335 bound to NS3/4A is of the HCV genotype 1b, and so the relevant 20 different amino acid residues were modeled to be the same residues as found in HCV genotype 1a from H77 strain as well as amino acid sequence of PDB entry code 2OC8 [67] using the protein preparation tool implemented in Discovery Studio 2.5 Accelrys Inc.

All system preparations and MD simulation processes were performed on the AMBER10 package program [72]. The protonation states of the ionizable amino acids; lysine (K), arginine (R), histidine (H), aspartic acid (D) and glutamic acid (E), were characterized by PROPKA 3.1 [73]. Note that the two catalytic residues H57 and D81 were ionized as the neutral histidine with protonated δ -NH (HID type) and negatively charged aspartate in the boceprevir, telaprevir and danoprevir systems. For the BI201335 complex, the protonated ϵ -NH (HIE type) H57 and neutral aspartic acid D81 were used as derived from the $^1\text{H-NMR}$ data [65]. The missing hydrogen atoms were added using the LeaP module in AMBER10. The AMBER ff03 force field was applied for the protein [74]. To prepare the partial atomic charges and parameters of each inhibitor, the structure was fully optimized by means of the HF/6-31g(d) level of theory using Gaussian03 [75]. The electrostatic potential (ESP) charges were consequently computed with the same method and basis set. The antechamber

package was employed to convert ESP charges to restrained ESP (RESP) charges. The AMBER ff03 force field [74] and general AMBER force field (GAFF) [76] were adopted for ligand parameters by the parmchk program.

In order to find the optimum structures of NS3/4A complex, the hydrogen atoms were minimized with 1500 steps of steepest descents (SD) and followed by 1500 steps of conjugated gradient (CG) using the SANDER module implemented in AMBER10 to diminish the bad contacts and steric hindrances. Each system was subsequently solvated with the TIP3P water model [77] in a cubic box within 10 Å around the protein surface and chloride counterions were added to neutralize the total positive charge of the complex. Afterwards, the SD and CG minimizations with 1500 steps were respectively applied to optimize the counterions and water molecules, whereas the proteins and inhibitor were constrained with a force constant of 500 kcal/mol·Å². Finally, the whole complex was kept free of any constraint and eventually minimized with 1500 steps each for SD and CG.

2.2.3 Molecular Dynamics (MD) simulations

Each prepared NS3/4A-inhibitor complex was performed by three independent MD simulations with different initial atomic velocities (namely MD1-MD3) under periodic a boundary condition with the *NPT* ensemble. All covalent bonds involving hydrogen atoms in each system were constrained with the SHAKE algorithm [78]. The short-range cut-off of 10 Å for non-bonded interactions was applied, whilst the particle mesh Ewald (PME) summation method [79] was used for calculating the long-range electrostatic interactions. The simulation time step was of 0.2 ps. The system was initially heated up to 298 K for 200 ps and was then

simulated at this temperature at 1 atm till 40 ns. The trajectories were collected every 2 ps for analysis. The root-mean square displacement (RMSD) and hydrogen bond (H-bond) were explored using the ptraj module of AMBER, whilst the per-residue decomposition of MM/GBSA binding free energy ($\Delta G_{bind}^{residue}$) and the total binding free energy (ΔG_{bind}) were calculated by means of MM/PBSA and MM/GBSA approaches using the mm_pbsa module.

2.2.4 Binding free energy

The MM/PBSA and MM/GBSA approaches have been widely succeeded in predicting the binding free energies (ΔG_{bind}) of many biomolecular systems [80-85]. In this study, both methods were applied to estimate the ΔG_{bind} between the NS3/4A protease and each ligand by computing $\Delta\Delta G_{bind}$ as the free energy difference between the complex (ΔG_{com}), protein (ΔG_{prot}) and ligand (ΔG_{lig}) as shown in Eq. (2.1).

$$\Delta\Delta G_{bind} = \Delta G_{com} - (\Delta G_{prot} + \Delta G_{lig}) \quad (2.1)$$

Each term was achieved from the averaged free energy over 100 trajectories taken from the last 20-ns simulation. The free energy was calculated separately from the enthalpy in the gas phase (ΔH) and the entropy term ($-T\Delta S$), as shown in Eq. (2.2).

$$\Delta G = \Delta H - T\Delta S \approx \Delta E_{MM} + \Delta G_{solv} - T\Delta S \quad (2.2)$$

The ΔH of the system was predicted from the summation of the gas phase (ΔE_{MM}) and solvation free (ΔG_{solv}) energies. The ΔE_{MM} term includes the internal (ΔE_{int}), electrostatic (ΔE_{ele}) and van der Waals (ΔE_{vdW}) energies, as shown in Eq. (2.3),

whilst the ΔG_{solv} term is the sum of the electrostatic and nonpolar components as outlined by Eq. (2.4).

$$\Delta E_{MM} = \Delta E_{int} + \Delta E_{ele} + \Delta E_{vdW} \quad (2.3)$$

$$\Delta G_{solv} = \Delta G_{ele,solv} + \Delta G_{nonpolar,solv} \quad (2.4)$$

The $\Delta G_{ele,solv}$ was investigated by means of either the Poisson-Boltzmann (PB) or the generalize Born (GB) models, while $\Delta G_{nonpolar,solv}$ is calculated using solvent accessible surface area (SASA) [86, 87] with a probe radius of 1.4 Å using Eq. (2.5).

$$\Delta G_{nonpolar,solv} = \gamma SASA \quad (2.5)$$

Note that the dielectric constants were set to 1 and 80 for the solute and surrounding solvent, respectively. The values for surface tension constant γ of 0.0072 kcal/mol·Å² was used.

2.2.5 Decomposition free energy

The contribution of each residue towards the ligand binding was estimated using the per-residue decomposition free energy ($\Delta G_{bind}^{residue}$), based on the MM/GBSA approach. One half of the electrostatic interaction (E_{ele}^i) between atoms i and j of the protein and ligand, respectively, was taken to calculate the electrostatic contribution as outlined in Eq. (2.6).

$$E_{ele}^i = \frac{1}{2} \sum_{i \neq j} \frac{q_i q_j}{r_{ij}}, \quad (2.6)$$

The q_i and q_j represent the atomic charges of atoms i and j , respectively, and r_{ij} is the distance between these two atoms. Alternatively, the per-residue

intermolecular vdW interaction (E_{vdW}^i) was similarly attributed but avoiding double counting. The internal energy (ΔE_{int}) was equal to zero because the internal energies of the complex, protein and ligand that were calculated separately from the same trajectory. Therefore, the electrostatic free energy component based on the GB method was calculated by Eq. (2.7).

$$\Delta G_{ele,solv} = -\frac{1}{2} \left(1 - \frac{e^{-\kappa f_{GB}}}{\epsilon_\omega} \right) \sum_{ij} \frac{q_i q_j}{f_{GB}} \quad (2.7)$$

The dielectric constant of solvent (ϵ_ω) and the Debye-Hückel screening parameter (κ) were identified as 80 and 0, respectively, and f_{GB} is a smooth function interpolating between atomic radii and the distance between atoms i and j , in which the double sum runs over all pairs of atoms. Note that the common expression of f_{GB} was given by Eq. (2.8).

$$f_{GB} = \left[r_{ij}^2 + \alpha_i \alpha_j \exp\left(\frac{-r_{ij}^2}{4\alpha_i \alpha_j}\right) \right]^{1/2} \quad (2.8)$$

The α_i and α_j are the effective Born radii of atoms i and j , respectively. According to the Eqs. (2.6) and (2.7), the contribution of atom i on the electrostatic free energy could be defined by Eq. (2.9).

$$\Delta G_{ele,solv}^i = -\frac{1}{2} \sum_{ij} \left(1 - \frac{e^{-\kappa f_{GB}}}{\epsilon_\omega} \right) \frac{q_i q_j}{f_{GB}(r_{ij})} + \frac{1}{2} \sum_{i \neq j} \frac{q_i q_j}{r_{ij}} \quad (2.9)$$

In addition, the *SASA* of atom i in the complex and the separated parts in the nonpolar component was given by Eq. (2.10).

$$\Delta G_{nonpolar,solv}^i = \gamma \times \left(SASA^{i,com} - (SASA^{i,prot} + SASA^{i,lig}) \right) \quad (2.10)$$

The $SASA^{i,prot}$ and $SASA^{i,lig}$ are equal to zero depending on which molecule the atom belonged to.

Taken altogether, the $\Delta G_{bind}^{residue}$ was the summation of E_{ele}^i , E_{vdW}^i , $\Delta G_{nonpolar,solv}^i$ and $\Delta G_{ele,solv}^i$. Similarly, the binding free energy contributions of the residue, backbone and side chain were calculated separately from the related atoms.

2.4 RESULTS AND DISCUSSION

2.4.1 Stability of global structures

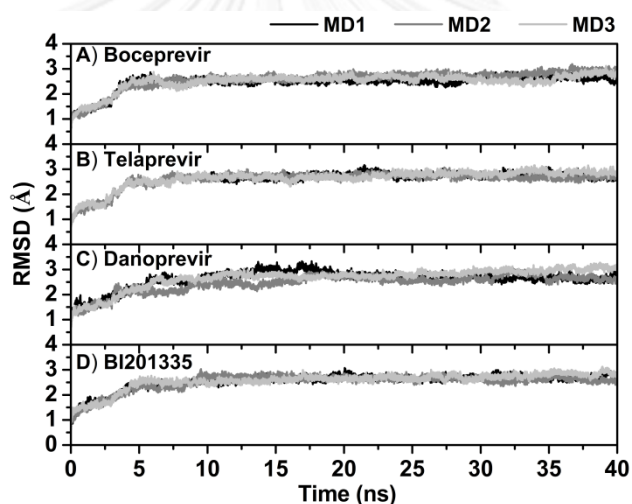


Figure 2.3 Root-mean square displacements (RMSDs) for all atoms of the four NS3/4A-inhibitor complexes compared to their initial structures from the three independent simulations (MD1-MD3)

To determine the stability of the four MD systems from three independent MD simulations, the RMSDs of all atoms relative to those of starting structure versus the simulation time was plotted (Fig. 2.3). The RMSD values rapidly increased in the first 5 ns and fluctuated at approximately 2.5 Å until 40 ns in all complexes. The NS3/4A-danoprevir complex showed a higher fluctuation level during 12-18 ns (about

2-3 Å) and subsequently reduced to 2.5 Å at 20 ns till end of simulation. This is therefore the MD trajectories from 20-40 ns of the four studied systems were extracted for further analysis.

2.4.2 Key residues for ligand binding

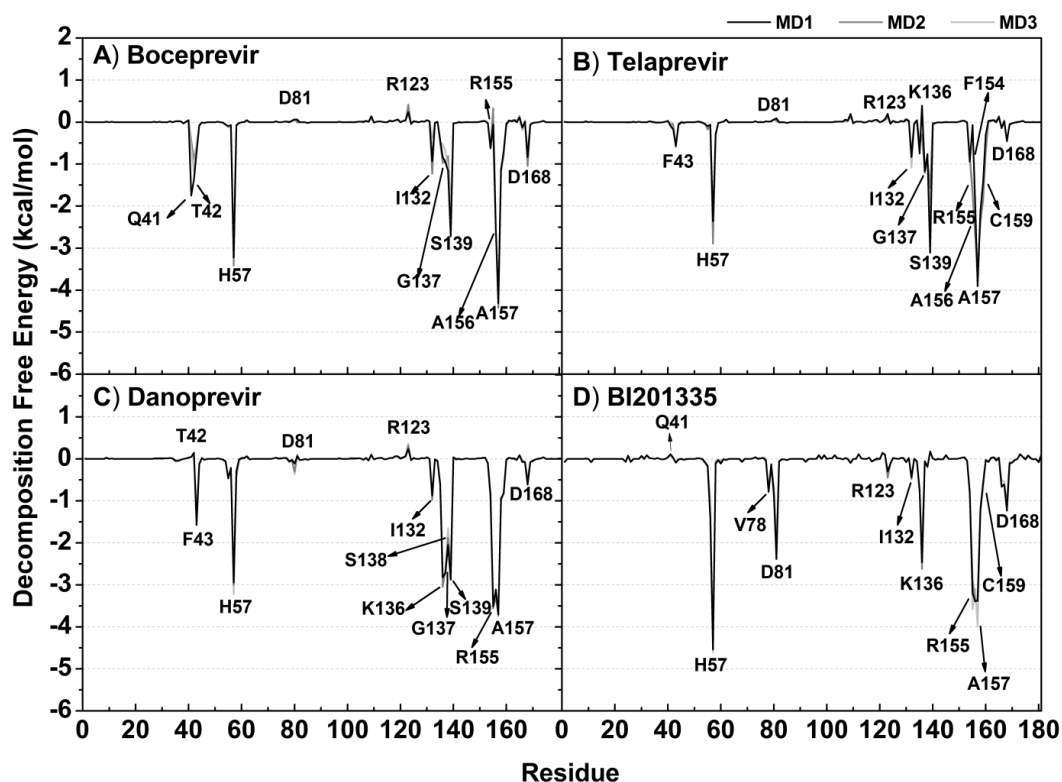


Figure 2.4 Per-residue decomposition free energy of NS3 protease for the four studied inhibitors from the three independent simulations

The per-residue decomposition of binding free energy ($\Delta G_{bind}^{residue}$) based MM-GBSA approach was used to scan the key residues important for ligand binding to the HCV NS3/4A protease, with the contribution of protease residues in the four complexes being shown in Fig. 2.4. Although the structures of the four inhibitors are significantly different (Fig. 2.2), they share similar orientations and binding interactions

at the protease active site (Fig. 2.1B). From the fingerprint in Fig. 2.4, NS3 residues 41-43, 57, 81, 132-139, 155-159 and 168 are likely to have provided an energy stabilization of < -1 kcal/mol towards ligand binding, whilst there is no contribution from the NS4A cofactor (data not shown). The stabilization from these residues including the other residues within 8 Å sphere around ligand was separately considered into the contribution from their backbone and side chain in Fig. 2.5 (left), as well as in terms of the electrostatic ($\Delta E_{\text{ele}} + \Delta G_{\text{polar}}$) and vdW ($\Delta E_{\text{vdW}} + \Delta G_{\text{nonpolar}}$) energies in Fig. 2.5 (right). Among the 24 residues plotted in Fig. 2.5 (left), most residues likely stabilized the ligand through the backbone, such as residues G137, S138, A157, V158 and D168. All the residues greatly contributed to ligand binding through the vdW energetic term (up to -4.5 kcal/mol) mainly at the residues H57, D81 (only for BI201335), R155, A156, A157, and V158 (only for telaprevir and BI201335) with interactions of < -2.0 kcal/mol (Fig. 2.5, right). Meanwhile, their electrostatic energies were detected in the range of 2.4 to -2.0 kcal/mol in which the positive and negative values indicated the ligand destabilization and stabilization, accordingly. The obtained data resulted from the hydrophobic S3 and S4 sub-sites, the partially hydrophobic/hydrophilic S1 and S1' sub-sites, and the extended hydrophilic S2 sub-site (Fig. 2.1) [88].

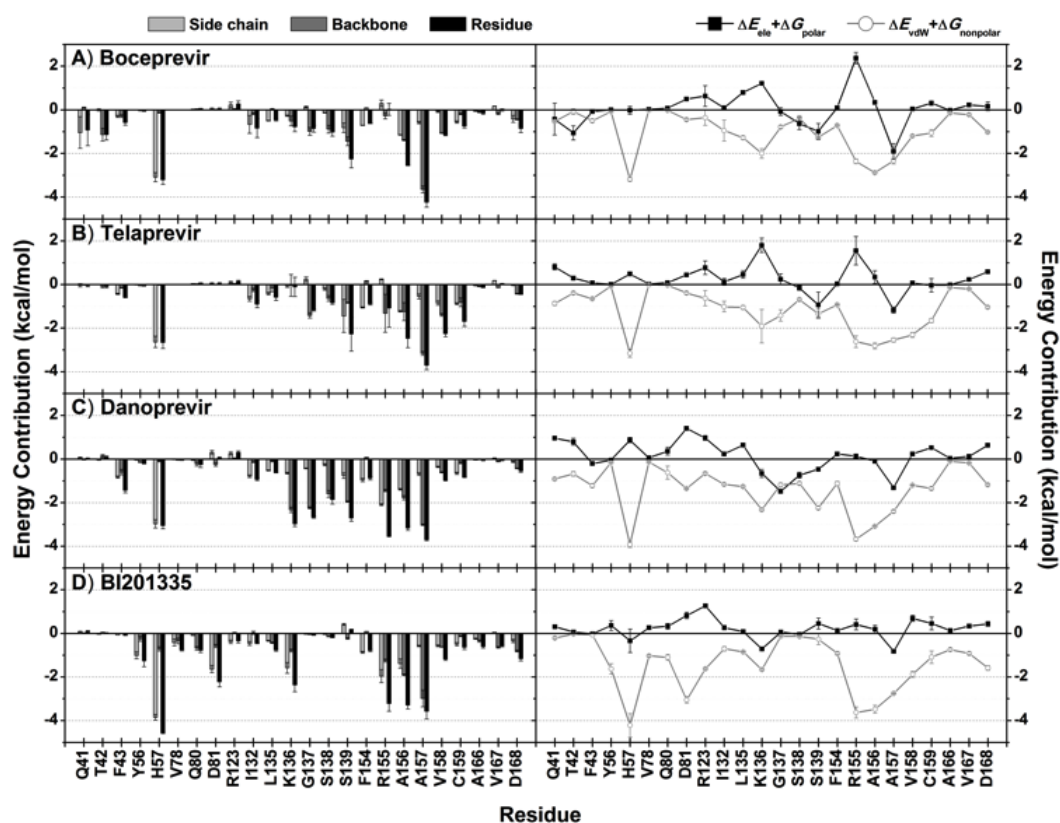


Figure 2.5 (Left) Averaged energy contributions over the three independent simulations from the residue backbone and side chain for the four studied complexes of the NS3/4A protease with (A) boceprevir, (B) telaprevir, (C) danoprevir and (D) BI201335. (Right) Averaged electrostatic and vdW energy contributions from each residue. Note the standard deviation among the three simulations is shown as error bar.

As mentioned above that the binding pattern of the four inhibitors were typically comparable, however, the interactions at the two side chains of covalent and non-covalent inhibitors were different (Fig. 2.5 (left)). For non-covalent inhibitors, the fluoro-isindoline and bromo-quinoline rings at the extended P2 site of danoprevir and BI201335 (Fig. 2.2) were highly stabilized by the R155 residue

especially by its aliphatic side chain through the vdW interaction. This strong hydrophobic contribution has been mostly found for protease inhibitors containing the aromatic ring at the extended P2 site [61, 69, 70, 89, 90] associated with the highly resistance to several anti-HCV drugs [68, 91-93]. Meanwhile, the K136 residue strongly interacted with their P1'-sulfonyl and P1-carboxylate groups, respectively. More different interactions were observed as follows. The strongest stabilization from the NS3/4A protease was found for danoprevir binding (Fig. 2.5, left), where the ten residues (F43, H57, K136, G137, S138, S139, R155, A156, A157 and V158) each provided an energetic contribution of < -1 kcal/mol. Of the three catalytic residues in the BI201335 complex, H57 provided the highest stabilization to the ligand (-4.6 kcal/mol in Fig. 2.5, left) while the attractive contribution from the neutral D81 residue was only found in this system. In contrast, there was rather low stabilization from S139 which is the residue center for the cleavage reaction in accordance with the predicted weak H-bonds at 11% and 47% occupancy (Fig. 2.6). Higher stabilization by residue D168 was found for BI201335 binding (-1.2 kcal/mol) and in addition the Y56, V78 and Q80 residues (-1.3 , -0.8 and -0.8 kcal/mol, respectively) likely supported its extended P2 site. In addition, the salt bridge formation between R155 and D168 was only detected in danoprevir and BI201335 complexes (Fig.2.7), therefore the R155 conformation can be eventually affected by D168 mutation possibly related to the macrocyclic drug resistances [26]. This was formerly seen in the NS3/4A-TMC435 complex in which the energy change profile of TMC435 suggested the interrupted interaction at the extended P2 site [90]. Alternatively, the Q41 and T42 residues at the N-terminus attractively interacted with the α -ketoamide at P1 site of boceprevir via electrostatic interactions of -0.5 and -1.1 kcal/mol,

respectively (Fig. 2.5, right) with a formation of three strong H-bonds (> 70% occupation in Fig. 2.6). Lastly, although the lowest energetic contribution was presented in the telaprevir complex, the C159 residue conferred a higher stabilization in this system than the other three inhibitors by ~1 kcal/mol (Fig. 2.5, left) mainly through vdW interaction (right).

2.4.3 Hydrogen bond (H-bond) interactions

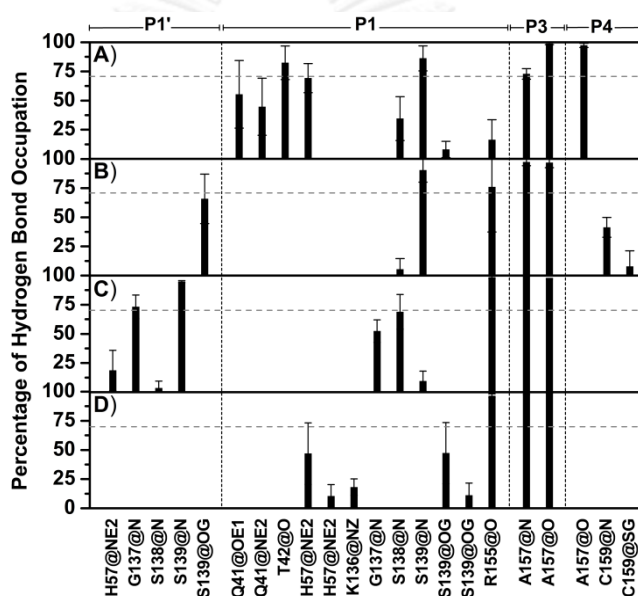


Figure 2.6 The averaged percentage of H-bond occupation of the NS3/4A residues contributed to (A) boceprevir, (B) telaprevir, (C) danoprevir and (D) BI201335 over the three MD simulations where the standard deviation is given as error bar.

Even though ligand binding was predominantly contributed by the vdW interactions as mentioned above, H-bond formation between the ligand and the surrounding residues of NS3/4A could be an important factor in the specific inhibition towards this targeted enzyme. Therefore, H-bond interactions were evaluated in

terms of the percentage of H-bond occupation using the criteria of (i) a distance between the proton donor and acceptor atoms $\leq 3.5 \text{ \AA}$ and (ii) the angle of the H-bond ≥ 120 degree. Boceprevir and BI201335 were comprised of P1-P4 sites, whereas the P1' site is additionally connected to the P1 site in the cases of telaprevir and danoprevir (see Fig. 2.2). In order to reveal the specific binding at each sub-site of NS3/4A, the H-bond interactions were separately considered for the individual P site of inhibitor as shown in Fig. 2.6 and the 3D structure taken from the last MD snapshot from the MD1 simulation was chosen to display the inhibitor binding and interaction at the protease active site in Fig. 2.7.

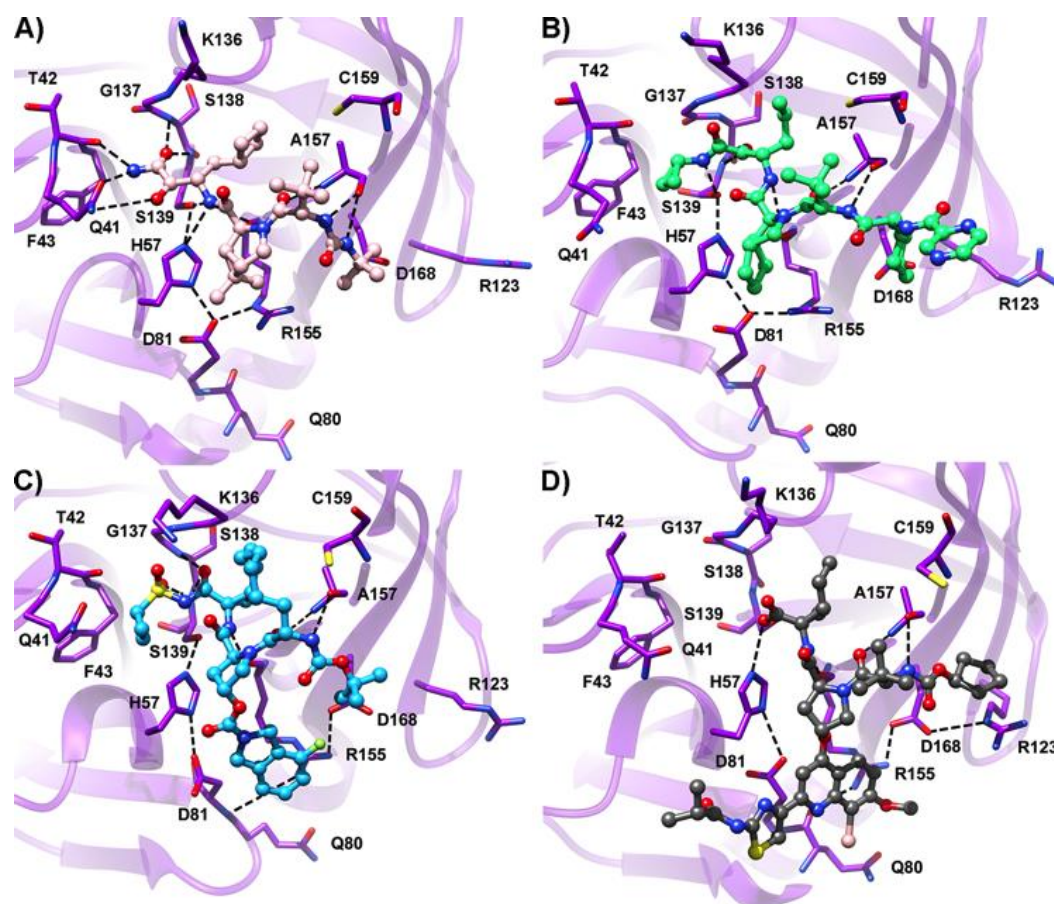


Figure 2.7 The binding pattern of (A) boceprevir, (B) telaprevir, (C) danoprevir and (D) BI201335 in the NS3/4A active site demonstrated from the last snapshot from MD1 simulation. Note that residue H57 is in the HIE type and D81 is in neutral form for the NS3/4A–BI201335 complex, whilst in the other complexes they are the HID type and negatively charged form, respectively.

By considering the number of strong H-bonds (> 70% occupancy) with NS3 residue (Fig. 2.6), the order of H-bond strength was of boceprevir (6) > danoprevir (5) > telaprevir (4) > BI201335 (3). All four inhibitors had no H-bond formation at the S2 sub-site, although the two non-covalent inhibitors, danoprevir and BI201335, consisted of the fluoro-isindoline and bromo-quinoline rings (Fig. 2.2). Only two

strong H-bonds with the backbone of A157 toward the P3 site at the carbamate nitrogen of danoprevir and BI201335 as well as the amide group of boceprevir and telaprevir were maintained as in their initial co-crystal structures [66, 88]. This might imply that the A157 backbone of the NS3 protease is a recognized site for ligand binding. They also shared the same interaction with R155 at the amide nitrogen of the P1 cleavage site but with different binding strengths. Note that these results were in accordance with the previous theoretical and experimental studies [61, 89]. Therefore the H-bond with R155 could be a common interaction between NS3/4A and inhibitors. In comparison with a potent macrocyclic inhibitor TMC435 [90], the H-bond formed between the backbone of A157 and the P3 nitrogen of TMC435 was absent because this nitrogen atom was capped by the methyl group. More than 75% H-bond occupation with R155 was detected for danoprevir, BI201335 and telaprevir, whereas the interaction was rather weak for boceprevir (< 17%) with increased H-bond distance by ~ 0.8 Å at the end of the MD simulations (Fig. 2.7A). Moreover, the P1-ketoamide of boceprevir in planar orientation (Fig. 2.7A) was well formed the five hydrogen bonds with Q41, T42, H57 and S139, while the interaction with S139 was only maintained in telaprevir due to the cyclopropyl termination at P1' site (Figs. 2.6 and 2.7). The latter one is somewhat similar to that found for danoprevir, which contains a cyclopropylsulfonyl group but the amide oxygen at the P1 site was stabilized by S138 instead. Differentially, the carboxylate group at the P1 site of BI201335 formed five weak H-bonds with H57, K136 and S139 (Fig. 2.6D). At the P4 site (Figs. 2.2 and 2.6), the peptide nitrogen of boceprevir strongly interacted with the A157 backbone oxygen, whilst this interaction could not be formed with danoprevir and BI201335 because of the change of this nitrogen to the carbamate oxygen.

Instead, a 41% and 8% H-bond occupation were detected between C159 and the P4-amino oxygen of telaprevir. The P1' site of telaprevir and danoprevir made a strong H-bond with the side chain and backbone of S139, respectively. Additionally, that of danoprevir also formed a strong H-bond with side chain of G137.

2.4.4 Binding affinity predictions

Both MM/PBSA and MM/GBSA methods were employed in this study to estimate and compare the inhibitory efficiency of the four studied inhibitors against the HCV NS3/4A protease in terms of the binding free energy (ΔG_{bind}) and its energetic components (gas phase energy (ΔE_{MM}), which is comprised of ΔE_{vdW} and ΔE_{ele} energies, solvation free energy (ΔG_{sol}) and entropic term ($-T\Delta S$)), as summarized in Table 2.1. It seems that the total negative charge (-1e) of BI201335 favorably enhanced electrostatic energy interaction towards the NS3/4A protease (ΔE_{ele} of -194.9 kcal/mol) by ~three- to five-folds relative to the other three inhibitors (-69.2, -44.3 and -39.8 kcal/mol for danoprevir, telaprevir and boceprevir, respectively). The ΔE_{vdW} and ΔE_{ele} almost equal contributed for the danoprevir binding, whilst the higher stabilization by ΔE_{vdW} of 6 and 12 kcal/mol was found for boceprevir and telaprevir. Although the ΔE_{ele} contribution was relatively high in BI201335 complex, the ΔE_{vdW} contribution in this complex (-67.3 kcal/mol) was in the same range to that of danaprevir complex (-66.8 kcal/mol). By including the solvation free energy, the vdW term ($\Delta G_{nonpolar,sol} + \Delta E_{vdW}$) is a favorable contribution to the total binding free energies of all four NS3/4A inhibitor complexes, which were opposed by the unfavorable electrostatic term ($\Delta G_{ele,sol} + \Delta E_{ele}$). This is due to relatively high positive values of polar solvation resulted from either PB or GB

models. So, the vdW interaction played an important role in the HCV NS3/4A protease with inhibitors in a good agreement with our previous study [94]. With a summation of the entropic term, both MM/PBSA and MM/GBSA methods agreed each other in binding free energy prediction of danoprevir (-27.5 and -36.4 kcal/mol) > BI201335 (-23.7 and -23.4 kcal/mol) > boceprevir (-16.3 and -19.4 kcal/mol) > telaprevir (-13.5 and -16.7 kcal/mol). The obtained results were relatively consistent with the experimental IC_{50} value⁸ rather than K_i value [56, 57].

Table 2.1 Comparison of the averaged binding free energy and energetic components (kcal/mol) calculated using 100x3 MD trajectories from the three independent simulations and experimental IC_{50} and K_i (nM) values of the four inhibitors binding to NS3/4A protease of HCV

	Boceprevir		Telaprevir		Danoprevir		BI201335	
	MM/PBSA	MM/GBSA	MM/PBSA	MM/GBSA	MM/PBSA	MM/GBSA	MM/PBSA	MM/GBSA
ΔE_{ele}	-39.8 ± 7.5		-44.3 ± 7.9		-69.2 ± 6.9		-194.9 ± 22.4	
ΔE_{vdW}	-46.3 ± 3.2		-56.0 ± 3.6		-66.8 ± 2.9		-67.3 ± 4.0	
ΔE_{MM}	-86.1 ± 7.9		-100.3 ± 8.8		-136.1 ± 7.2		-262.2 ± 21.8	
$\Delta G_{nonpolar,sol}$	-6.1 ± 0.3		-7.2 ± 0.4		-7.9 ± 0.3		-8.7 ± 0.3	
$\Delta G_{ele,sol}$	48.7 ± 3.8	45.7 ± 4.1	60.9 ± 6.8	57.7 ± 6.8	86.9 ± 6.0	78.1 ± 5.2	213.3 ± 20.3	213.7 ± 20.5
ΔG_{sol}	42.6 ± 3.8	39.6 ± 4.0	53.7 ± 6.7	50.5 ± 6.7	79.1 ± 6.0	70.2 ± 5.1	204.7 ± 20.2	205.1 ± 20.4
$\Delta G_{ele,sol} + \Delta E_{ele}$	8.9 ± 5.8	5.9 ± 5.8	16.6 ± 3.7	13.4 ± 3.2	17.7 ± 3.4	8.8 ± 3.3	18.4 ± 5.8	18.8 ± 3.8
$\Delta G_{nonpolar,sol} + \Delta E_{vdW}$	-52.4 ± 1.8		-63.2 ± 1.9		-74.7 ± 1.6		-75.9 ± 2.2	
ΔG_{total}	-43.5 ± 6.1	-46.5 ± 5.5	-46.6 ± 4.4	-49.8 ± 4.0	-56.9 ± 3.9	-65.8 ± 4.0	-57.5 ± 5.1	-57.2 ± 3.8
$-T\Delta S$	27.2 ± 16.6		33.1 ± 17.1		29.4 ± 16.1		33.8 ± 16.6	
ΔG_{bind}	-16.3 ± 11.4	-19.4 ± 11.1	-13.5 ± 10.8	-16.7 ± 10.6	-27.5 ± 10.0	-36.4 ± 10.0	-23.7 ± 10.9	-23.4 ± 10.2
IC_{50} (nM)	80 ± 15		87 ± 5		0.20 ± 0.01		-	
K_i (nM)	1.1 ± 0.3		3.2 ± 1.1		-		1.2 ± 0.2	

2.5 CONCLUSION

In this work, the multiple 40-ns classical MD simulations were applied to the HCV NS3/4A protease in complex with the two existing anti-HCV drugs, boceprevir and telaprevir, and the two highly potent inhibitors, danoprevir and BI201335,

currently in the clinical trial phase 2 and phase 3, respectively. Scanning of the per-residue decomposition free energy from the NS3 and NS4A domains revealed that the ligand binding was favorably stabilized by the NS3 residues 41-43, 57, 81, 132-139, 155-159 and 168 without any contribution from the NS4A domain. In addition to the free energy contributed from the individual residues, the total MM/PBSA and MM/GBSA binding free energies also likely suggested that the vdW energetic term is the key ligand-target interaction for NS3/4A protease of HCV. This is possibly because the binding site contains the hydrophobic residues at the extended S2, S3 and S4 sub-sites as well as partly at the S1' and S1 sub-sites. Besides the importance of vdW interaction, the intermolecular H-bonds were highly formed at the reactive P1 site of all inhibitors (the cleavage reaction center), whilst their P3 site sustainably interacted with the A157 backbone. Taken altogether, the ligand-target interactions and total binding free energies revealed that the order of the studied inhibitor susceptibilities was of danoprevir > BI201335 > boceprevir > telaprevir, which was in somewhat similar trend to the experimentally derived data.

CHAPTER 3
SEARCHING FOR POTENT NS3/4A PROTEASE INHIBITORS

In silico screening for potent inhibitors against the NS3/4A Protease of Hepatitis C Virus

Arthitaya Meeprasert¹, Thanyada Rungrotmongkol², Mai Suan Li³ and
Supot Hannongbua¹

¹*Department of Chemistry, Faculty of Science, Chulalongkorn University, 254 Phayathai Road, Patumwan, Bangkok 10330, Thailand*

²*Department of Biochemistry, Faculty of Science, Chulalongkorn University, 254 Phayathai Road, Bangkok 10330, Thailand*

³*Institute of Physics, Polish Academy of Sciences, Al. Lotnikow 32/46, 02-668 Warsaw, Poland*

This article has been accepted in Journal: Current Pharmaceutical Design Year:
2013

3.1 ABSTRACT

Hepatitis C virus (HCV) infections are a serious viral health problem globally, causing liver cirrhosis and inflammation that can develop to hepatocellular carcinoma and death. Since the HCV NS3/4A protease complex cleaves the scissile peptide bond in the viral encoded polypeptide to release the non-structural proteins during the viral replication process, this protease is then an important target for drug design. The computer-aided drug design and screening targeted at NS3/4A protease of HCV were reviewed. In addition, using steered molecular dynamics simulations, potent inhibitors of the NS3/4A complex were searched for by screening the ZINC database based upon the hypothesis that a high rupture force indicates a high binding efficiency. Nine top-hit compounds (**59500093**, **59784724**, **13527817**, **26660256**, **29482733**, **25977181**, **28005928**, **13527826** and **13527826**) were found that had the same or a greater maximum rupture force (and so assumed binding strength and inhibitory potency) than the four current drugs and so are potential candidates as anti-HCV chemotherapeutic agents. In addition, van der Waals interactions were found to be the main contribution in stabilizing the ligand-NS3/4A complex.

3.2 INTRODUCTION

Hepatitis C viruses (HCV) are enveloped positive single stranded RNA viruses in the *Flaviviridae* family, and are comprised of some eleven main genotypes (30-35% sequence difference between genotypes), multiple subtypes and some 100 strains that show different global distribution/infection patterns. Genotypes 1-3 tend to have a worldwide distribution with genotype 1a accounting for ~60% of the global infections, whilst genotypes 2 and 3 account for around 35% of global infections [23,

95-97]. Genotypes 4-11 are distributed more locally and typically account for a much lower proportion of infections, but local HCV populations and infection patterns can vary considerably from the above global average pattern. This is relevant since the virulence and optimal treatment can vary with each HCV genotype.

Infection with HCV causes liver inflammation that can develop into cirrhosis, hepatocellular carcinoma and death, making hepatitis C one of the public health problems [5, 6]. Moreover, the global number of people infected with HCV is continuously increasing by about 3-4 million each year. The current drug applications used for the treatment of infections are principally the long term (24-48 weeks) administration of (i) peg-interferon (PEG-IFN), (ii) PEG-IFN in combination with ribavirin, and (iii) PEG-IFN/ribavirin with either boceprevir (Victrelis®) or telaprevir (Incivek®), but these exhibit increasing sustained undesirable side effects, such as flu-like symptom, anemia and hemolysis [54, 55]. Moreover, for the common and virulent HCV genotype 1, PEG-IFN combined with ribavirin has an approximate success rate of only 40-50% of treated patients [1, 4, 98], compared to almost complete success in the treatment of infection with HCV genotypes 2 and 3. Therefore, HCV inhibitors with an increased efficiency and decreased side effects are urgently needed.

The HCV genome (~ 9,600 nucleotides) is initially translated as a precursor polyprotein (Fig. 3.1A) and then subsequently processed by host peptidases and viral proteases on the endoplasmic reticulum (ER) membrane into the four structural proteins (C, E1, E2 and p7) and six non-structural proteins (NS2, NS3, NS4A, NS4B, NS5A and NS5B), which is essential for viral replication cycle.

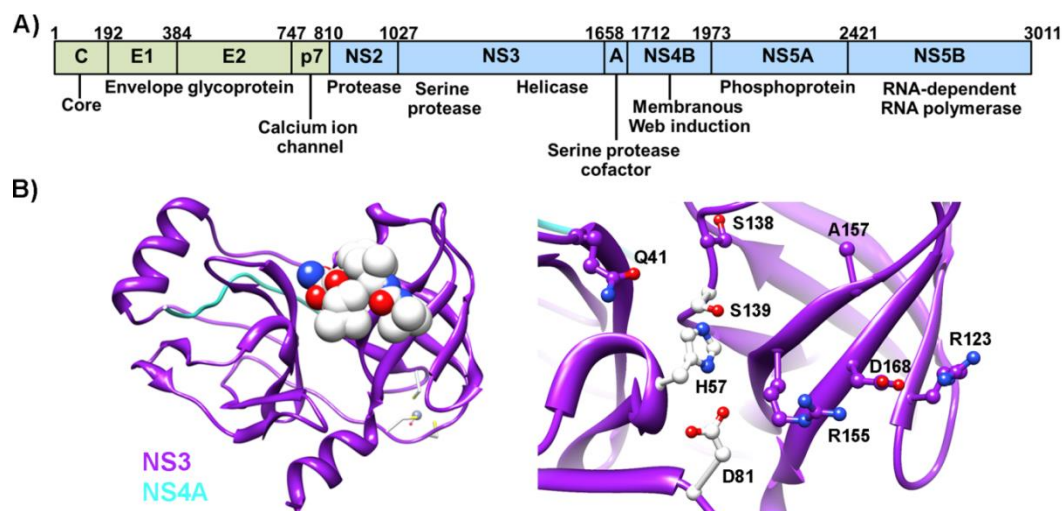


Figure 3.1 (A) Polyprotein of hepatitis C virus (HCV), where the green and blue present structural and non-structural proteins, respectively. (B) (Left) Structure of the NS3/NS4A cofactor complex with the inhibitor bound (vdW sphere), and (right) the catalytic triad residues (H57, D81 and S139 in white ball and sticks) and the other residues (violet ball and sticks) at the binding site.

HCV generally has two principal drug-targets; its RNA polymerase and the protease enzymes. The RNA-dependent RNA-polymerase (RdRp) of HCV, catalyzing the RNA replication, lacks a proofreading activity which results-in a high mutation rate and a large number of mutations [18]. The NS3/4A protease plays a critical role in producing the important components for viral RNA replication by cleaving the scissile peptide bond between the junctions of NS3/NS4A, NS4A/NS4B, NS4B/NS5A and NS5A/NS5B. NS3/4A is a serine protease belonging to trypsin/chymotrypsin superfamily, where the H57, D81 and S139 residues form an essential catalytic triad involved in the recognition of the D/EXXXC/T-S/A sequence of substrates [8, 62]. Based on the available structure of HCV protease [65, 99, 100], there are three possible sites used for drug design: (i) substrate binding pocket, (ii) NS4A binding

groove and (iii) zinc binding site. At the last site, zinc ion is linked to three cysteine residues and a histidine via a water molecule which forms the tetrahedral coordination geometry resulting to non-dominantly specific pocket to any compounds. Since NS4A cofactor binds tightly to NS3 protease, it is rather difficult to develop the suitable inhibitors at the protein-protein binding site [101]. This is thus the substrate binding site only has potential to serve as target for anti-HCV drug design. Since the binding pocket of HCV NS3/4A is likely solvent exposable, shallow and hydrophobic than that of the other proteases such as thrombin and elastase [11], the design and development of drugs that can act as inhibitors of this protease is more challenging. The design of most of the existing protease inhibitors have been designed based on the decapeptide (P6-P4') substrate of NS3/4A by subsequent modification of the functional group to prevent its cleavage by the catalytic residues (reversible competitive inhibitors). Since in other serine proteases the N-terminal products appear to be inhibitors of the enzyme itself including HCV protease (Table 1), then these cleaved products of NS3/4A have also been used to optimize peptidomimetic inhibitors using aldehyde, boronate and α -ketoamide groups [12, 102-105]. For example, the two current drugs, boceprevir and telaprevir (Fig. 3.2), that contain an α -ketoamide instead of a scissile peptide bond, have been used to inhibit the NS3/4A protease by forming a covalent bond to the hydroxyl group of the S139 residue in a reversible manner [104].

Table 3.1 The biological activities of NS3/4A substrates and their cleaved products

Substrate/Cleaved product	K_m (μM) ^a	K_i (μM) ^a
NS3-NS4A DLEVVT-STWV DLEVVT-OH	nd*	> 500.0
NS4A-NS4B DEMEEC-ASHLPYK-NH ₂ DEMEEC-OH DEMEEC-NH ₂ ASHLPYIEQG-NH ₂	10.0	0.6 80.0 > 500.0
NS4B-NS5A DCSTPC-SGSW-NH ₂ DCSTPC-OH SGSWLRDVWDKK-NH ₂	> 1000.0	180.0 > 300.0
NS5A-NS5B EDWVAbuC-SMSY-NH ₂ EDWVAbuC-OH SMSYWTGALKK-NH ₂	3.8	1.4 > 300.0

* nd, not determined

^a K_m and K_i are taken from the reference [12]

The NS3 protein is composed of a serine protease domain at the N-terminal and a helicase/NTPase domain at the C-terminal and forms a non-covalent complex with the NS4A cofactor (Fig. 3.1B). Among 631 residues of NS3 protein, the minimum residues required for the protease activity is 180 amino acids counting from the N-terminus and 14 amino acids of NS4A protein which is embedded in NS3 protease domain for activating the protease enzyme function. NS3 protease has two sub-domains, N-terminus (residues 1-93) and C-terminus (residues 94-180), where each sub-domain contains the conventional six-stranded β barrel [6, 8, 63]. Even though the reported full-length NS3/4A crystal structure [106] and molecular dynamics study [61] showed that the NS3/4A active site is located near helicase-protease interface resulting to the formation of ligand-helicase interactions, the kinetic properties of

truncated protease is likely similar to those of the full-length NS3/4A. Thereby, several previous studies on the HCV NS3/4A protease were focused on the truncated protease [59, 107-109]. In the crystal structure of NS3 protease without NS4A cofactor binding [110, 111], the imidazole ring of H57 catalytic residue is moved out from the S139 reaction center residue and thus it is unable to abstract the proton from the hydroxyl group of S139 while the carboxylic group of D81 turns away into the direction that cannot stabilize H57. Therefore, the presence of NS4A cofactor is needed to adjust the three catalytic residues of NS3 protease into the active conformation suitable for deprotonation of S139 and Michaelis addition.

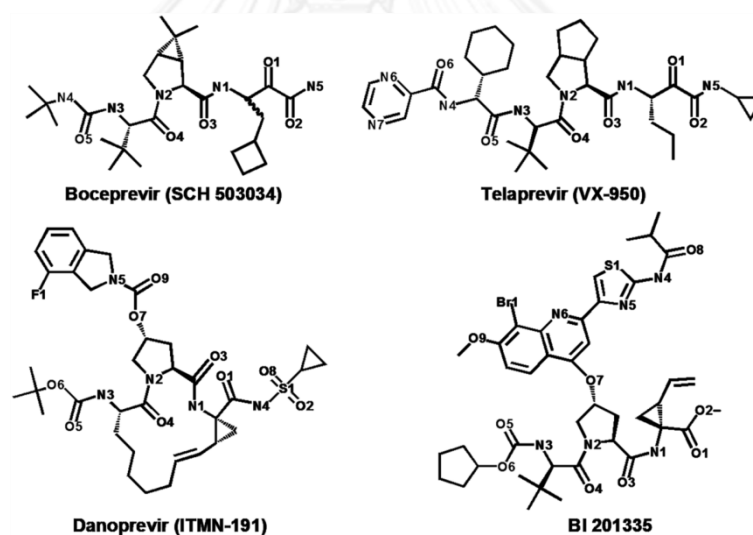


Figure 3.2 Chemical structures of the four NS3/4A protease inhibitors: boceprevir, telaprevir, danoprevir (ITMN-191) and BI201335

In addition, two non-covalent inhibitors with strong electrostatic interactions with the NS3/4A catalytic pocket have also been developed (BI201335 and danoprevir (ITMN-191); Fig. 3.2) and are currently in phase 3 and phase 2 clinical trials, respectively [112]. Danoprevir (0.2 nM) showed an approximately 400-fold

higher efficiency compared to boceprevir (80 nM) and telaprevir (87 nM) in the treatment of HCV genotype 1 infections in preclinical trials [56]. BI201335 (1.2 nM) inhibited the NS3/4A protease with a similar potency to boceprevir (1.1 nM), but was about three-fold more effective than telaprevir (3.2 nM). Moreover, whilst BI201335 showed a high capability to inhibit the NS3/4A activity of HCV genotypes 1, 4, 5 and 6, it was less potent against genotypes 2 and 3 being about 50-fold and 190-fold lower than against genotype 1 [57]. A subnanomolar inhibition activity of danoprevir was similarly found against these four genotypes, however its potency was decreased about 10-fold for inhibiting genotypes 2 and 3 [56]. Additionally, the side effects are commonly detected after treatment with boceprevir or PEG-IFN plus ribavirin [113]. The combination of these three drugs affect more serious anemia. Moreover, drug resistance has already been reported for the currently available commercial anti-HCV drugs, as summarized in Table 3.2, and is increasing in frequency.

Table 3.2 Drug resistance profile of the four currently available NS3 protease HCV inhibitors

Residue	Mutation	Inhibitors
V36 [19, 20, 23-25]	A, M, G	Boceprevir, Telaprevir
Q41 [24]	R	Boceprevir, Danoprevir
F43 [24]	S, C	Boceprevir, Telaprevir, Danoprevir
T54 [19, 20, 23-26]	A, S	Boceprevir, Telaprevir, BI201335
R155 [19, 20, 23, 24, 26]	K, T, Q	Boceprevir, Telaprevir, BI201335, Danoprevir
A156 [19, 20, 23, 24, 26]	S, T, V	Boceprevir, Telaprevir, BI201335, Danoprevir
D168 [23, 26]	A, V, G	BI201335, Danoprevir
V170 [23, 24]	A	Boceprevir, Telaprevir

Recently, various computational techniques are available and potentially useful for designing, developing and exploring the novel inhibitors with higher efficiency and specificity than the existing drugs as well as understanding the key

drug-target interactions in a variety of diseases such as influenza [114-116], human immunodeficiency virus (HIV) infection [117], tuberculosis [118], chikungunya [85] and cancer [82]. The current available tools are for example molecular docking, quantitative structure-activity relationship (QSAR), comparative molecular field analysis (CoMFA), comparative molecular indices analysis (CoMSIA), molecular dynamics (MD) simulation and etc.

da Cunha and co-workers [58] employed CoMFA approach to determine the best 3D-QSAR model on BILN 2061 derivatives. They predicted that substitution of the carbamate group of BILN 2061 with bulky group led to an increase in the inhibition efficiency, whereas the bulky group at the thiazole ring provided the unfavorable interaction. The potency of inhibitor can also be enhanced by replacing the thiazole ring with the low electron density functional group. It is well-known that the functional side chain of P2 and P3 residues of peptide inhibitors favors to be hydrophobic and hydrophilic groups, respectively. The 3D-QSAR contour maps of tetrapeptide analogue inhibitors [60] presented that the large favored negative charge contour of P3 residue apparently oriented toward the positively charged side chain of K136 while the favored hydrophobic contour allowed the P3 side chain to preferentially occupy in the hydrophobic pocket formed by V132, V158 and C159. In addition, the pharmacophore results suggested that the modification on P3 residue by extending its side-chain length could expand the binding interaction with the S3 subsite. From the observed success of these ketoamide substituted compounds in inhibiting the HCV NS3/4A, derivatives have been continuously developed so as to try to obtain a higher inhibition efficacy [119-122]. For example, nardaprevir, a second generation NS3/4A inhibitor, was designed based on the boceprevir structure and

gave about a 10-fold improved inhibition [119]. The CoMFA, CoMSIA and HQSAR techniques were applied to build a QSAR model to investigate the relationship between the structure of the inhibitor and its biological activity, an advantage if not prerequisite for the design and development of higher efficiency inhibitors, using the 190 derivatives of naltrexone as the initial source for screening [109, 123-129]. The CoMFA contour map (Fig. 3.3) suggested that the R1 and R2 groups of naltrexone should be modified with a larger chain, such as cyclic rings. A negatively charged R1 group (sulfonamide group for example) and positively charged R4 group were predicted to increase the inhibition efficiency. Notice that the activity becomes worse if the R4 group is a large side chain and so this side chain should be small. Among the 16 best designed compounds, the 4 compounds had the highest predicted binding affinities that might be the anti-HCV drug candidates.

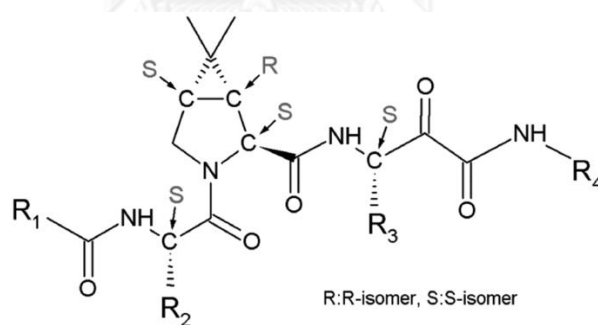


Figure 3.3 The structure of the naltrexone derivative scaffold [109]

The molecular docking approach is generally employed for virtual screening and predicting the binding pattern in an active site of bimolecular systems, since it computationally uses up less CPU time. However, if the movement of the receptor is regulated as a rigid molecule, the prediction ability of molecular docking is rather

limited and sometimes inaccurate [130, 131]. For example, a range of indole derivatives were designed as NS3/4A inhibitors and docked into the NS3/4A binding site using molecular docking but subsequently some of the docking results were found to be in contrast to the observed experimental inhibition activity [132]. Besides the standard molecular docking (flexible ligand docking) method, the flexible receptor docking or induced-fit docking (GENIUS) approach allows the conformational change of both the ligand and receptor [133]. This method was used on the NS3/4A protease of HCV to screen for novel inhibitors. Initially 97 compounds were screened out of 166,206 compounds using the ranked GENIUS scores, but only 27 of these 97 compounds were experimentally found to show more than 50% inhibition at 100 μM . The two common scaffolds from these 27 compounds were then used for a 2D-similarity search. Among the 140 matching compounds found the five compounds that was a new class of anti-NS3/4A candidate scaffold with IC_{50} values of $< 10 \mu\text{M}$. This finding may be useful for the further drug design and development. The higher accuracy approaches, such as molecular mechanics Poisson-Boltzmann surface area (MM-PBSA), molecular mechanics generalized Born surface area (MM-GBSA), linear interaction energy (LIE), thermodynamic integration, potential mean force (PMF) and so on, are widely used and provide more reliable results, but they require a significantly higher computational time that restricts their application to screening larger datasets. As in previous work [83], molecular docking, MD simulation and MM-PBSA methods were used in order to investigate the binding interaction between NS3/4A and polyphenol derivatives. Since the crystal structures of these complexes were not available, molecular docking was subsequently used to dock each compound into the substrate binding site (H57, D81, G137, S139, A156 and A157).

The MM-PBSA result gave the correlation coefficient between predicted and experimental binding free energies of 0.96. Ideally, a trustworthy method that demands a relatively low CPU time is optimal for high throughput screenings that are otherwise logistically impractical with the CPU intensive methods. The steered molecular dynamics (SMD) approach has been proposed as one such potential good choice as it can be rapidly used to investigate the unbinding process of ligands from the receptor, the unfolding mechanism of biomolecular systems, transportation of small molecules through channels and for screening hit-lead compounds [134-137]. In the last case, it is based on the hypothesis that the larger rupture force is required to pull a higher susceptible ligand out from its receptor. Recently, the SMD approach was successfully applied to evaluate the binding affinity of the neuraminidase inhibitors of influenza A pH1N1 virus as well as other designed compounds obtained from NCIDS library [136].

This work then focuses on screening for potential inhibitors of the HCV NS3/4A protease complex. To this end the search for ligands that are potential new potent anti-HCV drug candidates was performed by screening the ZINC database [37] using SMD simulations to remove each docked ligand from the NS3/4A (HCV genotype 1a) binding pocket with a constant velocity. Afterwards, the binding efficiency of each ligand was predicted from the maximum pulling force (F_{max}). Note that the four known HCV NS3/4A protease inhibitors (boceprevir, telaprevir, BI201335 and danoprevir) were also included in this SMD screen for validation by comparison of the obtained theoretical data to their known experimental inhibition activities [56, 57].

3.3 MATERIALS AND METHODS

3.3.2 NS3/4A protease and inhibitor complexes preparation

The three-dimensional structures for the complexes of NS3/4A protease of HCV genotype 1a bound with boceprevir, telaprevir and danoprevir were obtained from the Protein Data Bank (PDB) with PDB entry codes 2OC8 [88], 2P59 [66] and 3M5L [100], respectively. In contrast, the BI201335 complex was modeled from the X-ray structure of this compound bound to the HCV genotype-1b protease (3P8N [65]) by employing the macromolecules tool in the Discovery Studio 2.5^{Accerys Inc}. The protonation state of all ionizable amino acids (R, K, D, E and H) were considered at pH = 7.0. Additionally, the H protonation state was determined by considering the possibility of hydrogen bond formation with the surrounding residues. The development of atomic charges and empirical force field parameters for the inhibitor were developed according to the standard procedure [82, 84, 138, 139]. The atomic charges of each drug were calculated using the HF/6-31g(d) method with the Gaussian03 software [75], which were then fitted into RESP charges using the ANTECHAMBER module implemented in AMBER10 [72, 140]. The atom types and the other parameters of each ligand were assigned by AMBER force fields [74] and GAFF [76]. Afterwards, the ACPYPE [141] was used to convert the AMBER file format to GROMACS format.

3.3.2 Set of ligands and molecular docking

To search for potent inhibitors of the NS3/4A protease of HCV genotype 1a, the ZINC database [142] (over 21 million compounds in ready-to-dock 3D formats) was first selected to collect 40 compounds using the criteria that the ligand-target is

a serine protease enzyme and the net charge of the ligand is less than or equal to 1. Atomic charges, atom types and other parameters of all ligands were prepared as described above. Subsequently, each ligand was then flexibly docked into the rigid NS3/4A binding pocket using the GOLD (Genetic Optimization for Ligand Docking) suite version 5.1 from the Cambridge Crystallographic Data Center (CCDC). The Genetic Algorithm (GA) was applied to explore the possible conformations and orientations of all compounds in the drug binding site where CHEMPLP was used as the fitness function [143]. For each docking simulation, 30 GA runs were performed with 100,000 genetic operations and a population size of 100 chromosomes. Note that the docked results with 30 GA runs are relatively similar to the higher GA runs up to 50 and 100. The crossover, mutation and migration frequencies were set at 95, 95 and 10, respectively, while the selection pressure was fixed at 1.1. However, the GA will be terminated early if the top three dockings are within 0.15 nm of the RMSD of all atoms. With respect to the flexibility of the ligand, the protonated carboxylic acids and all planar moieties containing R-NR₁R₂ were allowed to flip. The 1.2 nm sphere radius around the catalytic residue S139 was defined as a binding site. The conformer with the highest CHEMPLP docking score and intensively interacting with the NS3/4A binding residues was considered as the best binding mode and adopted as the starting structure for SMD simulations in the next step. Again, the partial charges and parameters for each compound from the ZINC database were prepared in the same way as the known inhibitor (described above).

3.3.3 Steered Molecular Dynamics (SMD) simulations

The NS3/4A protease-ligand complexes were embedded in a rectangular box of dimensions of 7.0 × 7.5 × 10.0 nm that contained ~16,000 molecules of TIP3P

water [77]. Chloride ions were added to neutralize the whole system. The center of mass of the NS3/4A protease was placed at 3.50, 3.75 and 3.50 nm. The unbinding tunnel's vector starting from the protein active site to the calculated end point of tunnel was relocated and re-rotated to Z-direction using editconf module implemented in GROMACS. Note that the vector direction was checked by adding dummy atoms to identify its direction prior to SMD performed. All molecular dynamics (MD) and SMD simulations were performed using the GROMACS 4.5.5 package [144, 145] with the AMBER ff03 force field [74]. Firstly, the added solvent and ions were energetically minimized using steepest descent (SD) while the other molecules were constrained. The receptor was then minimized by SD method with a constrained solvent. Finally, the entire system was minimized by SD and conjugated gradient (CG), respectively. Each minimization converged when the maximum force was ≤ 100 kJ/mol·nm. MD simulations were initially heated from 0 to 298 K for 100 ps with the *NVT* ensemble using the Berendsen procedure. Afterwards, the simulations with *NPT* ensemble were performed at 298 K and a pressure of 1 atm (~ 101.33 kPa) for 200 ps using the Parrinello-Rahman pressure coupling approach to maintain a constant pressure, whilst the solute was restrained with 200 kJ/mol·nm². Thereafter, the restrained force was decreased to 100 kJ/mol·nm², and the simulation was continuously equilibrated for 200 ps. To ensure that the complex structure was stable prior to SMD calculation, the system was then fully equilibrated for 1000 ps. The LINC algorithm was applied to constrain all bonds [146]. A time step of 2 fs with a van der Waals interaction cut off of 1.4 nm was used. Meanwhile, the long-range electrostatic interactions were evaluated by means of the particle mesh

Ewald (PME) summation method [147, 148]. The non-bonded interaction pair-list was truncated at 1.0 nm and updated every 10 fs.

After equilibration, the bound ligand was pulled out from the binding pocket of the NS3/4A protease with a constant velocity (v) of 0.005 nm/ps along the z-direction using harmonic potential on the ligand, whereas the C-alpha atoms of all amino acids were restrained. The force was applied on an atom close to the center of mass of the ligand with a spring constant (k) of 600 kJ/mol·nm² (~996 pN/nm). While a pulled ligand was moving, the hydrogen bonds with NS3/4A were gradually ruptured. The total force can be measured via $F = k(vt-x)$, where x is the displacement of pulled atom from the starting position. Four and three independent simulations were performed for each known inhibitor and ZINC compound, respectively, using the different seed numbers in order to confirm the consistency of results.

3.4 RESULTS AND DISCUSSION

3.4.1 Choice of pulling path

Caver 2.1 [149, 150], implemented in Pymol, was employed to generate the possible pathways of pulling a ligand out from the drug binding site of the NS3/4A protease. As well-known that the rupture force is sensitive to the pulling direction [151, 152], therefore it is needed to verify which pathway is most suitable for ligand unbinding. The three possible pathways for unbinding ligands from the NS3/4A active site together with their average radius and depth are shown in Fig. 3.4A. Since the easiest or main unbinding pathway could confer the lowest rupture force, it is hypothesized that the shallowest and/or widest tunnel could be the easiest

pathway. This is because the leaving ligand supposes to interact with minimal number of amino acids along the tunnel. According to this hypothesis, the pathway 1 with an average radius of 0.13 nm and depth of 1.40 nm was chosen. Additionally, the seven possible pathways of pulling were generated (pathways 4-10 in Fig. S1 the supporting information) in order to assure that the pathway 1 is the main tunnel. Even though the tunnels 4 (0.17 nm), 9 (0.14 nm) and 10 (0.17 nm) seem rather wider in comparison with that of the tunnel 1 (0.13 nm), their lengths are significantly longer by approximately 0.81, 0.01 and 2.64 nm, respectively. Whereas, the rest tunnels (pathways 5-8) are slightly either narrower or deeper than those of pathway 1.

To ensure that the first tunnel had the smallest rupture force for pulling the ligand, boceprevir was pulled out from the pathways 1-3. The derived force-time and force-displacement profiles are summarized in Fig. 3.4B and 3.4C where the displacement (extension) refers to the distance between the ligand positions at time $t = t_x$ and $t = t_0$. The rupture force (F_{max}) obtained from the third tunnel was much higher than that in the other two tunnels, since its cavity (Fig. 3.4A) is rather narrow at the active site as well as significantly longer (3.52 nm). Interestingly, among pathways 1-3, the direction of the third tunnel is only pointed to HCV helicase domain [61, 106] leading to deeper tunnel which could consequently result in a higher rupture force. Meanwhile the average radius in pathway 2 was the smallest in width (0.09 nm) but the F_{max} of the first pathway displayed a slightly lower F_{max} than the second tunnel in accordance with its 0.89 nm shorter length. In addition, the first two pathways reached the maximum point at almost the same time (~226 ps), while the third pathway took ~ 50 ps longer (Fig. 3.4B and 3.4C). After that the interaction

between NS3/4A and boceprevir suddenly decreased together in all three cases to an elongation of the extended distance (ligand displacement) of more than ~ 1.5 nm (Fig. 3.4C).

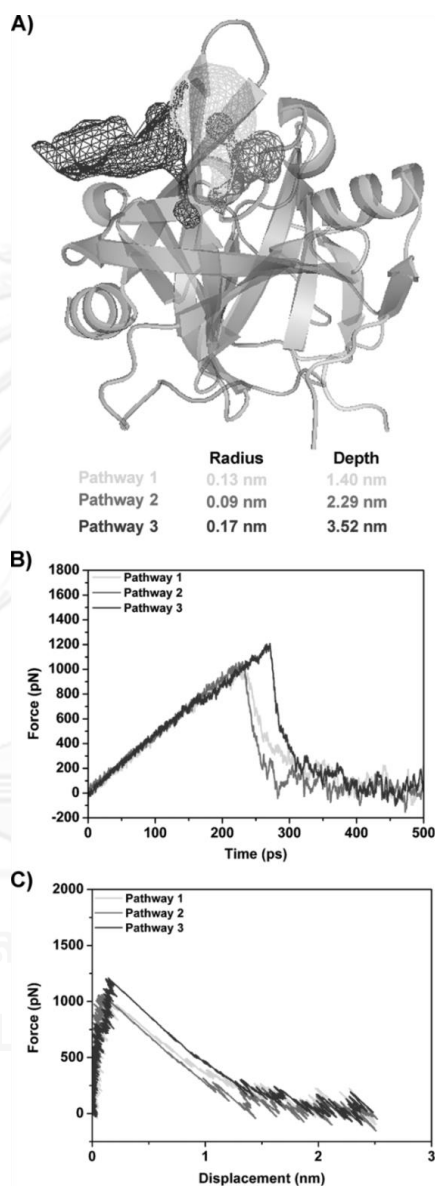


Figure 3.4 (A) Three possible pathways shown with their average radius and depth for ligand unbinding path constructed by pulling boceprevir from the NS3/4A binding site. (B) The force-time and (C) force-displacement profiles of boceprevir along the three pathways shown in (A).

Taken together, the first tunnel, which is surrounded by the V55, H57, S139, G140, F154, R155 and A156 residues of the NS3/4A complex, was the easiest way for the ligand to escape from the NS3/4A binding site to the bulk phase. Accordingly, this was used in further simulations for screening the compounds by SMD simulations.

3.4.2 Validity of the SMD approach

To test the potential reliability of the SMD simulations prior to using this approach to screen for hit-lead compounds for NS3/4A protease inhibition from the ZINC database, the four known NS3/4A protease inhibitors (boceprevir, telaprevir, BI201335 and danoprevir) were pulled out from the binding pocket along pathway 1 (Fig. 3.4). Their geometries at the equilibrium state were then superimposed, as shown in Fig. S3. The force-time and force-displacement profiles of each of the four inhibitors are plotted in Fig. 3.5, while the profiles obtained from the other three SMD simulations with different starting velocities are given in Fig. S2 (supporting information). With respect to the force-time profile (Fig. 3.5A), the force increased linearly over time to reach the maximum force, defined as the rupture force (F_{\max}), due to the gradual disruption of the hydrogen bonds, electrostatic and van der Waals interactions enforced by the increased distance between the ligand and binding site induced by the external applied force at a constant velocity of 0.005 nm/ps. After reaching F_{\max} the force immediately decreased, although a minor peak was possibly observed due to the newly formed interactions with the residues located along the pathway, as seen for BI201335 for example.

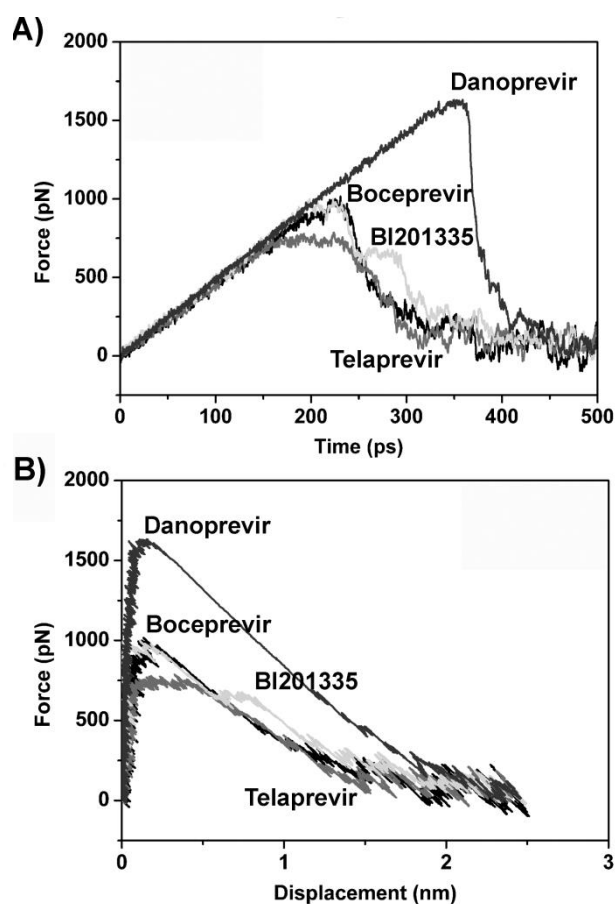


Figure 3.5 (A) The force-time and (B) the force-displacement profiles of the four inhibitors pulled from the NS3/4A protease binding site through the selected tunnel (pathway 1 in Fig. 3.4A), where in (A) the x-axis refers to the extended distance from the reference position of the ligand (at $t = 0$)

With respect to the force-displacement plot (Fig. 3.5B), the boceprevir, telaprevir and BI201335 ligands successfully escaped from the NS3/4A protease at nearly the same distance as each other at ~ 1.5 nm and after ~ 350 ps (Fig. 3.5A), whilst the danoprevir was freed later (~ 400 ps) at a distance of ~ 2.0 nm. That the NS3/4A-danoprevir complex takes the longest time and the highest force to remove it suggests that it is the most stable complex, whilst accordingly the NS3/4A-

telaprevir would be the worst due to the required lowest applied force to unbind it. The susceptibility of boceprevir towards the NS3/4A protease was predicted to be comparable to that of BI201335. For comparison with the experimentally derived data [22, 23], the theoretically (SMD) derived rupture force (F_{max} obtained from Fig. 3.5) was plotted with the experimental binding free energies, derived from their reported inhibition activities as IC_{50} [56] and K_i [57] values (Fig. 3.6). The F_{max} values obtained from the SMD simulations corresponded relatively well to the experimentally derived data, with the binding efficiency ranked (highest to lowest) as danoprevir > boceprevir ~ BI201335 > telaprevir. Therefore, the SMD approach was viewed as having the potential to obtain qualitatively reliable binding affinities and so could be used for screening the hit-lead compounds of the NS3/4A protease of HCV from the ZINC database.

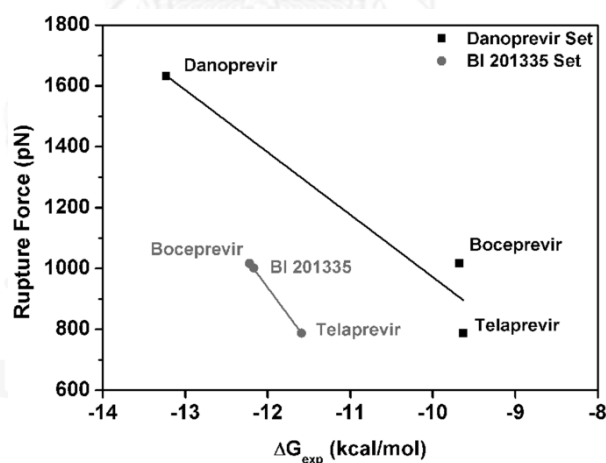


Figure 3.6 The correlation between the rupture force (F_{max}) and the calculated binding free energies obtained from the experimental values, based on where $R = 1.987 \times 10^{-3}$ kcal/mol, $T = 298$ K, K_i is inhibition constant and IC_{50} is the half maximal inhibitory concentration

3.4.3 Ranking of binding affinity of ligands

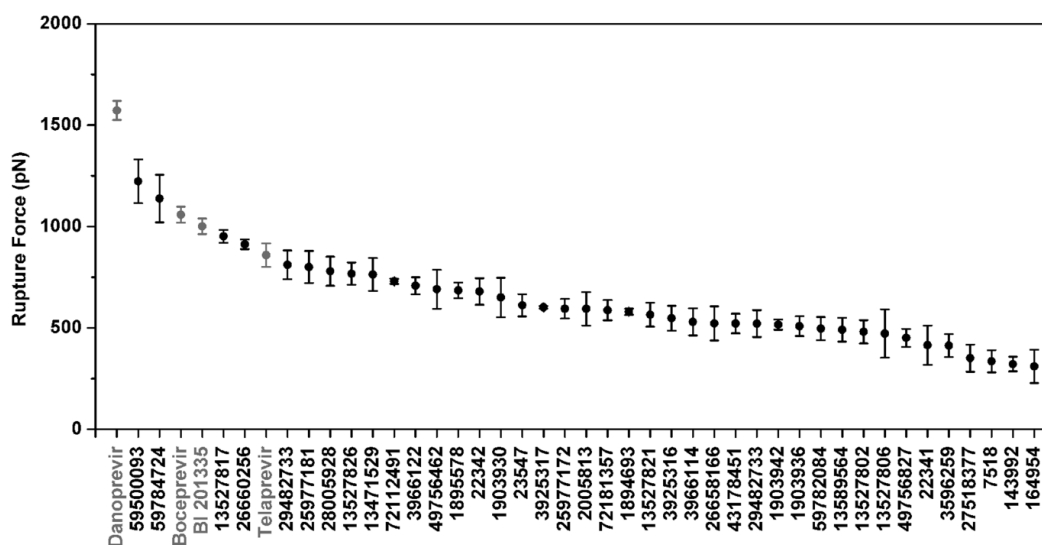


Figure 3.7 Ranking of the binding affinity to the NS3/4A protease of the top 40 ligands from the ZINC database and the four currently used HCV inhibitors (shown in grey) for comparison

After three independent MD simulations for each ligand-NS3/4A protease complex, each compound from the ZINC database was pulled out from the NS3/4A binding pocket using the same procedure applied for the known inhibitor-protease complex described above. The average F_{\max} values derived from the multi-simulations with their standard deviations for all 40 compounds were ranked with those of the four inhibitors in Table S1 (supporting information) and plotted in Fig. 3.7. The CHEMPLP scores derived from the docking analysis are also given in Table S1 for comparison.

In comparison between docking score and SMD rupture force for the 44 ligands (Table S1), although the best potent ligand predicted from both methods is danoprevir, the docking cannot well predict the binding affinity of the known

inhibitors (danoprevir > BI201335 >> telaprevir > boceprevir) unlike the SMD (danoprevir > boceprevir ~ BI201335 > telaprevir). This is because the docking method contains the uncontrollable factors such as neglecting the protein dynamics and limiting in the trial number of ligand position. Additionally, the CHEMPLP scoring function is a force field based scoring which ignores the internal protein energy [153]. Therefore, the top-hit ligands screened from the calculated rupture force are further discussed in details.



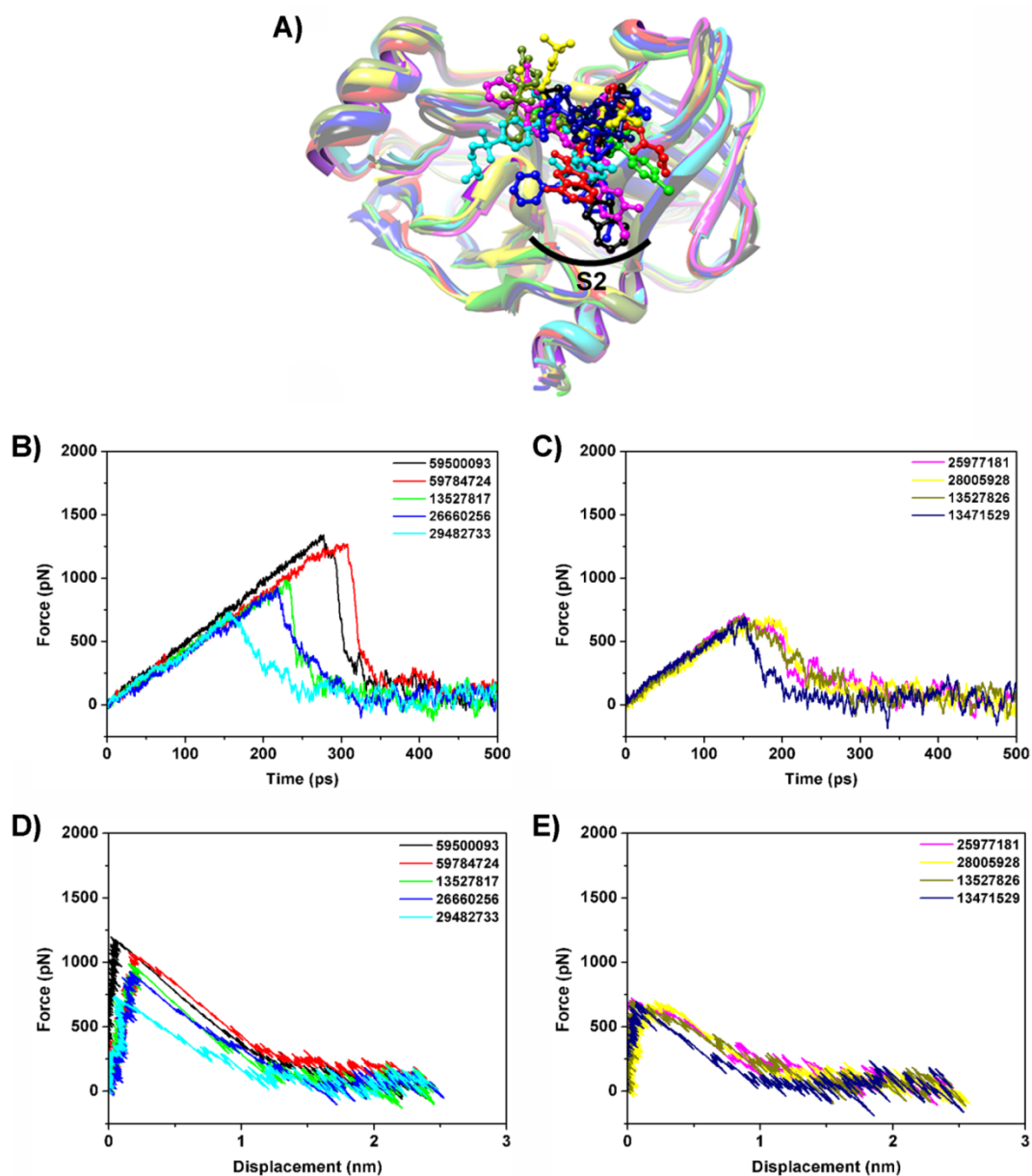


Figure 3.8 (A) Superimposition of the last snapshots for NS3/4A in complex with the best nine screened compounds from the ZINC database: 59500093 (black), 59784724 (red), 13527817 (green), 26660256 (blue), 29482733 (cyan), 25977181 (pink), 28005928 (yellow), 13527826 (olive green) and 13471529 (navy blue). The (B) and (C) force-time profiles, and (D) and (E) force-displacement profiles were obtained from the representative trajectories.

From the F_{\max} values, danoprevir, which is currently in phase 2 clinical trials, was predicted to have the highest efficiency of ligand binding against the NS3/4A protease of HCV (genotype 1a) with an F_{\max} value of approximately 1572 pN. The ZINC compounds **59500093** and **59784724** (F_{\max} values of 1222 and 1137 pN, respectively) were predicted to interact with the NS3/4A protease considerably better than the two approved drugs of boceprevir and telaprevir (F_{\max} values of 1058 and 859 pN, respectively) and better than BI201335 (1000 pN) that is currently in phase 3 clinical trials. In addition, compounds **13527817** (951 pN) and **26660256** (912 pN) are predicted to form a more stable complex with NS3/4A than telaprevir. However, there were an additional five ligands (**29482733**, **25977181**, **28005928**, **13527826** and **13471529**; at 811, 800, 780, 767 and 763 pN, respectively) that were capable of binding to the NS3/4A protease within the range of one standard deviation of that for telaprevir (859 ± 58 pN). Apart from these nine compounds, the remaining 31 ligands from the top 40 hits obtained from screening the ZINC database showed lower F_{\max} values (< 750 pN) that were less than the one standard deviation limit of telaprevir (800 pN) and so are likely to be inferior inhibitors. Accordingly, these nine best (highest F_{\max}) compounds from the ZINC database (**59500093**, **59784724**, **13527817**, **26660256**, **29482733**, **25977181**, **28005928**, **13527826** and **13527826**) were selected as potential candidates for NS3/4A inhibitors of HCV genotype 1. Their force-time and force-displacement profiles are summarized in Fig. 3.8. It can be seen that these compounds were placed in the similar orientation as the four known inhibitors (Fig. S3). Interestingly, the four screened compounds (**59500093**, **59784724**, **13527817** and **26660256**) with F_{\max} values that were greater

than that for telaprevir all contain an aromatic ring that occupied the S2 binding pocket.

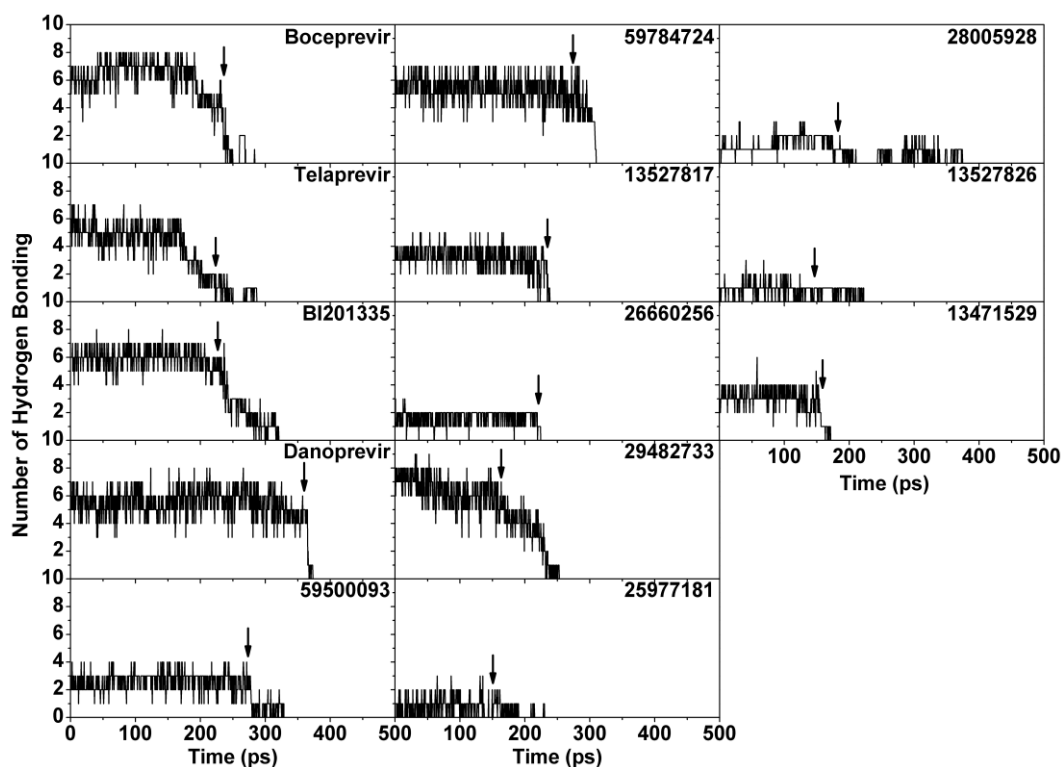
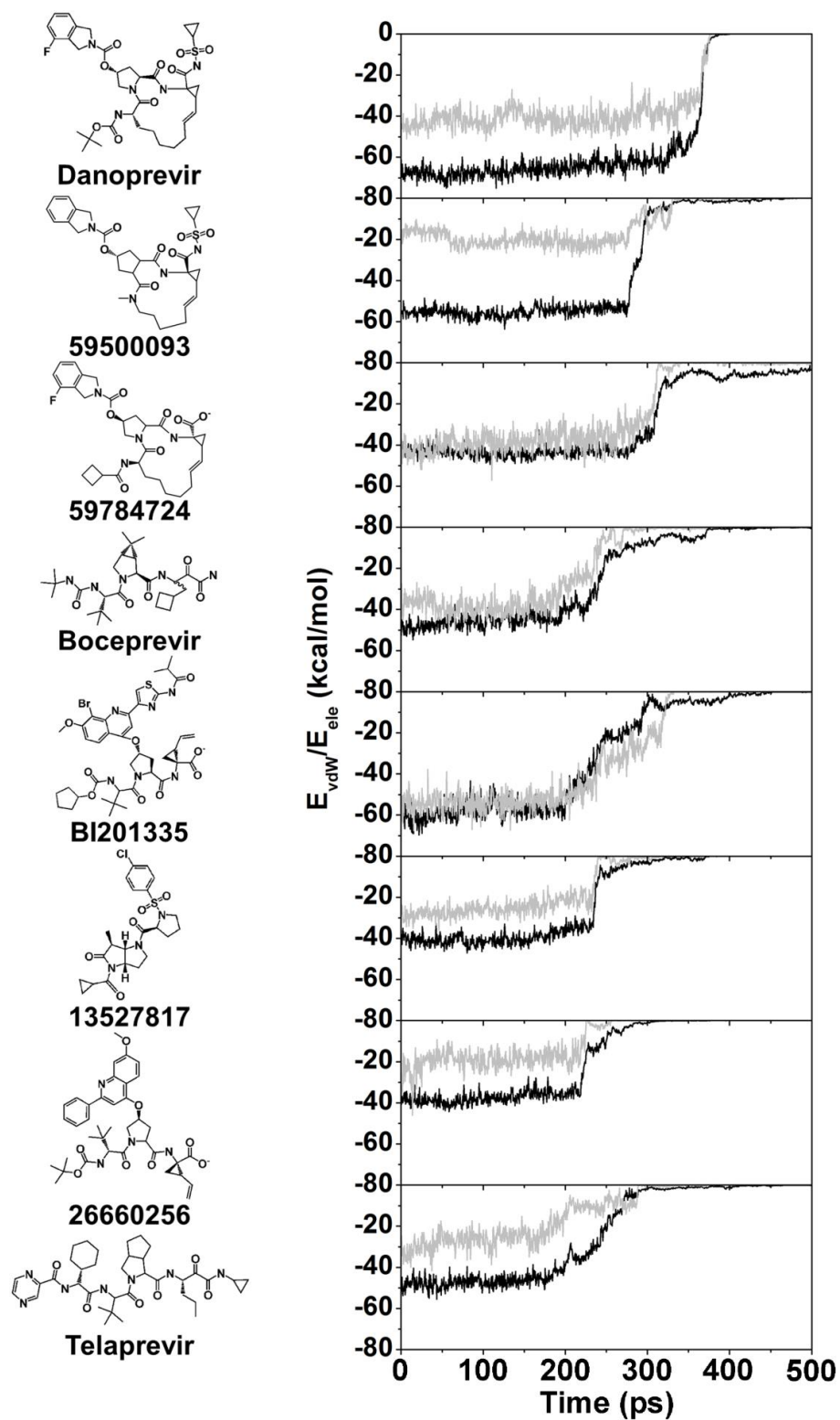


Figure 3.9 Time dependencies of the hydrogen bonding number of top 13 ligands, the arrow pointed at F_{max}

The time dependence of the van der Waals (E_{vdW}) and electrostatic (E_{ele}) interactions between the top ranked 13 ligands and the NS3/4A residues obtained from the first simulation are depicted in Fig. 3.10. The number of hydrogen bonds per unit time is plotted in Fig. 3.9. It is worth noting that in all the systems except for **59784724**, BI201335 and **29482733**, the vdW interaction is noticeably higher than electrostatic interaction along the pulling time. To understand the ligand-target interactions that potentially correspond to the binding efficiency, the summation of the vdW and electrostatic energies obtained at F_{max} were considered. Among the 13

ligands, danoprevir, formed six hydrogen bonds with active site residues, showed the lowest energy summation of -82 kcal/mol (E_{vdW} and E_{ele} of -49 and -33 kcal/mol) at $t \approx 375$ ps and afterwards all the interactions were suddenly lost. The screened **59500093** and **59784724** compounds, which contain macrocyclic and isoindole rings as per danoprevir, had a relatively high energy summation (-78 and -72 kcal/mol, at $t \approx 250$ ps). In the case of BI201335, the carboxylate group at the P1 moiety can interact with the G137 and S139 residues at the NS3/4A catalytic pocket leading to a higher net negative value than for the other compounds. At $t \approx 200$ ps, compounds **13527817** and **26660256** provided a kcal/mol higher E_{ele} contribution at F_{max} than telaprevir, whilst their vdW energies were almost equal. Although the energy summation of the other eight ligands was not significantly lower, they moved out of the NS3/4A binding pocket faster ($t < 200$ ps).



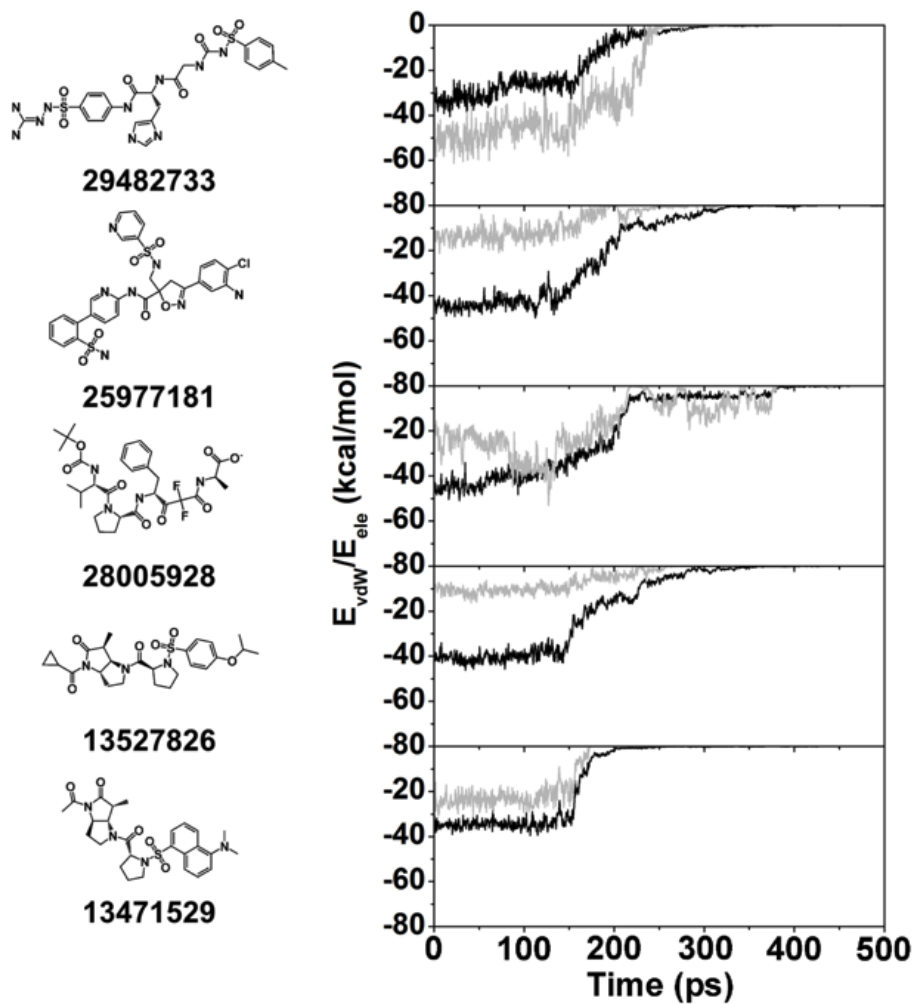


Figure 3.10 Electrostatic (E_{ele}) and van der Waals (E_{vdW}) energies (shown in grey and black line, respectively) as the ligand is withdrawn at a constant force per unit time for the top thirteen ligands

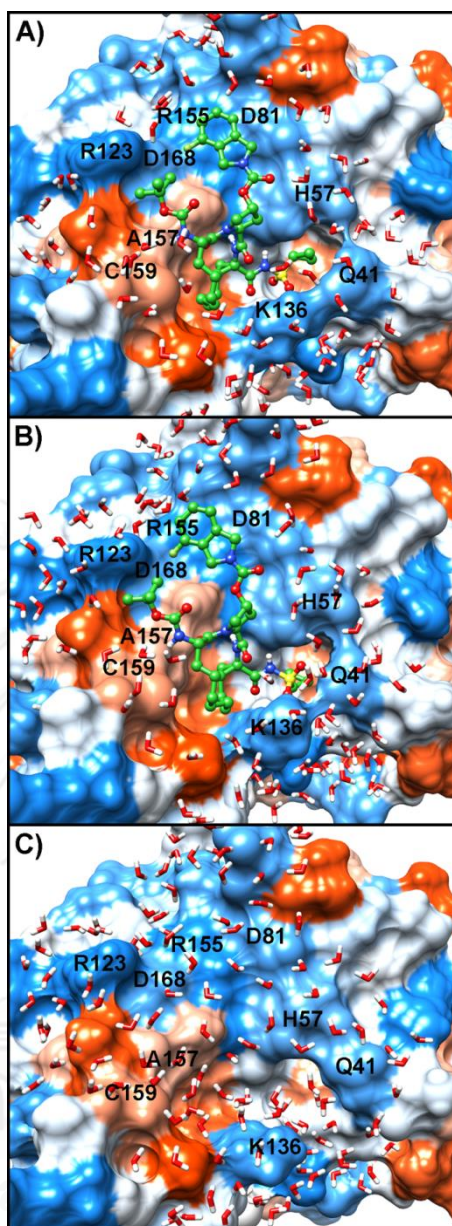


Figure 3.11 Close up of the NS3/4A protease in complex with danoprevir (green ball and stick model) at (A) the equilibrium state (before pulling), (B) the maximum point (Fmax at $t = 385$ ps in Fig. 3.4), and (C) the independent state (after passing the maximum point at $t = 450$ ps). The blue and orange colors represent hydrophilic and hydrophobic surfaces, respectively

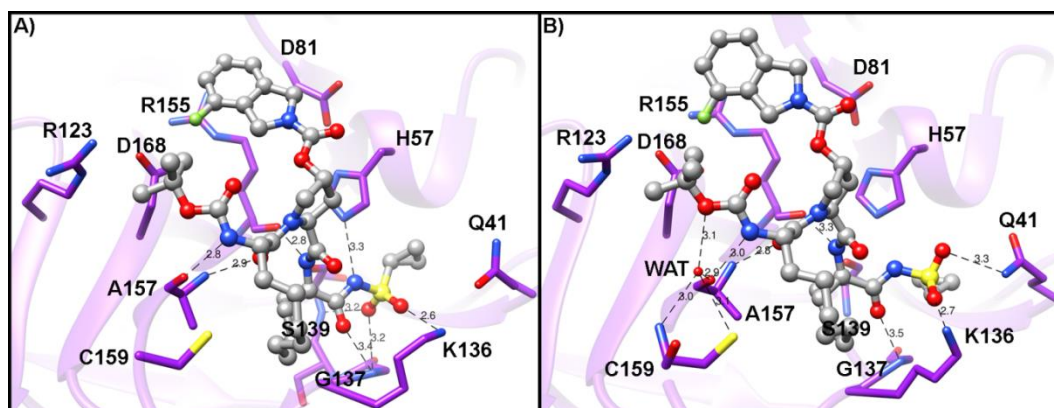


Figure 3.12 Hydrogen bond formation between danoprevir and its binding residues in HCV NS3/4A protease at (A) the equilibrium state, (B) the maximum pulling force in correspondence to Fig. 3.11

By following the SMD snapshot of NS3/4A-danoprevir complex at the equilibrium state (before pulling the ligand out of pocket), it was presented that the danoprevir was surrounded by Q41, T42, F43, V55, H57, Q80, D81, R123, I132, L135, K136, G137, S138, S139, F154, R155, A156, A157, C159 and D168 (Fig. 11A where the nine selected residues were shown). This inhibitor was strongly stabilized via the hydrogen bonds with H57, K136, G137, S139, R155 and A157 (Fig. 3.12A). At the maximum peak of pulling force (Fig. 5 at $t = 385$ ps), the sulfone group of danoprevir and the side chain of Q41 were flipped together to form a new hydrogen bonding interaction (with a distance of 0.33 nm in Fig. 3.12B), while one more water was detected and acted as a center of hydrogen bond network between its carbamate oxygen atom and the two residues, A157 and C159. Meanwhile, the other binding site residues were slightly changed since the center of mass of danoprevir was moved away only about 0.16 nm from the pocket resulting in a loss of interaction with H57. Likewise, many water molecules gradually came closer to the drug binding

site in an effort to solvate, occupy and stabilize the binding pocket instead of a pulled ligand (Fig. 3.11).

3.5 CONCLUSION

The SMD technique was applied to screen for potentially potent anti-HCV agents from the ZINC database based on the hypothesis that a high required rupture force (F_{\max}) for pulling the ligand out of the NS3/4A binding site equates to a high predicted binding affinity and so inhibition efficiency. To validate the method, the four known HCV inhibitors (boceprevir, telaprevir, danoprevir and BI201335) were also subjected to the same SMD analyses, where the derived F_{\max} values were found to be in good agreement with the experimentally derived inhibition activity data. According to the ranked F_{\max} , the 40 top hit compounds from the ZINC database were reduced to nine (**59500093**, **59784724**, **13527817**, **26660256**, **29482733**, **25977181**, **28005928**, **13527826** and **13471529**) that were, from the above assumption, likely to be as good as or better than the four current inhibitors. Compounds **59500093** and **59784724** were predicted to have a higher potential than the existing commercial drugs (boceprevir and telaprevir) and the BI201335 inhibitor that is currently in clinical phase III trials. Compounds **13527817** and **26660256** were suggested to have a better inhibition efficiency than telaprevir (but not boceprevir or BI201335), whereas the remaining five compounds were predicted to be broadly the same as telaprevir. Therefore, these nine top-hit ligands may serve as potential NS3/4A protease inhibitors or be further used as templates for lead optimization. In addition to the predicted binding affinities, derived from the theoretically obtained F_{\max} values, the vdW interaction was found to have a higher contribution towards stabilizing the ligand NS3/4A interaction than electrostatic interactions.

CHAPTER 4
THE REACTION MECHANISM OF NS3/4A PROTEASE OF HCV WITH BOCEPREVIR
AND TELAPREVIR

Insight into the Reaction Mechanism of BOC- and TVR-NS3/4A Using QM/MM MD
Simulations

Arthitaya Meeprasert¹, Marc W. van der Kamp², Thanyada Rungrotmongkol³,
Adrian J. Mulholland² and Supot Hannongbua¹

¹*Department of Chemistry, Faculty of Science, Chulalongkorn University, 254
Phayathai Road, Patumwan, Bangkok 10330, Thailand*

²*Centre for Computational Chemistry, School of Chemistry, University of Bristol,
Bristol BS8 1TS, United Kingdom*

³*Department of Biochemistry, Faculty of Science, Chulalongkorn University, 254
Phayathai Road, Bangkok 10330, Thailand*

This article is in preparation for publication (2014).

4.1 INTRODUCTION

Since the number of infected people by hepatitis C virus (HCV) in worldwide has been increased about 3-4 millions every year [5, 6], HCV becomes one of global public health problems. It causes of liver inflammation, cirrhosis and hepatocellular carcinoma etc. Currently, Food and Drug Administration (FDA) approved four anti-HCV drugs; ribavirin, peg-interferon (PEG-IFN), boceprevir (BOC) and telaprevir (TVR), however some side effects have been found such as flu-like symptoms, anemia, hemolysis and neutropenia after the treatment [54, 55]. Approximately a half of patients infected with HCV genotype 1 has non-responded to the treatment with the combination of ribavirin and PEG-IFN [1, 4]. In order to design and develop the novel anti-HCV drugs, understanding of the function of NS3/4A protease with how the current drugs inhibit is very important. Note that NS3/4A serine protease is one of the highly attractive drug targets of HCV because it is responsible for cleavage the scissile peptide bond in an encoded polyprotein during the viral replication. In the present work, the inhibition mechanism of boceprevir and telaprevir against NS3/4A were investigated based on the combined self-consistent charge density functional tight-binding and molecular mechanics molecular dynamics (SCC-DFTB/MM MD) simulation.

HCV is a single-stranded RNA (ssRNA) virus in the *Hepacivirus* genus of *Flaviviridae* family containing approximately 3000 amino acids of encoded protein. After a gene encoding, the polyprotein precursor is subsequently processed to generate four structural proteins (C, E1, E2 and p7), while six non-structural proteins (NS2, NS3, NS4A, NS4B, NS5A and NS5B) produced by host and viral proteases [154]. The 631 residues of NS3 protein are consisted of serine protease (N-terminal) and

helicase (C-terminal) domains. The 180 amino acids of NS3 protease are the minimal residues required to enzyme of cleavage the peptide bond between the four junctions of the non-structural proteins; NS3/NS4A, NS4A/NS4B, NS4B/NS5A and NS5A/NS5B [8]. To activate the NS3 protease, a non-covalent heterodimer, NS4A cofactor could be in complex with NS3 protease. Deletion of the NS4A cofactor leads to the decreased proteolytic activity of NS3 protease owing to the H57 and D81 conformations are unaligned, and thus H57 is unable to abstract a proton from S139 side chain [9, 10]. In addition, a zinc (Zn^{2+}) ion tetrahedrally coordinated with three deprotonated cysteine residues (C97, C99 and C145) and H149 through a water molecule locating ~ 20 Å away from the binding pocket. From the previous work [155], a Zn^{2+} cation was proposed to play a role only in structural stabilization.

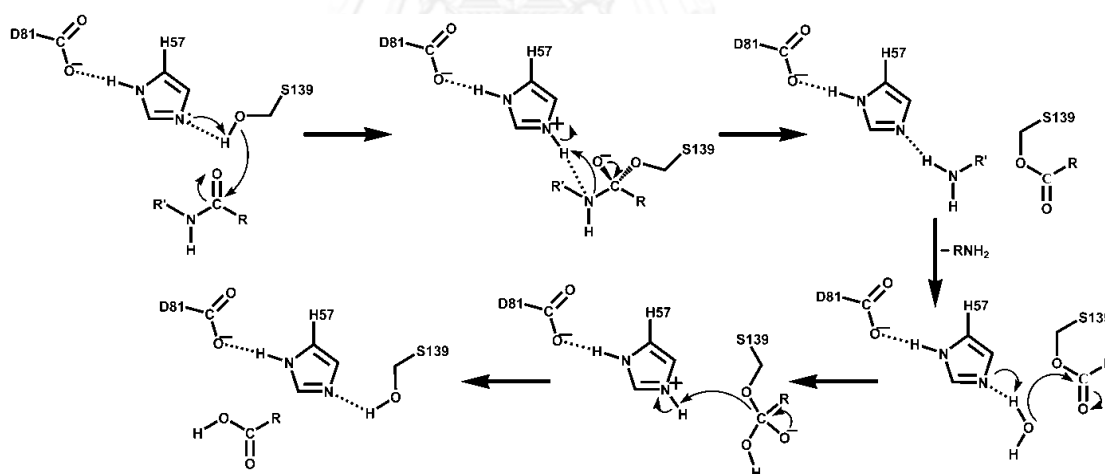


Figure 4.1 The catalytic mechanism of the peptide cleavage reaction by the HCV NS3/4A protease

From the previous QM/MM study [154], the mechanistic reaction in NS3/4A protease was likely to be similar to other serine proteases as depicted in Fig. 4.1. Firstly, the peptide substrate binds to the NS3/4A pocket forming a Michaelis

complex. The imidazole nitrogen of H57 subsequently abstracts the proton from the S139 hydroxyl group gaining a negatively charged hydroxyl group on Ser139, and this group then acts as a nucleophile to attack the carbonyl carbon of the peptide bond between the P1-P1' residues of the substrate (so-called the first step of the acylation process). This leads to a tetrahedral intermediate formation in which the negatively charged carbonyl oxygen is stabilized by the oxyanion hole formed by residues 135-139. Consequently, the previously relocated electrons on the carbonyl oxygen move back to release the N-terminal of the substrate that accepts the proton from the protonated H57. Afterwards, this residue activates the hydrolysis reaction by accepting the proton from the water molecule that concomitantly attacks the reacting carbonyl carbon to form the second tetrahedral intermediate. Finally, the covalent bond between the carbonyl carbon and hydroxyl oxygen of S139 is broken to gain the final hexapeptide product and the proton is transferred back to S139 [64, 110, 156].

Recently, several theoretical studies on the reaction mechanism of serine proteases with their native substrates including the NS3/4A protease have already been reported [156-159]. However, the reaction mechanism of NS3/4A with the covalent inhibitors has not been yet theoretically studied in the molecular level. Thus, the reaction mechanism (acylation and proton transfer) of NS3/4A with BOC and TVR has been focused in this study. Since the most protease inhibitors have been designed and developed in according to the substrate, intermediate or transition state mimics, we supposed that the reaction mechanism of NS3/4A with its inhibitors is likely similar to its natural substrates. We hope that understanding this

inhibitory mechanism might lead to development of the higher potent NS3/4A inhibitors.

4.2 MATERIALS AND METHODS

The initial structures of NS3/4A with boceprevir and telaprevir bound were obtained from the X-ray structures with 2.66 and 1.40 Å of resolution (Protein Data Bank (PDB) entry codes 2OC8 [67] and 3SV6 [70]). Note that in the crystal structures, the ligands covalently formed with the S139, hence the mechanistic studies were started with a backward reaction from acyl enzyme (product) to reactant. The cationic dummy atom model [160] was used for Zn²⁺ parameter. The AMBER ff12SB force fields were applied for the protein [161]. All system preparations and QM/MM molecular dynamics (MD) simulations were performed with the AMBER12 package program [162]. The PROPKA 3.1 [73] and the surrounding environment were used to consider the protonation state of the ionizable amino acids. Importantly, the two catalytic residues, H57 and D81, have been ionized as the neutral histidine with a hydrogen atom at delta position (δ -NH) and a negatively charged aspartate for both NS3/4A-boceprevir and telaprevir complexes. The missing hydrogen atoms were added and the system was consequently solvated in TIP3P [77] water box with a radius of 10 Å from protein surface by the LeaP module. In addition, chloride counterions were also added in order to neutralize the protein-ligand complexes.

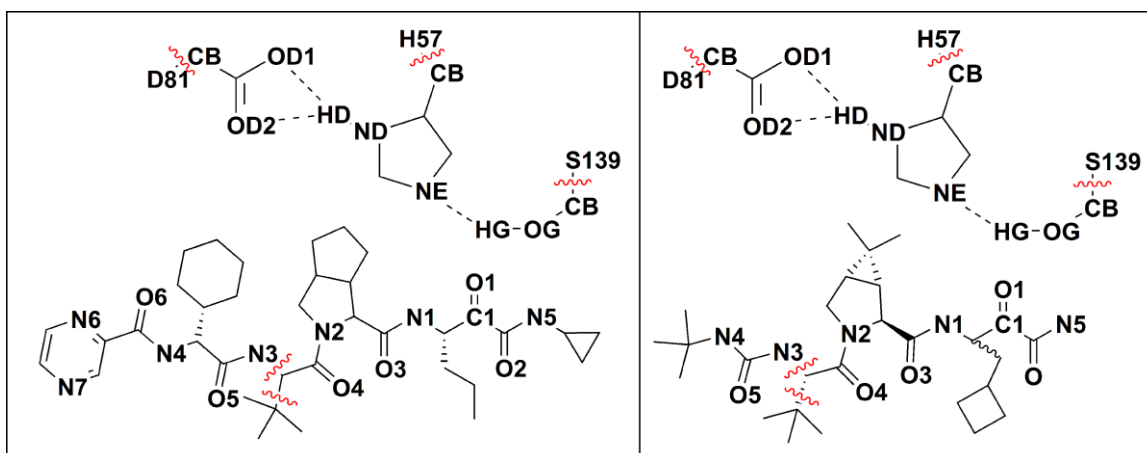


Figure 4.2 Fragments of the NS3 catalytic residues and telaprevir (left) and boceprevir (right) included in the QM region, where the QM and MM parts are partitioned by the red line

The combined QM/MM MD approach has been widely used to investigate the reaction mechanism such as bond making and breaking such as a proton transfer in the enzymatic systems [53, 163-165]. In this work, the studied complex has been divided into two subsystems; QM and MM. The QM region contains the side chains of the catalytic residues (H57, D81 and S139) and the fragment of ligand as depicted in Fig. 4.2. Totally, there were 72 and 75 atoms, respectively with $-1e^-$ in the QM region for both systems. The QM atoms were treated with self-consistent charge density functional tight-binding (SCC-DFTB) [166], semi-empirical method based on density functional theory approach, whilst the rest of system was treated by molecular mechanics (ff12SB). To consider the boundary region between the QM and MM regions, the link-atom approach [167] was employed. The five hydrogen link atoms were used for separating the QM and MM regions. Afterwards, the QM/MM energy minimization was carried out with 100 steps of steepest descents (SD) and followed

by 1900 steps of conjugate gradient (CG) algorithms. Then the entire system was heated up from 50 to 300 K in 50 ps and then equilibrated by means of the QM/MM MD under periodic boundary condition in two steps; (i) the 20 kcal/mol·Å of force constant was applied to restrain the distance between H57 and D81 for 30 ps and (ii) the system was continuously simulated till 300 ps without any restraint. The QM/MM MD snapshots were collected every 1 ps. The non-bonded cut-off of 10 Å and the simulation time step of 1 fs were used, while the Particle Mesh Ewald (PME) [167] approach was applied to calculate the long-range QM-QM and QM-MM electrostatic interactions. The SHAKE [78] algorithm was used to constrain all covalent bonds in the MM region involving with hydrogen atoms.

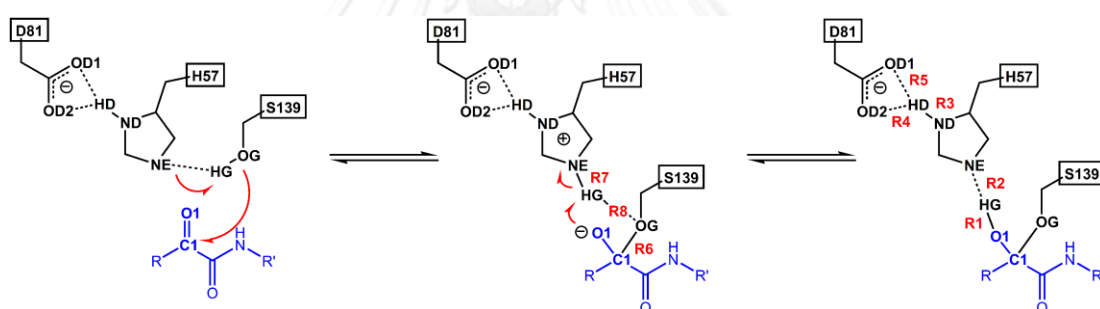


Figure 4.3 Proposed reaction mechanism of NS3/4A protease with the ketoamide inhibitor

To investigate the free energy profile (FEP) of the mechanistic reaction of NS3/4A protease with boceprevir and telaprevir, the SCC-DFTB/MM MD coupled with the umbrella sampling implemented in AMBER program and weighted histogram analysis method (WHAM) [168, 169] were employed. In addition, three snapshots of each complex obtained from the equilibration phase at 200, 250 and 300 ps were chosen as the starting configuration for the calculations. From the product or acyl-

enzyme structure, the three reaction coordinates (RCs) were considered to study the two steps of reaction; (i) the proton transfer between the carbonyl oxygen of ligand and NE of H57 relating to the difference between O1-HG and HG-NE distances, $RC1 = R1 - R2$ and (ii) the nucleophilic attack of S139 on the carbonyl carbon, C1 of ligand (OG-C1 distance) and the proton transfer between H57 and S139 (difference of NE-HG and HG-OG distances), $RC2 = R6$ and $RC3 = R7 - R8$ as shown in Fig. 4.3. The latter step generates the tetrahedral intermediate (TI). Note that one- and two-dimensional umbrella sampling calculations have been applied to the first and second steps, respectively. For each window of the reaction coordinate, the 2 ps equilibration and 5 ps production runs were carried out. The reaction coordinate was increased by 0.1 Å for each step of sampling, whilst the harmonic restrained potential was applied with 200 kcal/mol·Å of force constant. Finally, the production run of every window in the reaction coordinate was taken and consequently calculated the relative free energy of all simulations by the WHAM in order to outline the FEP.

4.3 RESULTS AND DISCUSSION

To determine the stability of the NS3/4A-BOC and -TVR complexes during the QM/MM MD, the RMSD has been plotted as depicted in Fig. 4.4. The result shows that since 100 ps the RMSD values of both complexes are fluctuated in the range of 1.5 Å suggesting the systems have reached an equilibrium. Therefore the structures at 200, 250 and 300 ps were used as the initial structures for the SCC-DFTB/MM MD with the umbrella sampling to explore the free energy profile and characterize the reaction mechanism of NS3/4A protease.

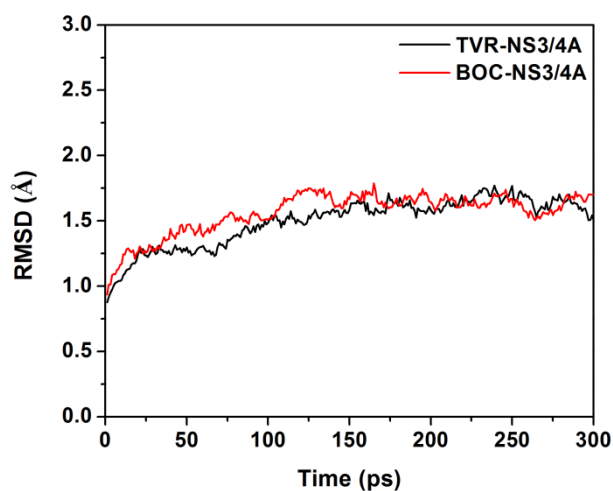


Figure 4.4 The root mean-square displacements (RMSDs) relative to the initial structures of NS3/4A protease with boceprevir (BOC) and telaprevir (TVR) bound as shown in the red and black lines, respectively.

For the first step of the backward reaction, the proton was transferred from the keto-amide hydroxyl group of the ligands to ϵ N or named as NE of catalytic H57, where their FEPs obtained from WHAM analysis were shown in Fig. 4.4. According to the energy barriers of the 2 drugs, it seems that the free energy monotonically increased along the reaction coordinate of the proton transfer reaction. However, the shallow minimum was observed from the FEPs at the SCC-DFTB/MM level of theory where the curvatures were changed nearly $RC1 \approx 0.5 \text{ \AA}$ (Fig. 4.4). This is therefore the TI structures taken from this path are rather similar to the transition state (TS) structures. Note that the free energies at the $RC1 \approx 0.5 \text{ \AA}$ are $\sim 14.3 \pm 0.3$ and $\sim 14.3 \pm 0.8$ kcal/mol relative to the acyl enzyme or the product state (at $RC1 \approx -1.0 \text{ \AA}$) for BOC and TVR, respectively. After the minimal free energy of TI, the free energy still increased continuously because the proton was moved too more close to the ϵ N of H57. Subsequently, the TI complex was used as the initial structure for the 2D-umbrella sampling calculation of the proton transfer from H57 to S139 and the nucleophilic attack of S139 to the carbonyl carbon of keto-amide group. The 2D-FES result was shown in Fig. 4.5. It showed that the acylation step of both systems occurred in a concerted reaction which also supposed to be the rate limiting step as the native substrates according to their had the higher free energy barriers compared

with the proton transfer step (between keto-amide group of inhibitor and histidine). The free energies of the backward reaction relative to the tetrahedral intermediate for generating Michaelis complexes (reactant, R) are ~ 22.2 and ~ 20.1 kcal/mol for boceprevir and telaprevir systems, respectively. These free energy values are moderately similar to the experimental activation free energies (~ 23.2 and ~ 23.4 kcal/mol for boceprevir and telaprevir) [170]. Note that these values were converted from the rate constant of the backward reaction at temperature 298 K.

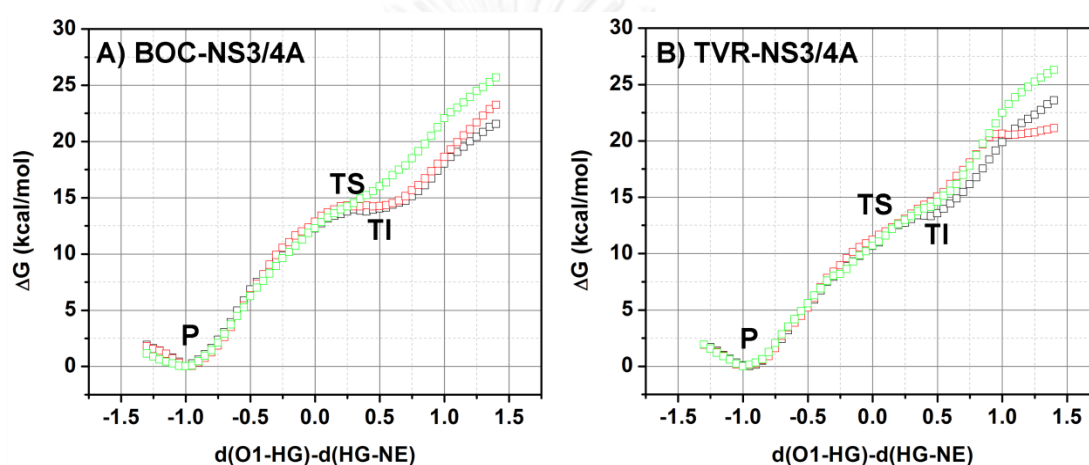


Figure 4.5 Free energy profile (FEP) obtained from WHAM of 3 umbrella sampling calculations for the proton transfer between H57 and the hemiketal oxygen of (A) BOC-NS3/4A and (B) TVR-NS3/4A

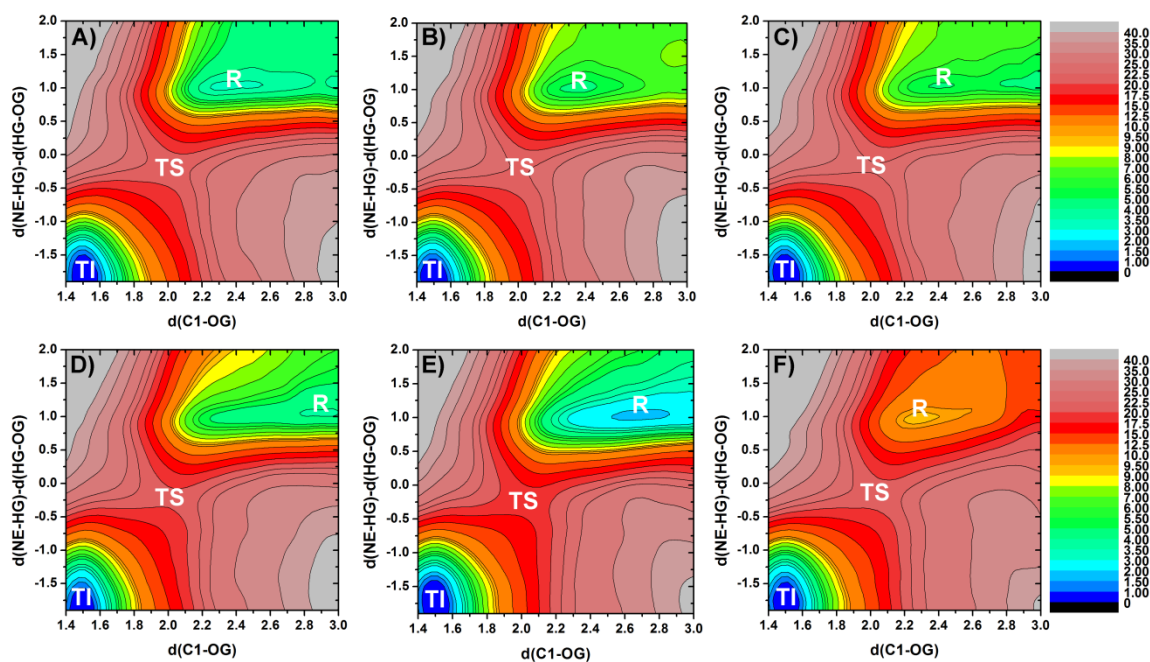


Figure 4.6 The three individual SCC-DFTB/MM free energy surfaces (FESs) for the acylation mechanism of NS3/4A protease binding to (A-C) boceprevir and (D-E) telaprevir with different initial structures

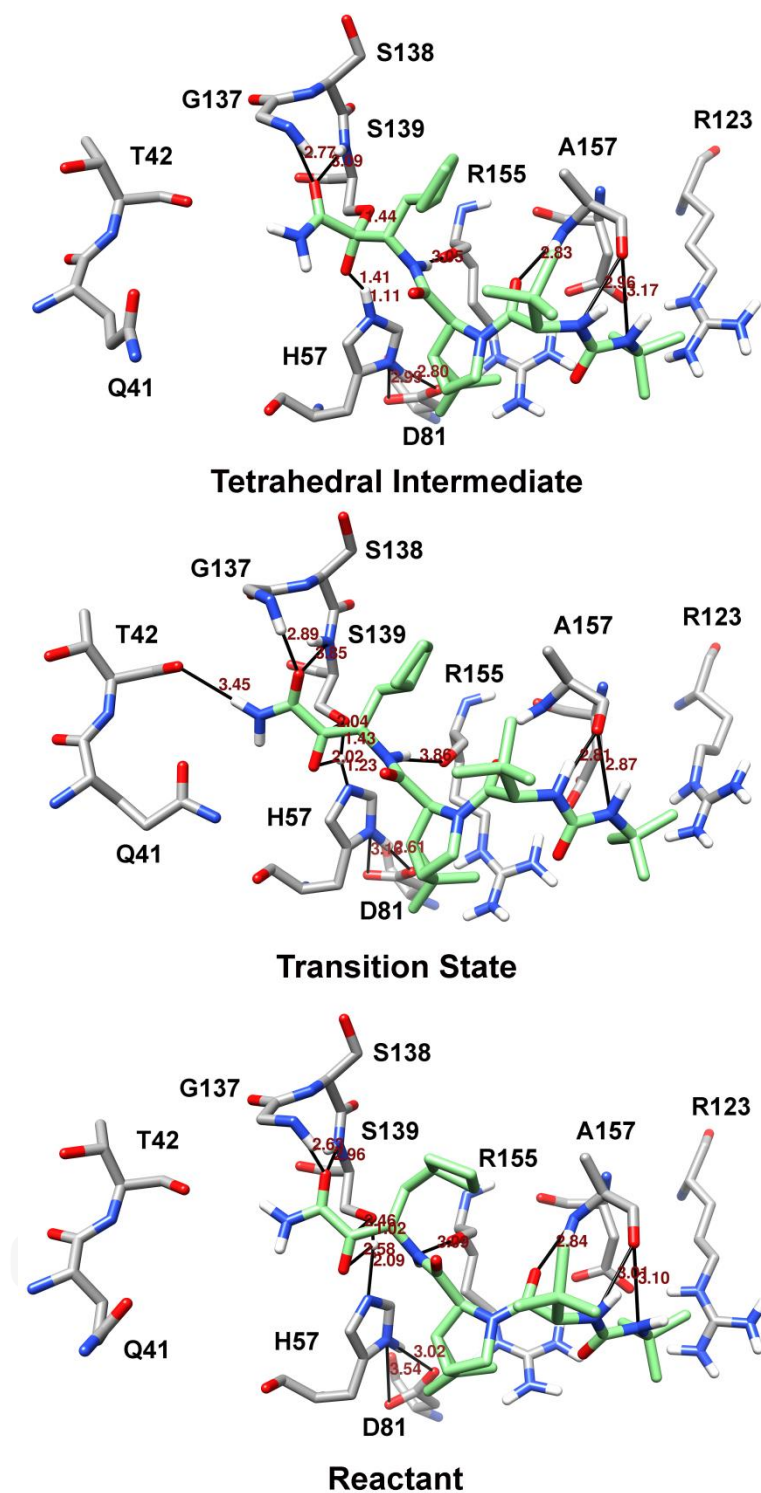


Figure 4.7 Structures and distances of the tetrahedral intermediate, transition state and reactant of NS3/4A-boceprevir complex in the acylation reaction

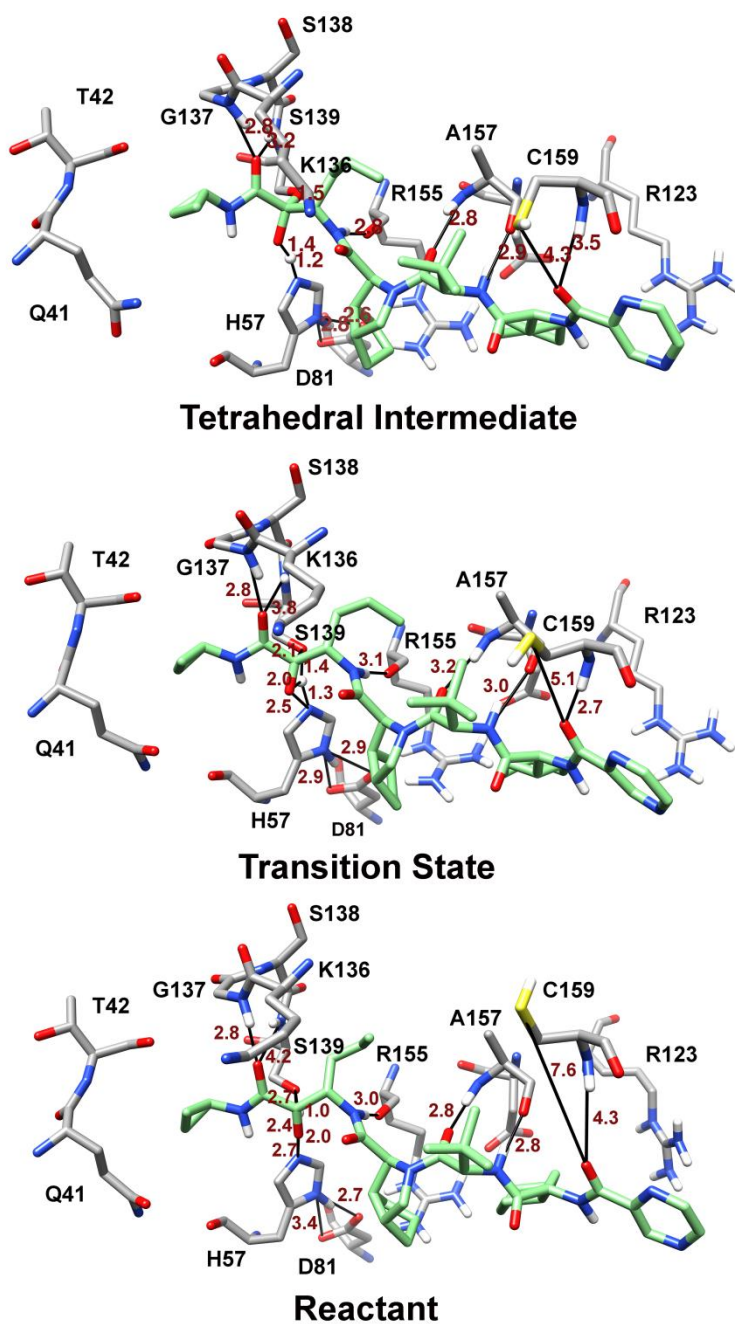


Figure 4.8 Structures and distances of the tetrahedral intermediate, transition state and reactant of NS3/4A-telaprevir complex in the acylation reaction

4.4 CONCLUSIONS

The inhibition mechanism of boceprevir and telaprevir towards NS3/4A protease has been examined using the semi-empirical SCC-DFTB/MM MD technique in couple with umbrella sampling, and subsequently their free energy profiles have been calculated by means of WHAM. Since these two drugs were developed based on the natural substrates of HCV NS3/4A protease, we presumed that their mechanism for producing an acyl enzyme could be similar to that of natural substrates. The SCC-DFTB/MM MD calculations predicted that the acylation mechanisms with a formation of tetrahedral intermediate for these drugs were occurred in concerted reaction. In addition, the acyl enzymes were much more stable than the tetrahedral intermediate and Michaelis complex. In the next step, the structural properties and the contribution of the binding site residues that stabilized the ligands will be intensively investigated, and the higher level of theory such as DFT or *ab initio* QM/MM calculations should be carried out.

CHAPTER 5

PROTEIN STRUCTURE AND LIGAND-TARGET INTERACTIONS OF THE NEURAMINIDASE
SUBTYPES A/H5N1 AND A/pH1N1 COMPLEXED LANINAMIVIR

Binding pattern of the long acting neuraminidase inhibitor laninamivir towards
influenza A subtypes H5N1 and pandemic H1N1

Arthitaya Meeprasert¹, Wasinee Khuntawee², Kittiwat Kamlungsua¹, Nadtanet
Nunthaboot³, Thanyada Rungrotmongkol⁴ and Supot Hannongbua¹

¹*Department of Chemistry, Faculty of Science, Chulalongkorn University, 254
Phayathai Road, Patumwan, Bangkok 10330, Thailand*

²*Nanoscience and Technology Program, Graduate School, Chulalongkorn
University, 254 Phayathai Road, Bangkok 10330, Thailand*

³*Department of Chemistry, Faculty of Science, Mahasarakham University,
Khamriang, Kantarawichai, Mahasarakham 44150, Thailand*

⁴*Department of Biochemistry, Faculty of Science, Chulalongkorn University, 254
Phayathai Road, Bangkok 10330, Thailand*

This article has been published in Journal: Journal of Molecular Graphics and
Modelling Page 148-154. Volume: 38 Year:2012

5.1 ABSTRACT

Influenza A H5N1 and pH1N1 viruses have broadly emerged and become widespread in various countries around the world. Oseltamivir, the most commonly used antiviral drug against the seasonal and pandemic influenza viruses, is targeted at the viral neuraminidase (NA), but some isolates of this virus have become highly resistant to this drug. The novel long-acting drug, laninamivir, was recently developed to inhibit influenza A and B viruses of either the wild-type (WT) or the oseltamivir resistant mutant of NA. To understand the high efficiency of laninamivir, all-atom molecular dynamics simulations were performed on the WT and H274Y mutant of H5N1 and pH1N1 NAs with laninamivir bound. As a result, the novel drug was found to directly interact with 11 binding residues mainly through salt bridge and hydrogen bond formation (as also seen by electrostatic contribution). These are comprised of 7 of the catalytic residues (R118, D151, R152, R224, E276, R292 and R371), and 4 of the framework residues (E119, W178, E227 and E277). Laninamivir showed a similar binding pattern to all four NAs, but strong hydrogen bonding interactions were only found in the WT strain, with a slightly lowered contribution at some drug contact residues being observed in the H274Y mutation. This is in good agreement with the experimental data that the H274Y mutant has a small increase (1.3- to 7.5-fold, which was not statistically significant) in the IC_{50} value of laninamivir.

5.2 INTRODUCTION

The avian flu (H5N1) and 2009 pandemic H1N1 (pH1N1) viruses are wide spread throughout the world and some isolates have become resistant to oseltamivir, the most common and (formerly) effective anti-influenza drug [31, 171] (Fig. 5.1), leading to a potentially global public health problem. A new drug,

laninamivir (R-125498), was approved and marketed in Japan in September, 2010 [40]. With a long term inhibitory efficiency against the neuraminidase (NA) enzyme of influenza A and B viruses as well as their current oseltamivir resistant mutations [39, 40, 172], laninamivir is thus a very interesting drug not only for good efficacy but also in terms of a stockpile for future pandemic influenza. Although, the three dimensional structures of laninamivir binding to the wild-type (WT) NA subtypes N1 (from pH1N1, Fig. 5.2) N2 and N5 have recently been crystalized [173], the drug orientation and binding patterns towards the H5N1 virus and the H274Y (N2 numbering) mutant of both the pH1N1 and H5N1 viruses are not yet revealed. Therefore, the main goal of this present study was to provide a detailed comparative understanding of the drug-target interactions of laninamivir binding to the NA of both the WT and the H274Y mutant of these two N1 virus strains.

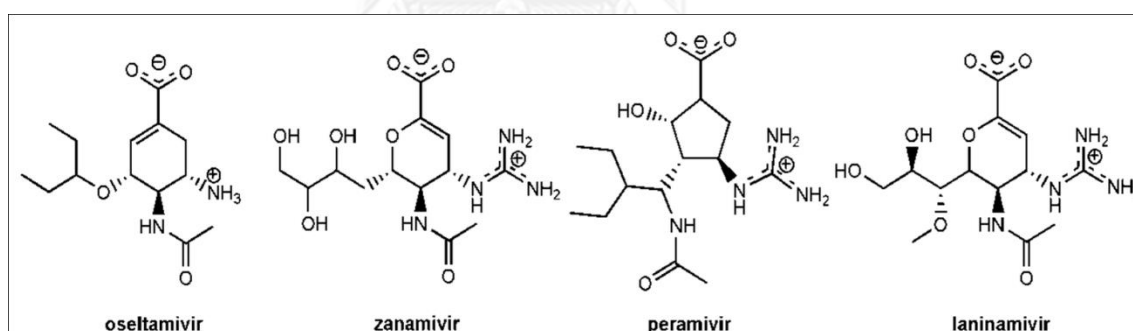


Figure 5.1 The chemical structures of four NA inhibitors (NAIs) in the active metabolite form: oseltamivir, zanamivir, peramivir and laninamivir

NA is a glycoside hydrolase enzyme (EC 3.2.1.18) that is found on the surface of the influenza virus and plays a pivotal role in the viral life cycle [174]. As such, NA cleaves the glycosidic bond of the terminal sialic acid from the host cell receptor with a new viral progeny release to infect other cells. Up to date, oseltamivir

(Tamiflu®) and zanamivir (Relenza®), shown in Fig. 5.1, are the two common anti-influenza drugs targeted against, and operating as inhibitors of NA (NAIs). While oseltamivir is medicated as a tablet, zanamivir is administered by oral inhalation. Therefore, the oseltamivir is more commonly used to treat influenza patients. Another NAI drug, peramivir, was made available during the outbreak of the 2009 pandemic H1N1 virus until June, 2010 under the Emergency Use Authorization (EUA) by the Food and Drug Administration (FDA) [175]. Recently, the second generation flu NAI drug, laninamivir, was discovered by Yamashita et al. [49] and manufactured by Daiichi Sankyo Co. Ltd. in Japan and Biota. It is an active metabolite converted in lung from the CS-8959 (laninamivir octanoate) prodrug [38, 172, 176]. Besides the long term efficient activity, with a single inhaled dose being comparable to that from taking oseltamivir twice daily for 5 days, laninamivir is effective against the wild-type strain of both influenza A (seasonal H1N1, pH1N1, H5N1 and H3N2) and B viruses as well as the oseltamivir-resistant H274Y mutations of H5N1, pH1N1 and seasonal H1N1 viruses, [177, 178] as summarized in Table 5.1. It is worth noting that the virus strain order, in terms of the fold increase in resistance to laninamivir, relative to wild type is pH1N1 (1.36) < seasonal H1N1 (1.85) < H5N1 (3.44 or 7.50). In agreement with the experimental data, laninamivir and its prodrug were theoretically predicted to have high binding affinities with A/H5N1 complexes through the rupture forces and so that laninamivir could be used to inhibit both the WT and the oseltamivir-resistance providing N294S and H274Y mutations [179].

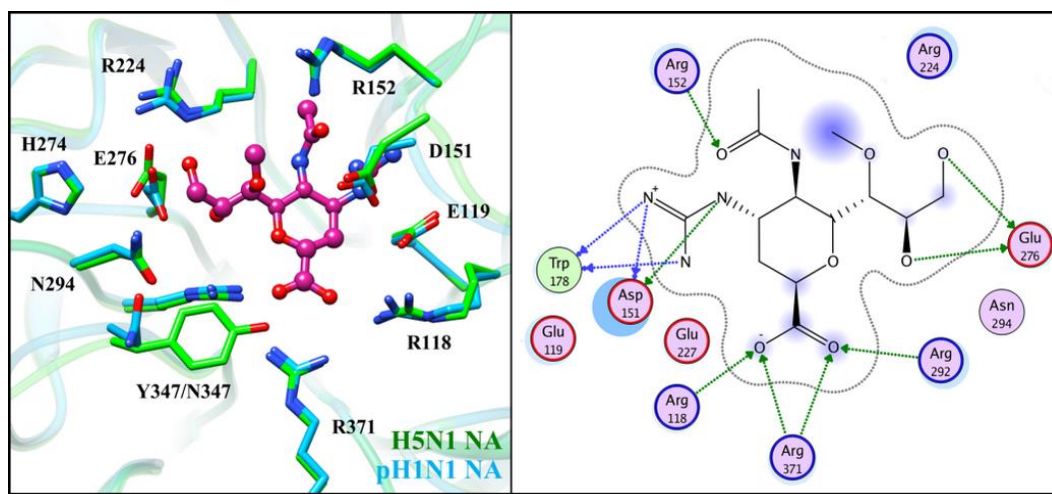


Figure 5.2 (Left) Close up of laninamivir binding to the catalytic pocket of the pH1N1 NA (cyan) obtained from the 3TI3 crystal structure[170] with a superimposition of the H5N1 NA (2HU4 [42], green). (Right) From the X-ray structure of the laninamivir-NA complex, the hydrogen bond formations through the backbone and side chain of the surrounding residues are represented by blue and green arrows, respectively.

In order to understand the high susceptibility of NA from both the WT and H274Y mutant isolates of the influenza viruses towards the NAI laninamivir, molecular dynamics (MD) simulations were performed on the two influenza subtypes, H5N1 and pH1N1. The drug-target interactions, in terms of the hydrogen bonds, electrostatic and vdW forces, with the surrounding residues at the catalytic site of NA were intensively analyzed, discussed and compared with the co-crystal structure of pH1N1 NA with laninamivir bound, as well as with previous theoretical studies on the other anti-influenza NAI drugs.

Table 5.1 The 50% inhibitory concentration (IC₅₀) values of laninamivir for neuraminidase (NA) from various influenza strains.

Virus strain	NA change	IC ₅₀ (nM)	Resistance fold
A/H1N1 (seasonal flu) [172]	WT	1.79	
pH1N1 [172]	WT	1.83	
A/H3N2 [172]	WT	2.13	
Influenza B [172]	WT	11-26	
A/Yogohama/67/2006 (seasonal H1N1) [178]	WT	3.03	
A/Yogohama/67/2006 (seasonal H1N1) [178]	H274Y	5.62	1.85
A/Washington/29/2009 (pH1N1) [177]	WT	1.57 ^a	
A/Washington/29/2009 (pH1N1) [177]	H274Y	2.14 ^a	1.36
A/Hanoi/30408/05 (HPAI H5N1) [178]	WT	0.32	
A/Hanoi/30408/05 (HPAI H5N1) [178]	H274Y	1.10	3.44
A/Vietnam/1203/04 (H5N1) [178]	WT	0.28	
A/Vietnam/1203/04 (H5N1) [178]	H274Y	2.10	7.50

^a Flurescein leakage (MUNANA) assay

5.3 METHODOLOGY

5.3.1 System preparation

All system preparations and MD simulations were performed using the AMBER10 software¹⁶. The four simulated systems of the WT and H274Y mutant of the NA from both the pH1N1 and H5N1 virus strains were prepared as follows. The starting structure of WT pH1N1 NA-inhibitor complex was taken from the recently determined co-crystal structure of the WT NA of pH1N1 virus with laninamivir bound (PDB entry code: 3TI3 [173]). To build the H274Y mutant system, the histidine at residue number 274 was changed to tyrosine from the refined crystal structure of apo pH1N1 NA (PDB code: 3NSS¹⁷). This procedure was done using the LEaP module implemented in AMBER10. The laninamivir was later added into the active site of the

mutated H274Y pH1N1 NA. For the two laninamivir-H5N1 systems, the X-ray structures of the WT and H274Y forms of NA from H5N1 strains complexed with oseltamivir (PDB codes 2HU4 [42] and 3CLO [171], respectively) were used where the atomic coordinates of oseltamivir were replaced by laninamivir. The Ca^{2+} and water molecules from the crystal structure were retained in the system. The ionizable amino acids, including K, R, D and E, were categorized at pH 7.0. The protonation state of histidine was assigned according to the identified hydrogen bond with the interacting partner. A possible disulfide bridge between two cysteines was assigned to maintain the protein stability. The missing hydrogen atoms of the NA protein and the laninamivir NAI in each system were added by the LEaP module.

The energy minimization with 2000 steps of steepest descent (SD) and continued by 1000 steps of conjugated gradient (CG) were initially performed on the hydrogen atoms to reduce bad steric contacts. Subsequently, each system was solvated by TIP3P waters [77], with a minimum distance of 12 Å from the protein surface. The water box size was 98×98×98 Å and 89×87×95 Å for the pH1N1 wide type and H274Y, respectively, while those of H5N1 systems was 84×85×88 Å. The total negative charges were neutralized by adding Na^+ counterions. Afterwards, the crystal and modeled waters were minimized by 2000 steps of SD and 1000 steps of CG, and finally the whole system was optimized using the same procedure.

5.3.2 Partial Charge and Force Field Development for laninamivir

The partial atomic charges and empirical force field parameters of laninamivir were developed according to the standard scheme as in previous studies [135, 180, 181]. By considering the hybridization of the covalent bonds, the coordinates of the

22 missing hydrogen atoms were added to laninamivir structure. The ligand structure was optimized with the HF/6-31* basis set to adjust the bond lengths and bond angles using Gaussian 03 program [75]. To obtain electrostatic potential (ESP) surrounding ligand molecule, the single point calculation was performed at the same method and level of theory on the optimized geometry. Consequently, the restrained electrostatic potential (RESP) charges were evaluated with the charge-fitting procedure using the RESP module of AMBER program. The laninamivir parameters were derived from the generalized amber force field (GAFF) [76], while the standard van der Waals (vdW) parameters were utilized to adequate transferability of intermolecular interaction.

5.3.3 Molecular Dynamics (MD) simulations

A single continuous MD simulation was applied on each of the four NA-laninamivir simulated complexes, being NA from the WT and H274Y mutation of both H5N1 and pH1N1 viral strains, where the periodic boundary with the NPT ensemble at 1 atm and a time step of 2 fs were employed. The whole system was heated up to 300 K for 50 ps and subsequently simulated at this temperature for 20 ns using the SANDER module in AMBER. The SHAKE algorithm was used to constrain all bonds involving hydrogen atoms [78]. The cutoff distance for non-bonded interactions was set at 12 Å and the particle mesh Ewald method [79] was applied to account for long-range electrostatic interactions. After the simulations were found to reach equilibrium, the MD trajectories were extracted from the production phase for analysis. The ptraj and MM-GBSA modules, as implemented in the AMBER software, were used to analyze the global root mean-square displacement (RMSD), hydrogen

bond occupancy, decomposition of free energies per residue and their energy components, between laninamivir and each of the four targeted NA isoforms.

5.4 RESULTS AND DISCUSSION

5.4.1 Stability of the global structure

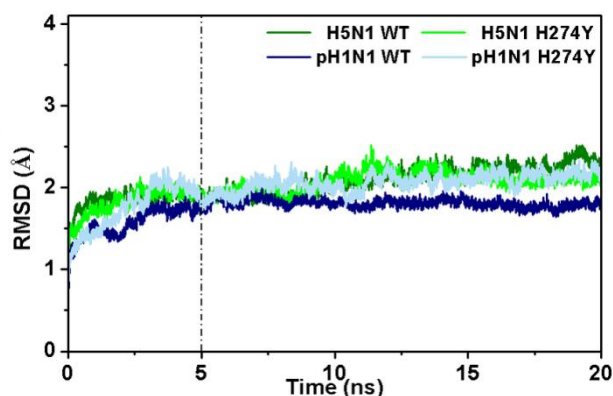


Figure 5.3 Root mean-square displacements (RMSDs) relative to the starting structure for all atoms of the laninamivir binding to the WT and H274Y NAs of the influenza H5N1 and pH1N1 viruses

To monitor the stability of the four studied systems, the RMSD values of the all atoms of the laninamivir NAI complexed to each of the four NAs (WT and H274Y NAs of the H5N1 and pH1N1 viruses) relative to the starting structure versus simulation time were measured and are shown in Fig. 5.3. As can be seen from the plot, the RMSD fluctuations are similar in three systems around 2.2 Å, excluding the pH1N1 WT shows lower fluctuation around 1.8 Å (after 3 ns). All complexes were likely to reach equilibrium at 5 ns. Therefore, the MD trajectories from the last 15 ns were extracted for all further analysis.

5.4.2 Laninamivir binding patterns

To understand the mechanism of action and drug-target interactions of the laninamivir binding to both the WT and H274Y mutation of both the H5N1 and pH1N1 NAs, hydrogen bonding interaction and the role of key acting residues on the basis of decomposition of binding free energy were investigated as follows.

5.4.3 Hydrogen bonding interactions

Since the active metabolite of laninamivir is a zwitterion with the $-\text{COO}^-$ and $-\text{NHC}(\text{NH}_2)_2^+$ groups, hydrogen bonding and salt bridge interactions play a critical role in stabilizing the protein-ligand complex. To gain further insight into the efficiency of the laninamivir binding to the NAs from the WT and H274Y mutation of the H5N1 and pH1N1 viruses, the percentage occupancy and the number of hydrogen bonds between this NAI and the surrounding NA residues were investigated according to the subsequent criteria: (i) the distance between proton donor (D) and acceptor (A) atoms was $\leq 3.5 \text{ \AA}$; and (ii) the D-H...A angle was $\geq 120^\circ$. The hydrogen bond results and representative MD snapshots for the four complexes are depicted and compared in Fig. 5.4. Strong and moderate hydrogen bonding interactions are defined as having hydrogen bond occupations of $> 75\%$ and $50 - 75\%$, respectively.

As can be seen in Fig. 5.4, the major hydrogen bonding interactions between the laninamivir and the NA binding residues are almost similar among all four NA-laninamivir complexes, although they are slightly different at some amino acids. Even though the Y347 of H5N1 is replaced by N347 in pH1N1, the NA-laninamivir interaction still slightly changes. Differentially, the interaction between pH1N1 NA and oseltamivir was weakened due to the outwardly oriented N347 from the binding site

which decreased the average number of hydrogen bonds over simulation time with a presence of the wider pocket as noticed in the previous theoretical study [136]. The ether oxygen of the dihydropyran ring and the carbonyl oxygen of the -NHAc moiety established moderate and strong hydrogen bonding interactions with the nitrogen atoms of the guanidinium of NA residues R292 and R152, respectively. Interestingly, the former hydrogen bond with R292 was only observed in the laninamivir complexes of both strains. This phenomenon is not always found in zanamivir complexes, where the moderate hydrogen bond formation with dihydropyran scaffold was detected in pH1N1 NA, but not in H5N1 NA [136]. Meanwhile the latter one with R152 is typically detected in the other anti-influenza NA drugs and potent compounds [180-186]. In contrast to that for laninamivir-NA seen here, the H274Y mutation of NA was observed to disrupt the hydrogen bond of oseltamivir with the NA R152 residue [185, 187, 188], thereby probably resulting in the low drug inhibitory potency of oseltamivir. In contrast, this strong interaction with R152 and laninamivir could possibly account for the high NAI activity of laninamivir against the oseltamivir-resistant H274Y mutation. From the electrostatic surface study of oseltamivir binding pathway [187], the mutated residue 274 positioned directly onto the negatively charged funnel at the mouth of the binding pocket has perhaps caused a different electrostatic drug-target interaction. Moreover, the Y274 replacement significantly reduced the hydrophobic pocket size for the oseltamivir's bulky group as seen by an increase of solvent accessible surface area (SASA), instead of disrupting E276-R224 salt bridge [31, 188].

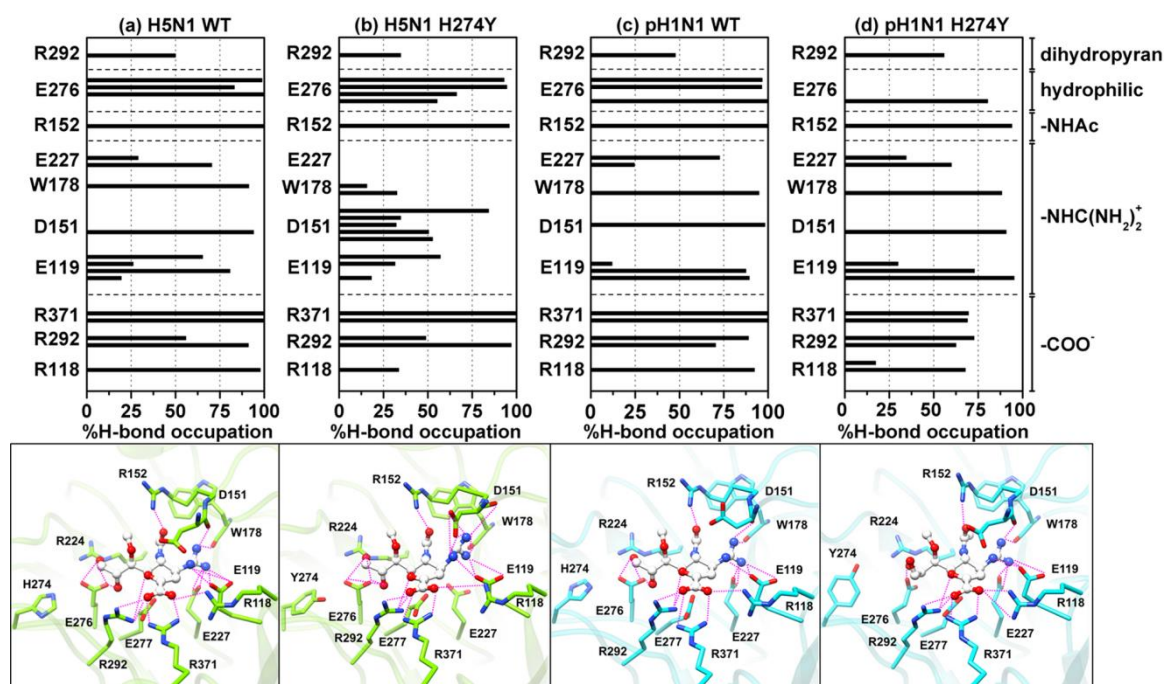


Figure 5.4 Percent occupation pattern of hydrogen bonds formed from the dihydropyran ring and the four side chains of laninamivir to the binding residues (label given along y-axis) in the active site of the four NAs: (a) H5N1 WT, (b) H5N1 H274Y, (c) pH1N1 WT and (d) pH1N1 H274Y.

However, some noticeable differences between the four H-bond patterns were detected at the 2,3-dihydroxy-1-methoxypropyl (hydrophilic bulky), $-NHC(NH_2)_2^+$ and $-COO^-$ moieties of the laninamivir ligand. The strong interaction strength between the hydrophilic bulky group of laninamivir and the E276 residue of NA was likely maintained in all complexes, although the percentage and number of hydrogen bonds were different. Stronger and larger numbers of hydrogen bond formations were observed in the case of the WT NA of both viruses and for the H5N1 H274Y mutant, while only one strong interaction was observed in the case of the H274Y NA from pH1N1. Conversely, the replacement of the hydrophilic group by

hydrophobic side chain such as in oseltamivir or peramivir usually brings a loss of hydrogen bond formation with NA [42, 172, 189, 190]. The change to a methoxy group at this hydrophilic side chain, instead of all three hydroxyl groups in zanamivir, led to no interaction with NA residue R224 in the H5N1 WT [180] and N294 (N2 numbering) in the pH1N1 WT [182].

At the $-\text{NHC}(\text{NH}_2)_2^+$ group, the positively charged side chain was well stabilized by the three negatively charged residues, E119, D151 and E227, as well as the W178 backbone (Fig.5.4, and discussed below), similar to that which was observed in the previous studies on the zanamivir- and peramivir-NA systems [180, 182, 185]. This part of the laninamivir formed a rather strong salt bridge interaction with NA residue E119 in the case of WT strains for H274Y mutant. A strong interaction with NA residue D151 was conserved in all four complexes although that with the H5N1 H274Y form of NA provided a larger number of weak and moderate salt bridge interactions than the other three NA-laninamivir systems. With almost 100% occupation of this laninamivir-NA interaction in the H5N1 WT and the two pH1N1 strains, one can imply that in complex with laninamivir the 150-loop of NA eventually and tightly moved to lock the inhibitor. Again, the guanidinium nitrogen of laninamivir created a strong hydrogen bond with the backbone carbonyl oxygen of NA residue W178 in all strains except the H274Y mutant of H5N1 complex which showed weakened interaction. This observation is different from those of oseltamivir binding to the WT and H274Y NA mutant of both H5N1 and pH1N1, where the hydrogen bond to W178 was completely lost [185, 188, 191], with a consequence of an increased resistance to this NAI in comparison to that for laninamivir. In addition, moderate hydrogen bonding between laninamivir and NA residue E227 was detected

in H5N1 WT and two of pH1N1, but this was totally lost in the case of H5N1 H274Y. It should be mentioned that the replacement of $-(\text{NH}_3)^+$ in oseltamivir by the longer $-\text{NHC}(\text{NH}_2)_2^+$ group in laninamivir (also in zanamivir) introduced the interaction with the NA residue E227.

As expected, the three conserved arginines of NA, R118, R292 and R371, were found to contribute extensively through salt bridge interactions to stabilize the COO^- moiety of laninamivir in the two WT NA strains. These important drug-target interactions are commonly detected in all NAs and drug candidates containing a negatively charged group [115, 116, 181, 184, 192]. Interestingly, the H274Y mutation has been found to interrupt the drug-target interactions with R118 (to 34% occupation) in H5N1 NA and partially disturb the arginine triad (to ~70%) in pH1N1 NA. The interaction with R118 was dramatically reduced from ~90% in the oseltamivir-NA (WT) complex of the pH1N1 to ~5% in the oseltamivir-NA (H274Y) complex [191].

5.4.4 Key residues for drug binding

To pinpoint the important residues for the binding of laninamivir in the NA active site of influenza H5N1 and H1N1 viruses, the interaction energy from the individual residues of NA that contributed to laninamivir binding were evaluated according to the MM-GBSA method [85, 193, 194] using the decomposition energy module of AMBER. Note that the measured residues are comprised of the eight catalytic residues (R118, D151, R152, R224, E276, R292, R371 and Y406) and the 11 framework residues (E119, R156, W178, S179, D198, I222, E227, H274, E277, N294, and E425). The binding free energy decomposition as a pairwise per-residue basis (

$\Delta G_{bind}^{residue}$), and the contribution separated into the residue backbone ($\Delta G_{bind}^{backbone}$) and the side chain ($\Delta G_{bind}^{sidechain}$), are plotted in Fig. 5.5 (left), whereas the corresponding electrostatic ($E_{ele}+G_{polar}$) and vdW ($E_{vdW}+G_{nonpolar}$) energy terms are shown in Fig. 5.5 (right).

Almost all the NA residues (except for D151 and W178) provided some energy stabilizations towards laninamivir through their side chains, in correspondence with the observed presence of drug-target hydrogen bonds. Among the NA residues in the WT strain of the two viruses (Fig. 5.5a and 5.5c, left), the highest contribution was likely gained from the laninamivir contacting NA residues through a strong salt-bridge (in terms of electrostatic energy in Fig. 5.5, right) and hydrogen bond interactions with the charged groups of laninamivir (mentioned above). These are the R292 and R371 residues in the catalytic site and the E119 (pH1N1) residue in the framework site with $\Delta G_{bind}^{residue}$ of less than -6 kcal/mol. Additionally, the residues R118, E119 (H5N1), D151, R152, W178, E227 and E276 gave an energy contribution in the range of $-2 \leq \Delta G_{bind}^{residue} \leq -6$ kcal/mol. Although most NA residues preferentially stabilized the laninamivir binding to NA, destabilization can be found at the framework residues R156 and E277. Contrary to the oseltamivir complex, the R118 residue plays the role to disrupt the binding stability between oseltamivir and receptor by ~ 2 kcal/mol of energy contribution as reported in the previous work [195].

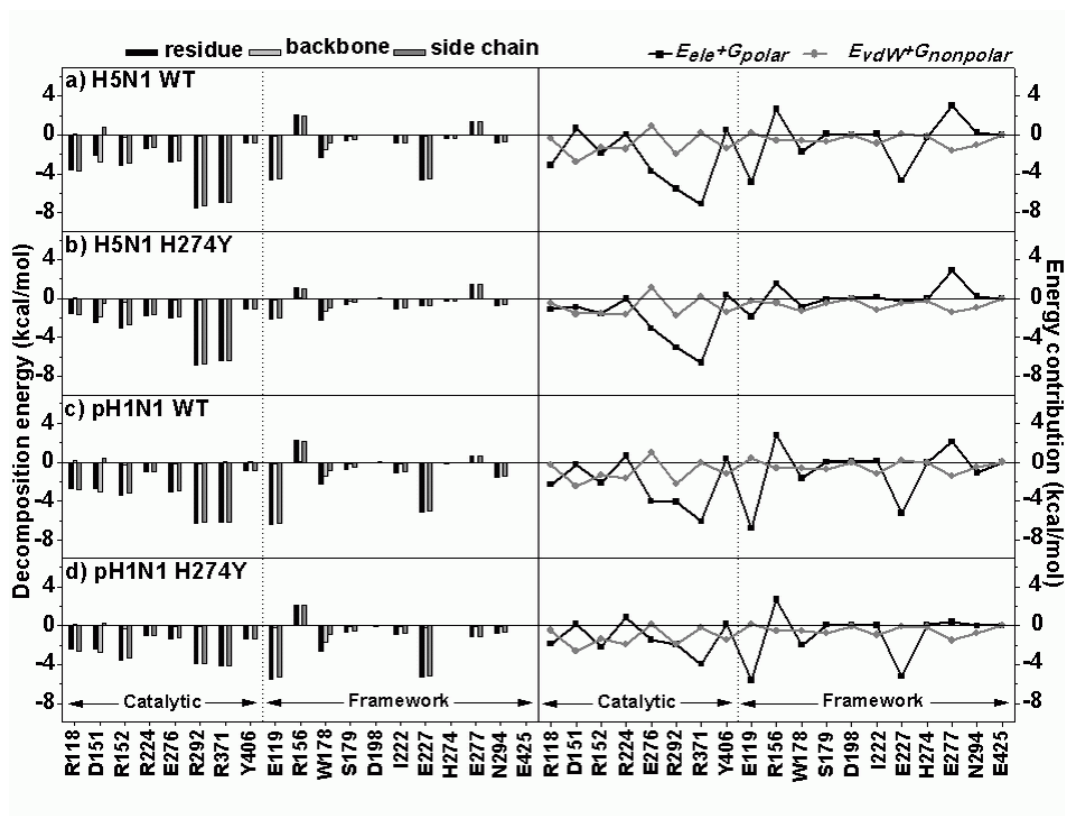


Figure 5.5 The (Left) decomposition of the binding free energy in pairwise per-residue basis, and its energy contributions from the backbone and side chain atoms, and (Right) the electrostatic and vdW energy

In the H274Y NA mutation, the laninamivir-NA interactions were apparently reduced to at least half-strength for H5N1 at the catalytic residue R118 and at the framework residues E119 and E227 (Fig. 5.5b, left), in accord with the observed decrease in the number and/or occupation of predicted hydrogen bonds (Fig. 5.5b). In some similar features, the situation is different for the pH1N1 H274Y NA mutant, in which the energy reduction was primarily found at the catalytic residue E276 (by ~ -2 kcal/mol) and a lowered interaction at the two conserved arginines R292 and R371 (energy increased to ~ -4 kcal/mol).

Taking into account the hydrogen bonding and per-residue binding free energy decomposition, the laninamivir-NA interactions were somewhat lowered in the H274Y NA isoform relative to that of the WT form both the H5N1 and pH1N1 viruses. This is in good agreement with the experimental evidence that shows slightly increased IC_{50} values, *i.e.*, 1.36-fold resistance for pH1N1 [177], and 3.4- and 7.5- fold resistance for H5N1 [178] compared to the WT (Table 5.1). However, most contributions to the laninamivir-NA were largely conserved. This information could support the high inhibitory potency of laninamivir against not only the wild type NA strain but also the H274Y mutant of the viral influenza subtypes H5N1 and H1N1.

5.5 CONCLUSIONS

MD simulations were applied to investigate the susceptibility of the WT and H274Y mutant isoforms of NA from the influenza A virus subtypes H5N1 and pH1N1 towards the NAi laninamivir, in terms of the structure and dynamic properties, drug-target interactions and binding pattern. The results show all the important interactions of laninamivir with NA are conserved. Indeed, even when histidine at the 274 position was transformed to tyrosine only slightly decreased interaction strength at some residues was observed (R118, W178 and R152). In comparison to oseltamivir, the laninamivir guanidinium and hydrophilic side chains are indispensable to lock the two framework residues (W178 and E227) and a catalytic residue (E276), respectively, better than those groups of oseltamivir at the relative positions. Most positive contributions to the interaction were found from the side chains of 7 of the catalytic NA residues (R118, D151, R152, R224, E276, R292 and R371), and 4 of the framework residues (E119, W178, E227 and E277), through electrostatic interactions and in particular salt bridge interactions and hydrogen bond formation. In contrast, in the

case of oseltamivir (the most widely used NAI anti-influenza drug), the important drug-target interactions were dramatically reduced and totally lost in the H274Y NA isoforms from the H5N1 and pH1N1 viral strains with a result of a high-level of resistance to oseltamivir. For the example, the oseltamivir interaction with W178 and R152 was significantly dwindled. This is, therefore, the likely explanation for the high susceptibility of both the WT and H274Y strains of H5N1 and pH1N1 viruses to laninamivir, in contrast to oseltamivir. However, it must be noted that only a single simulation was performed for each system, so the stability and preponderance of the interactions were unable to extrapolate conclusively. Based on overall data gained from the present study, the simulated results suggested that the drug hydrophilic moieties, $-\text{COO}^-$ and $-\text{NHC}(\text{NH}_2)_2^+$, are necessary for strong hydrogen bonding formation with NA, therefore modification on these groups may bring to a more powerful anti-influenza drugs. The replacement of the $-\text{COO}^-$ group by more negatively charged group such as phosphate or sulfonate possibly leads to higher interact with the conserved arginine triad, while the positively charged group might be lengthened in order to increase in drug-target interaction for the open 150-loop conformation of NA.

CHAPTER 6

CONCLUSIONS

Conventional MD simulation was applied to the NS3/4A protease of HCV binding to its inhibitors (boceprevir, telaprevir, danoprevir and BI201335) and the WT and H274Y variant neuraminidase of influenza A/H5N1 and A/pH1N1 viruses in order to investigate the drug-target interactions, binding efficiency, structural and dynamical properties. In addition, the potent inhibitor against NS3/4A protease was searched by pulling the 40 ZINC compounds from the drug binding pocket using the SMD approach based on the hypothesis that the higher force is needed for the stronger ligand binding. Thus the ligand that had a higher rupture force than the current NS3/4A inhibitors may serve as anti-HCV drug or used as a template for a further drug development. The QM/MM MD simulation, using semi-empirical SCC-DFTB level for describing the QM region and ff12SB AMBER force field for MM region, has also been employed to characterize and explore the reaction pathway of NS3/4A binding to boceprevir and telaprevir for both acylation and proton transfer.

For the MD calculation of the NS3/4A systems, all ligands were predominantly stabilized by the NS3 domain through van der Waals interactions suggested by the free energy contribution of individual residues, binding free energies from the MM/GBSA and MM/PBSA calculations. However, the hydrogen bonding interactions between ligand and surrounding residues are certainly important for the specificity in the ligand binding, especially for the hydrogen bond formation with A157 that has been conserved in all complexes. Altogether, the binding free energy calculation established the order of protease inhibitor susceptibilities is of danoprevir > BI201335 > boceprevir > telaprevir, which moderately agreed with the biological activities.

There are 9 top-hit compounds (ZINC ID **59500093**, **59784724**, **13527817**, **26660256**, **29482733**, **25977181**, **28005928**, **13527826** and **13471529**) out of 40 compounds exhibiting resemble susceptibility or higher than that of the 4 studied ligands. Especially, the first 2 compounds were predicted to have higher potential than the approved drugs (boceprevir and telaprevir). It is anticipated that these compounds may be used as NS3/4A inhibitor or be further used for drug development. Additionally, these top 9 compounds were also mainly stabilized via van der Waals interaction as the existing inhibitors. For the reaction mechanism of NS3/4A binding to boceprevir and telaprevir, it was found that the acylation reaction which is supposed to be the rate limiting step as in natural NS3/4A substrates was predicted to be occurred with the concerted manner in order to produce the tetrahedral intermediate. This result was calculated based on the SCC-DFTB/MM MD calculations. Comparing with the free energy of an intermediate, the estimated free energies barrier of the acylation are ~ 22.2 and ~ 20.1 kcal/mol for boceprevir and telaprevir binding, respectively, which quite agree with the experiment. Moreover, the acyl enzymes of both systems were predicted to be very stable compared with tetrahedral intermediate and Michaelis complex.

In the MD simulation of the 4 NA complexed with laninamivir, the results have shown that all essential interactions between NAs and laninamivir were mostly conserved, even H274 mutated to tyrosine showed only a slight decrease of interactions. On the contrary with NS3/4A, the ligand binding were largely contributed by electrostatic and salt-bridge interactions including hydrogen bond formation with the residues 118-119, 151-152, 178, 224, 227, 276, 292 and 371. Interestingly, several interactions were dramatically decreased in the H274Y mutant NA of H5N1 and

pH1N1 strains, therefore the highly efficient laninamivir can be served as anti-influenza drug for both WT and oseltamivir-resistant of H5N1 and pH1N1.



REFERENCES

- [1] Fried, M.W., Shiffman, M.L., Reddy, K.R., Smith, C., Marinos, G., Goncales, F.L., Jr., Haussinger, D., Diago, M., Carosi, G., Dhumeaux, D., Craxi, A., Lin, A., Hoffman, J. and Yu, J. Peginterferon alfa-2a plus ribavirin for chronic hepatitis C virus infection. **N. Engl. J. Med.** 347 (2002): 975-982.
- [2] Kiser, J.J., Burton, J.R., Anderson, P.L. and Everson, G.T. Review and management of drug interactions with boceprevir and telaprevir. **Hepatology** 55 (2012): 1620-1628.
- [3] Ramachandran, P., Fraser, A., Agarwal, K., Austin, A., Brown, A., Foster, G.R., Fox, R., Hayes, P.C., Leen, C., Mills, P.R., Mutimer, D.J., Ryder, S.D. and Dillon, J.F. UK consensus guidelines for the use of the protease inhibitors boceprevir and telaprevir in genotype 1 chronic hepatitis C infected patients. **Alimentary Pharmacology & Therapeutics** 35 (2012): 647-662.
- [4] Yi, M., Villanueva, R.A., Thomas, D.L., Wakita, T. and Lemon, S.M. Production of infectious genotype 1a hepatitis C virus (Hutchinson strain) in cultured human hepatoma cells. **Proc. Natl. Acad. Sci. U. S. A.** 103 (2006): 2310-2315.
- [5] Bostan, N. and Mahmood, T. An overview about hepatitis C: A devastating virus. **Crit. Rev. Microbiol.** 36 (2010): 91-133.
- [6] Lauer, G.M. and Walker, B.D. Hepatitis C virus infection. **N. Engl. J. Med.** 345 (2001): 41-52.
- [7] Scheel, T.K.H. and Rice, C.M. Understanding the hepatitis C virus life cycle paves the way for highly effective therapies. **Nature Medicine** 19 (2013): 837-849.
- [8] Lin, C. **HCV NS3-4A serine protease**. In: Hepatitis C viruses: Genomes and molecular biology, Tan, S.L. Ed., Horizon Bioscience, Norfolk, 2006, pp. 163-206.
- [9] McCoy, M.A., Senior, M.M., Gesell, J.J., Ramanathan, L. and Wyss, D.F. Solution structure and dynamics of the single-chain hepatitis C virus NS3 protease NS4A cofactor complex. **Journal of Molecular Biology** 305 (2001): 1099-1110.
- [10] Yan, Y., Li, Y., Munshi, S., Sardana, V., Cole, J.L., Sardana, M., Kuo, L.C., Chen, Z., Steinkuehler, C., Tomei, L. and Francesco, R.D. Complex of NS3 protease and NS4A peptide of BK strain hepatitis C virus: A 2.2 Å resolution structure in a hexagonal crystal form. **Protein Science** 7 (1998): 837-847.
- [11] Tong, L., Wengler, G. and Rossmann, M.G. Refined structure of sindbis virus core protein and comparison with other chymotrypsin-like serine proteinase structures. **J. Mol. Biol.** 230 (1993): 228-247.

- [12] Steinkühler, C., Biasiol, G., Brunetti, M., Urbani, A., Koch, U., Cortese, R., Pessi, A. and De Francesco, R. Product inhibition of the hepatitis C virus NS3 protease. **Biochemistry** 37 (1998): 8899-8905.
- [13] Frecer, V., Kabelac, M., De Nardi, P., Pricl, S. and Miertus, S. Structure-based design of inhibitors of NS3 serine protease of hepatitis C virus. **J. Mol. Graph. Model.** 22 (2004): 209-220.
- [14] Gallinari, P., Brennan, D., Nardi, C., Brunetti, M., Tomei, L., Steinkühler, C. and De Francesco, R. Multiple enzymatic activities associated with recombinant NS3 protein of hepatitis C virus. **J. Virol.** 72 (1998): 6758-6769.
- [15] Johansson, A., Hubatsch, I., Akerblom, E., Lindeberg, G., Winiwarer, S., Danielson, U.H. and Hallberg, A. Inhibition of hepatitis C virus NS3 protease activity by product-based peptides is dependent on helicase domain. **Bioorg. Med. Chem. Lett.** 11 (2001): 203-206.
- [16] Chu, H.M., Zhou, Y., Bartels, D.T., Khunvichai, A., Rao, B.G., Kwong, A.D. and Lin, C. Telaprevir (VX 950)-resistant variants exhibit reduced replication capacity compared to wild-type HCV in vivo and in vitro. **J. Hepatol.** 46 (2007): S230-S231.
- [17] Manns, M.P., Bourliere, M., Benhamou, Y., Pol, S., Bonacini, M., Trepo, C., Wright, D., Berg, T., Calleja, J.L., White, P.W., Stern, J.O., Steinmann, G., Yong, C.L., Kukolj, G., Scherer, J. and Boecher, W.O. Potency, safety, and pharmacokinetics of the NS3/4A protease inhibitor BI201335 in patients with chronic HCV genotype-1 infection. **J. Hepatol.** 54 (2011): 1114-1122.
- [18] Sarrazin, C. and Zeuzem, S. Resistance to direct antiviral agents in patients with hepatitis C virus infection. **Gastroenterology** 138 (2010): 447-462.
- [19] Kieffer, T.L., Sarrazin, C., Miller, J.S., Welker, M.W., Forestier, N., Reesink, H.W., Kwong, A.D. and Zeuzem, S. Telaprevir and pegylated interferon-alpha-2a inhibit wild-type and resistant genotype 1 hepatitis C virus replication in patients. **Hepatology** 46 (2007): 631-639.
- [20] Sarrazin, C., Kieffer, T.L., Bartels, D., Hanzelka, B., Muh, U., Welker, M., Wincheringer, D., Zhou, Y., Chu, H.M., Lin, C., Weegink, C., Reesink, H., Zeuzem, S. and Kwong, A.D. Dynamic hepatitis C virus genotypic and phenotypic changes in patients treated with the protease inhibitor telaprevir. **Gastroenterology** 132 (2007): 1767-1777.
- [21] Lin, C., Gates, C.A., Rao, B.G., Brennan, D.L., Fulghum, J.R., Luong, Y.P., Frantz, J.D., Lin, K., Ma, S., Wei, Y.Y., Perni, R.B. and Kwong, A.D. In vitro studies of cross-resistance mutations against two hepatitis C virus serine protease inhibitors, VX-950 and BILN 2061. **J. Biol. Chem.** 280 (2005): 36784-36791.

- [22] Guo, Z., Prongay, A., Tong, X., Fischmann, T., Bogen, S., Velazquez, F., Venkatraman, S., Njoroge, F.G. and Madison, V. Computational study of the effects of mutations A156T, D168V, and D168Q on the binding of HCV protease inhibitors. **J. Chem. Theory Comput.** 2 (2006): 1657-1663.
- [23] Rydberg, E.H., Cellucci, A., Bartholomew, L., Mattu, M., Barbato, G., Ludmerer, S.W., Graham, D.J., Altamura, S., Paonessa, G., De Francesco, R., Migliaccio, G. and Carfi, A. Structural basis for resistance of the genotype 2b hepatitis C virus NS5B polymerase to site a non-nucleoside inhibitors. **J. Mol. Biol.** 390 (2009): 1048-1059.
- [24] Tong, X., Bogen, S., Chase, R., Girijavallabhan, V., Guo, Z., Njoroge, F.G., Prongay, A., Saksena, A., Skelton, A., Xia, E. and Ralston, R. Characterization of resistance mutations against HCV ketoamide protease inhibitors. **Antiviral Res.** 77 (2008): 177-185.
- [25] Zhou, Y., Bartels, D.J., Hanzelka, B.L., Muh, U., Wei, Y., Chu, H.M., Tigges, A.M., Brennan, D.L., Rao, B.G., Swenson, L., Kwong, A.D. and Lin, C. Phenotypic characterization of resistant Val36 variants of hepatitis C virus NS3-4A serine protease. **Antimicrob. Agents Chemother.** 52 (2008): 110-120.
- [26] Lagace, L., White, P.W., Bousquet, C., Dansereau, N., Do, F., Llinas-Brunet, M., Marquis, M., Massariol, M.J., Maurice, R., Spickler, C., Thibeault, D., Triki, I., Zhao, S. and Kukolj, G. In vitro resistance profile of the hepatitis C virus NS3 protease inhibitor BI 201335. **Antimicrob. Agents Chemother.** 56 (2012): 569-572.
- [27] Susser, S., Welsch, C., Wang, Y., Zettler, M., Domingues, F.S., Karey, U., Hughes, E., Ralston, R., Tong, X., Herrmann, E., Zeuzem, S. and Sarrazin, C. Characterization of resistance to the protease inhibitor boceprevir in hepatitis C virus-infected patients. **Hepatology** 50 (2009): 1709-1718.
- [28] Lenz, O., Verbinnen, T., Lin, T.I., Vijgen, L., Cummings, M.D., Lindberg, J., Berke, J.M., Dehertogh, P., Fransen, E., Scholliers, A., Vermeiren, K., Ivens, T., Raboisson, P., Edlund, M., Storm, S., Vrang, L., de Kock, H., Fanning, G.C. and Simmen, K.A. In vitro resistance profile of the hepatitis C virus NS3/4A protease inhibitor TMC435. **Antimicrob. Agents Chemother.** 54 (2010): 1878-1887.
- [29] Rungrotmongkol, T., Yotmanee, P., Nunthaboot, N. and Hannongbua, S. Computational studies of influenza A virus at three important targets: hemagglutinin, neuraminidase and M2 protein. **Curr Pharm Des** 17 (2011): 1720-1739.
- [30] Emergence of a Novel Swine-Origin Influenza A (H1N1) Virus in Humans. **New England Journal of Medicine** 360 (2009): 2605-2615.
- [31] Neumann, G., Noda, T. and Kawaoka, Y. Emergence and pandemic potential of swine-origin H1N1 influenza virus. **Nature** 459 (2009): 931-939.

- [32] Webster, R.G. and Govorkova, E.A. H5N1 Influenza — Continuing Evolution and Spread. **New England Journal of Medicine** 355 (2006): 2174-2177.
- [33] Fiore, A.E., Fry, A., Shay, D., Gubareva, L., Bresee, J.S., Uyeki, T.M., Centers for Disease, C. and Prevention Antiviral agents for the treatment and chemoprophylaxis of influenza --- recommendations of the Advisory Committee on Immunization Practices (ACIP). **MMWR Recomm Rep** 60 (2011): 1-24.
- [34] Earhart, K.C., Elsayed, N.M., Saad, M.D., Gubareva, L.V., Nayel, A., Deyde, V.M., Abdelsattar, A., Abdelghani, A.S., Boynton, B.R., Mansour, M.M., Essmat, H.M., Klimov, A., Shuck-Lee, D., Monteville, M.R. and Tjaden, J.A. Oseltamivir resistance mutation N294S in human influenza A(H5N1) virus in Egypt. **J Infect Public Health** 2 (2009): 74-80.
- [35] Ferraris, O. and Lina, B. Mutations of neuraminidase implicated in neuraminidase inhibitors resistance. **Journal of Clinical Virology** 41 (2008): 13-19.
- [36] Hurt, A.C., Holien, J.K., Parker, M.W. and Barr, I.G. Oseltamivir resistance and the H274Y neuraminidase mutation in seasonal, pandemic and highly pathogenic influenza viruses. **Drugs** 69 (2009): 2523-2531.
- [37] van der Vries, E., Jonges, M., Herfst, S., Maaskant, J., Van der Linden, A., Guldemeester, J., Aron, G.I., Bestebroer, T.M., Koopmans, M., Meijer, A., Fouchier, R.A.M., Osterhaus, A.D.M.E., Boucher, C.A. and Schutten, M. Evaluation of a rapid molecular algorithm for detection of pandemic influenza A (H1N1) 2009 virus and screening for a key oseltamivir resistance (H275Y) substitution in neuraminidase. **Journal of Clinical Virology** 47 (2010): 34-37.
- [38] Koyama, K., Takahashi, M., Oitate, M., Nakai, N., Takakusa, H., Miura, S.-i. and Okazaki, O. CS-8958, a prodrug of the novel neuraminidase inhibitor R-125489, demonstrates a favorable long-retention profile in the mouse respiratory tract. **Antimicrob. Agents Chemother.** 53 (2009): 4845-4851.
- [39] Kubo, S., Tomozawa, T., Kakuta, M., Tokumitsu, A. and Yamashita, M. Laninamivir prodrug CS-8958, a long-acting neuraminidase inhibitor, shows superior anti-influenza virus activity after a single administration. **Antimicrob. Agents Chemother.** 54 (2010): 1256-1264.
- [40] Yamashita, M., Tomozawa, T., Kakuta, M., Tokumitsu, A., Nasu, H. and Kubo, S. CS-8958, a prodrug of the new neuraminidase inhibitor R-125489, shows long-acting anti-influenza virus activity. **Antimicrob. Agents Chemother.** 53 (2009): 186-192.
- [41] Moscona, A. Neuraminidase inhibitors for influenza. **N Engl J Med** 353 (2005): 1363-1373.

- [42] Russell, R.J., Haire, L.F., Stevens, D.J., Collins, P.J., Lin, Y.P., Blackburn, G.M., Hay, A.J., Gamblin, S.J. and Skehel, J.J. The structure of H5N1 avian influenza neuraminidase suggests new opportunities for drug design. **Nature** 443 (2006): 45-49.
- [43] Bianco, A., Brufani, M., Manna, F. and Melchioni, C. Synthesis of a carbocyclic sialic acid analogue for the inhibition of influenza virus neuraminidase. **Carbohydrate Research** 332 (2001): 23-31.
- [44] von Itzstein, M., Wu, W.Y., Kok, G.B., Pegg, M.S., Dyason, J.C., Jin, B., Van Phan, T., Smythe, M.L., White, H.F., Oliver, S.W. and et al. Rational design of potent sialidase-based inhibitors of influenza virus replication. **Nature** 363 (1993): 418-423.
- [45] Holzer, C.T., von Itzstein, M., Jin, B., Pegg, M.S., Stewart, W.P. and Wu, W.Y. Inhibition of sialidases from viral, bacterial and mammalian sources by analogues of 2-deoxy-2,3-didehydro-N-acetylneuraminic acid modified at the C-4 position. **Glycoconj J** 10 (1993): 40-44.
- [46] Lew, W., Chen, X. and Kim, C.U. Discovery and development of GS 4104 (oseltamivir): an orally active influenza neuraminidase inhibitor. **Curr Med Chem** 7 (2000): 663-672.
- [47] Gubareva, L.V., Webster, R.G. and Hayden, F.G. Comparison of the activities of zanamivir, oseltamivir, and RWJ-270201 against clinical isolates of influenza virus and neuraminidase inhibitor-resistant variants. **Antimicrob Agents Chemother** 45 (2001): 3403-3408.
- [48] Le, Q.M., Kiso, M., Someya, K., Sakai, Y.T., Nguyen, T.H., Nguyen, K.H., Pham, N.D., Ngyen, H.H., Yamada, S., Muramoto, Y., Horimoto, T., Takada, A., Goto, H., Suzuki, T., Suzuki, Y. and Kawaoka, Y. Avian flu: isolation of drug-resistant H5N1 virus. **Nature** 437 (2005): 1108.
- [49] Honda, T., Masuda, T., Yoshida, S., Arai, M., Kaneko, S. and Yamashita, M. Synthesis and anti-Influenza virus activity of 7-O-Alkylated derivatives related to zanamivir. **Bioorg. Med. Chem. Lett.** 12 (2002): 1925-1928.
- [50] Florin, E.L., Moy, V.T. and Gaub, H.E. Adhesion forces between individual ligand-receptor pairs. **Science** 264 (1994): 415-417.
- [51] Xu, Y., Shen, J., Luo, X., Silman, I., Sussman, J.L., Chen, K. and Jiang, H. How does huperzine A enter and leave the binding gorge of acetylcholinesterase? Steered molecular dynamics simulations. **J Am Chem Soc** 125 (2003): 11340-11349.
- [52] Warshel, A. and Levitt, M. Theoretical studies of enzymic reactions: dielectric, electrostatic and steric stabilization of the carbonium ion in the reaction of lysozyme. **J Mol Biol** 103 (1976): 227-249.

- [53] Lonsdale, R., Harvey, J.N. and Mulholland, A.J. A practical guide to modelling enzyme-catalysed reactions. **Chem Soc Rev** 41 (2012): 3025-3038.
- [54] Durantel, D., Escuret, V. and Zoulim, F. Current and emerging therapeutic approaches to hepatitis C infection. **Expert. Rev. Anti. Infect. Ther.** 1 (2003): 441-454.
- [55] Ferguson, M.C. Current therapies for chronic hepatitis C. **Pharmacotherapy** 31 (2010): 92-111.
- [56] Seiwert, S.D., Andrews, S.W., Jiang, Y., Serebryany, V., Tan, H., Kossen, K., Rajagopalan, P.T., Misialek, S., Stevens, S.K., Stoycheva, A., Hong, J., Lim, S.R., Qin, X., Rieger, R., Condroski, K.R., Zhang, H., Do, M.G., Lemieux, C., Hingorani, G.P., Hartley, D.P., Josey, J.A., Pan, L., Beigelman, L. and Blatt, L.M. Preclinical characteristics of the hepatitis C virus NS3/4A protease inhibitor ITMN-191 (R7227). **Antimicrob. Agents Chemother.** 52 (2008): 4432-4441.
- [57] White, P.W., Llinas-Brunet, M., Amad, M., Bethell, R.C., Bolger, G., Cordingley, M.G., Duan, J., Garneau, M., Lagace, L., Thibeault, D. and Kukolj, G. Preclinical characterization of BI 201335, a C-terminal carboxylic acid inhibitor of the hepatitis C virus NS3-NS4A protease. **Antimicrob. Agents Chemother.** 54 (2010): 4611-4618.
- [58] da Cunha, E.F.F., Ramalho, T.C., Taft, C.A. and de Alencastro, R.B. Computer-assisted analysis of the interactions of macrocyclic inhibitors with wild type and mutant D168A hepatitis C virus NS3 serine protease. **Lett. Drug. Des. Discov.** 3 (2006): 17-28.
- [59] Ontoria, J.M., Di Marco, S., Conte, I., Di Francesco, M.E., Gardelli, C., Koch, U., Matassa, V.G., Poma, M., Steinkühler, C., Volpari, C. and Harper, S. The design and enzyme-bound crystal structure of indoline based peptidomimetic inhibitors of hepatitis C virus NS3 protease. **J. Med. Chem.** 47 (2004): 6443-6446.
- [60] Wei, H.Y., Lu, C.S. and Lin, T.H. Exploring the P2 and P3 ligand binding features for hepatitis C virus NS3 protease using some 3D QSAR techniques. **J. Mol. Graph. Model.** 26 (2008): 1131-1144.
- [61] Xue, W., Wang, M., Jin, X., Liu, H. and Yao, X. Understanding the structural and energetic basis of inhibitor and substrate bound to the full-length NS3/4A: insights from molecular dynamics simulation, binding free energy calculation and network analysis. **Mol. Biosyst.** 8 (2012): 2753-2765.
- [62] Lin, K. Development of novel antiviral therapies for hepatitis C virus. **Viol. Sin.** 25 (2010): 246-266.
- [63] Lindenbach, B.D. and Rice, C.M. Unravelling hepatitis C virus replication from genome to function. **Nature** 436 (2005): 933-938.

- [64] Love, R.A., Parge, H.E., Wickersham, J.A., Hostomsky, Z., Habuka, N., Moomaw, E.W., Adachi, T. and Hostomska, Z. The crystal structure of hepatitis C virus NS3 proteinase reveals a trypsin-like fold and a structural zinc binding site. **Cell** 87 (1996): 331-342.
- [65] Lemke, C.T., Goudreau, N., Zhao, S., Hucke, O., Thibeault, D., Llinas-Brunet, M. and White, P.W. Combined X-ray, NMR, and kinetic analyses reveal uncommon binding characteristics of the hepatitis C virus NS3-NS4A protease inhibitor BI 201335. **J. Biol. Chem.** 286 (2011): 11434-11443.
- [66] Perni, R.B., Chandorkar, G., Cottrell, K.M., Gates, C.A., Lin, C., Lin, K., Luong, Y.-P., Maxwell, J.P., Murcko, M.A., Pitlik, J., Rao, G., Schairer, W.C., Drie, J.V. and Wei, Y. Inhibitors of hepatitis C virus NS3-4A protease. Effect of P4 capping groups on inhibitory potency and pharmacokinetics. **Bioorg. Med. Chem. Lett.** 17 (2007): 3406-3411.
- [67] Prongay, A.J., Guo, Z., Yao, N., Pichardo, J., Fischmann, T., Strickland, C., Myers, J., Weber, P.C., Beyer, B.M., Ingram, R., Hong, Z., Prosise, W.W., Ramanathan, L., Taremi, S.S., Yarosh-Tomaine, T., Zhang, R., Senior, M., Yang, R.-S., Malcolm, B., Arasappan, A., Bennett, F., Bogen, S.L., Chen, K., Jao, E., Liu, Y.-T., Lovey, R.G., Saxena, A.K., Venkatraman, S., Girijavallabhan, V., Njoroge, F.G. and Madison, V. Discovery of the HCV NS3/4A protease inhibitor (1R,5S)-N-[3-amino-1-(cyclobutylmethyl)-2,3-dioxopropyl]-3-[2(S)-[[[(1,1-dimethylethyl)amino]carbonyl]amino]-3,3-dimethyl-1-oxobutyl]-6,6-dimethyl-3-azabicyclo[3.1.0]hexan-2(S)-carboxamide (Sch 503034) II. Key steps in structure-based optimization. **J. Med. Chem.** 50 (2007): 2310-2318.
- [68] Perz, J.F., Armstrong, G.L., Farrington, L.A., Hutin, Y.J. and Bell, B.P. The contributions of hepatitis B virus and hepatitis C virus infections to cirrhosis and primary liver cancer worldwide. **J. Hepatol.** 45 (2006): 529-538.
- [69] Decha, P., Rungrotmongkol, T., Intharathep, P., Malaisree, M., Aruksakunwong, O., Laohpongspaisan, C., Parasuk, V., Sompornpisut, P., Pianwanit, S., Kokpol, S. and Hannongbua, S. Source of high pathogenicity of an avian influenza virus H5N1: Why H5 is better cleaved by furin. **Biophys. J.** 95 (2008): 128-134.
- [70] Rungrotmongkol, T., Decha, P., Sompornpisut, P., Malaisree, M., Intharathep, P., Nunthaboot, N., Udommaneethanakit, T., Aruksakunwong, O. and Hannongbua, S. Combined QM/MM mechanistic study of the acylation process in furin complexed with the H5N1 avian influenza virus hemagglutinin's cleavage site. **Proteins: Struct., Funct., Bioinf.** 76 (2009): 62-71.
- [71] De Francesco, R. and Steinkuhler, C. Structure and function of the hepatitis C virus NS3-NS4A serine proteinase. **Curr. Top. Microbiol. Immunol.** 242 (2000): 149-169.

- [72] Case, D.A., Cheatham, T.E., Darden, T., Gohlke, H., Luo, R., Merz, K.M., Onufriev, A., Simmerling, C., Wang, B. and Woods, R.J. The amber biomolecular simulation programs. **J. Comput. Chem.** 26 (2005): 1668-1688.
- [73] Olsson, M.H.M., Søndergaard, C.R., Rostkowski, M. and Jensen, J.H. PROPKA3: Consistent treatment of internal and surface residues in empirical pKa predictions. **J. Chem. Theory Comput.** 7 (2011): 525-537.
- [74] Duan, Y., Wu, C., Chowdhury, S., Lee, M.C., Xiong, G., Zhang, W., Yang, R., Cieplak, P., Luo, R., Lee, T., Caldwell, J., Wang, J. and Kollman, P. A point-charge force field for molecular mechanics simulations of proteins based on condensed-phase quantum mechanical calculations. **J. Comput. Chem.** 24 (2003): 1999-2012.
- [75] Frisch, M.J., Trucks, G.W., Schlegel, H.B., Scuseria, G.E., Robb, M.A., Cheeseman, J.R., Montgomery, J.A., Jr., Vreven, T., Kudin, K.N., Burant, J.C., Millam, J.M., Iyengar, S.S., Tomasi, J., Barone, V., Mennucci, B., Cossi, M., Scalmani, G., Rega, N., Petersson, G.A., Nakatsuji, H., Hada, M., Ehara, M., Toyota, K., Fukuda, R., Hasegawa, J., Ishida, M., Nakajima, T., Honda, Y., Kitao, O., Nakai, H., Klene, M., Li, X., Knox, J.E., Hratchian, H.P., Cross, J.B., Bakken, V., Adamo, C., Jaramillo, J., Gomperts, R., Stratmann, R.E., Yazyev, O., Austin, A.J., Cammi, R., Pomelli, C., Ochterski, J.W., Ayala, P.Y., Morokuma, K., Voth, G.A., Salvador, P., Dannenberg, J.J., Zakrzewski, V.G., Dapprich, S., Daniels, A.D., Strain, M.C., Farkas, O., Malick, D.K., Rabuck, A.D., Raghavachari, K., Foresman, J.B., Ortiz, J.V., Cui, Q., Baboul, A.G., Clifford, S., Cioslowski, J., Stefanov, B.B., Liu, G., Liashenko, A., Piskorz, P., Komaromi, I., Martin, R.L., Fox, D.J., Keith, T., Al-Laham, M.A., Peng, C.Y., Nanayakkara, A., Challacombe, M., Gill, P.M.W., Johnson, B., Chen, W., Wong, M.W., Gonzalez, C. and Pople, J.A. **Gaussian 03, Revision C.02**. Wallingford CT, Gaussian, Inc., 2004.
- [76] Wang, J., Wolf, R.M., Caldwell, J.W., Kollman, P.A. and Case, D.A. Development and testing of a general amber force field. **J. Comput. Chem.** 25 (2004): 1157-1174.
- [77] Jorgensen, W.L., Chandrasekhar, J., Madura, J.D., Impey, R.W. and Klein, M.L. Comparison of simple potential functions for simulating liquid water. **J. Chem. Phys.** 79 (1983): 926-935.
- [78] Ryckaert, J.-P., Ciccotti, G. and Berendsen, H.J.C. Numerical integration of the cartesian equations of motion of a system with constraints: molecular dynamics of n-alkanes. **J. Comput. Phys.** 23 (1977): 327-341.
- [79] York, D.M., Darden, T.A. and Pedersen, L.G. The Effect of Long-Range Electrostatic Interactions in Simulations of Macromolecular Crystals - a Comparison of the Ewald and Truncated List Methods. **J. Chem. Phys.** 99 (1993): 8345-8348.

- [80] Hou, T., Wang, J., Li, Y. and Wang, W. Assessing the performance of the MM/PBSA and MM/GBSA methods. 1. The accuracy of binding free energy calculations based on molecular dynamics simulations. **J. Chem. Inf. Model.** 51 (2011): 69-82.
- [81] Kaiyawet, N., Rungrotmongkol, T. and Hannongbua, S. Effect of halogen substitutions on dUMP to stability of thymidylate synthase/dUMP/mTHF ternary complex using molecular dynamics simulation. **J. Chem. Inf. Model.** 53 (2013): 1315-1323.
- [82] Khuntawee, W., Rungrotmongkol, T. and Hannongbua, S. Molecular dynamic behavior and binding affinity of flavonoid analogues to the cyclin dependent kinase 6/cyclin D complex. **J. Chem. Inf. Model.** 52 (2012): 76-83.
- [83] Li, X., Zhang, W., Qiao, X. and Xu, X. Prediction of binding for a kind of non-peptic HCV NS3 serine protease inhibitors from plants by molecular docking and MM/PBSA method. **Bioorg. Med. Chem.** 15 (2007): 220-226.
- [84] Meeprasert, A., Khuntawee, W., Kamlungso, K., Nunthaboot, N., Rungrotmongkol, T. and Hannongbua, S. Binding pattern of the long acting neuraminidase inhibitor laninamivir towards influenza A subtypes H5N1 and pandemic H1N1. **J. Mol. Graph. Model.** 38 (2012): 148-154.
- [85] Rungrotmongkol, T., Nunthaboot, N., Malaisree, M., Kaiyawet, N., Yotmanee, P., Meeprasert, A. and Hannongbua, S. Molecular insight into the specific binding of ADP-ribose to the nsP3 macro domains of chikungunya and venezuelan equine encephalitis viruses: Molecular dynamics simulations and free energy calculations. **J. Mol. Graphics Modell.** 29 (2010): 347-353.
- [86] Gohlke, H. and Case, D.A. Converging free energy estimates: MM-PB(GB)SA studies on the protein-protein complex Ras-Raf. **J. Comput. Chem.** 25 (2004): 238-250.
- [87] Kollman, P.A., Massova, I., Reyes, C., Kuhn, B., Huo, S., Chong, L., Lee, M., Lee, T., Duan, Y., Wang, W., Donini, O., Cieplak, P., Srinivasan, J., Case, D.A. and Cheatham, T.E. Calculating structures and free energies of complex molecules: Combining molecular mechanics and continuum models. **Acc. Chem. Res.** 33 (2000): 889-897.
- [88] Prongay, A.J., Guo, Z., Yao, N., Pichardo, J., Fischmann, T., Strickland, C., Myers, J., Weber, P.C., Beyer, B.M., Ingram, R., Hong, Z., Prosise, W.W., Ramanathan, L., Taremi, S.S., Yarosh-Tomaine, T., Zhang, R., Senior, M., Yang, R.-S., Malcolm, B., Arasappan, A., Bennett, F., Bogen, S.L., Chen, K., Jao, E., Liu, Y.-T., Lovey, R.G., Saksena, A.K., Venkatraman, S., Girijavallabhan, V., Njoroge, F.G. and Madison, V. Discovery of the HCV NS3/4A protease inhibitor (1R,5S)-N-[3-amino-1-(cyclobutylmethyl)- 2,3-dioxopropyl]-3-[2(S)-[[[(1,1- dimethylethyl)amino]carbonyl]amino]- 3,3-dimethyl-1-

- oxobutyl]-6,6-dimethyl-3-azabicyclo [3.1.0] hexan-2(S)-carboxamide (Sch 503034) II. Key steps in structure-based optimization. **J. Med. Chem.** 50 (2007): 2310-2318.
- [89] Romano, K.P., Ali, A., Aydin, C., Soumana, D., Ozen, A., Deveau, L.M., Silver, C., Cao, H., Newton, A., Petropoulos, C.J., Huang, W. and Schiffer, C.A. The molecular basis of drug resistance against hepatitis C virus NS3/4A protease inhibitors. **PLoS Pathog.** 8 (2012): e1002832.
- [90] Xue, W., Pan, D., Yang, Y., Liu, H. and Yao, X. Molecular modeling study on the resistance mechanism of HCV NS3/4A serine protease mutants R155K, A156V and D168A to TMC435. **Antiviral Res.** 93 (2012): 126-137.
- [91] Hansson, T., Oostenbrink, C. and van Gunsteren, W. Molecular dynamics simulations. **Curr. Opin. Struct. Biol.** 12 (2002): 190-196.
- [92] Karplus, M. and Petsko, G.A. Molecular dynamics simulations in biology. **Nature** 347 (1990): 631-639.
- [93] Simmonds, P. The origin of hepatitis C virus. **Curr. Top. Microbiol. Immunol.** 369 (2013): 1-15.
- [94] van Gunsteren, W.F. and Berendsen, H.J.C. Computer simulation of molecular dynamics: Methodology, applications, and perspectives in chemistry. **Angew. Chem., Int. Ed. Engl.** 29 (1990): 992-1023.
- [95] Chevaliez, S., Bouvier-Alias, M., Brillet, R. and Pawlotsky, J.-M. Hepatitis C virus (HCV) genotype 1 subtype identification in new HCV drug development and future clinical practice. **PLoS One** 4 (2009): e8209.
- [96] Simmonds, P. Genetic diversity and evolution of hepatitis C virus – 15 years on. **J. Gen. Virol.** 85 (2004): 3173-3188.
- [97] Simmonds, P., Bukh, J., Combet, C., Deleage, G., Enomoto, N., Feinstone, S., Halfon, P., Inchauspe, G., Kuiken, C., Maertens, G., Mizokami, M., Murphy, D.G., Okamoto, H., Pawlotsky, J.M., Penin, F., Sablon, E., Shin, I.T., Stuyver, L.J., Thiel, H.J., Viazov, S., Weiner, A.J. and Widell, A. Consensus proposals for a unified system of nomenclature of hepatitis C virus genotypes. **Hepatology** 42 (2005): 962-973.
- [98] Manns, M.P., McHutchison, J.G., Gordon, S.C., Rustgi, V.K., Shiffman, M., Reindollar, R., Goodman, Z.D., Koury, K., Ling, M.-H. and Albrecht, J.K. Peginterferon alfa-2b plus ribavirin compared with interferon alfa-2b plus ribavirin for initial treatment of chronic hepatitis C: A randomised trial. **Lancet** 358 (2001): 958-965.
- [99] Cummings, M.D., Lindberg, J., Lin, T.-I., de Kock, H., Lenz, O., Lilja, E., Felländer, S., Baraznenok, V., Nyström, S., Nilsson, M., Vrang, L., Edlund, M., Rosenquist, Å., Samuelsson, B., Raboisson, P. and Simmen, K. Induced-fit binding of the macrocyclic

- noncovalent inhibitor TMC435 to its HCV NS3/NS4A protease target. **Angew. Chem. Int. Ed.** 49 (2010): 1652-1655.
- [100] Romano, K.P., Ali, A., Royer, W.E. and Schiffer, C.A. Drug resistance against HCV NS3/4A inhibitors is defined by the balance of substrate recognition versus inhibitor binding. **Proc. Natl. Acad. Sci.** 107 (2010): 20986-20991.
- [101] McHutchison, J.G. and Patel, K. Future therapy of hepatitis C. **Hepatology** 36 (2002): s245-s252.
- [102] Lamarre, D., Anderson, P.C., Bailey, M., Beaulieu, P., Bolger, G., Bonneau, P., Bos, M., Cameron, D.R., Cartier, M., Cordingley, M.G., Faucher, A.-M., Goudreau, N., Kawai, S.H., Kukolj, G., Lagace, L., LaPlante, S.R., Narjes, H., Poupert, M.-A., Rancourt, J., Sentjens, R.E., St George, R., Simoneau, B., Steinmann, G., Thibeault, D., Tsantrizos, Y.S., Weldon, S.M., Yong, C.-L. and Llinas-Brunet, M. An NS3 protease inhibitor with antiviral effects in humans infected with hepatitis C virus. **Nature** 426 (2003): 186-189.
- [103] Llinàs-Brunet, M., Bailey, M., Fazal, G., Goulet, S., Halmos, T., Laplante, S., Maurice, R., Poirier, M., Poupert, M.-A., Thibeault, D., Wernic, D. and Lamarre, D. Peptide-based inhibitors of the hepatitis C virus serine protease. **Bioorg. Med. Chem. Lett.** 8 (1998): 1713-1718.
- [104] Shu-Hui, C., Jason, L., Yvonne, Y., Frantz, V., Robert, B.J., Wang, Q.M., John, I.G., Beverly, H., Joseph, C., Deqi, G., Mark, T. and John, E.M. P1 and P1; optimization of 3,4-bicycloproline P2 incorporated tetrapeptidyl alpha-ketoamide based HCV protease inhibitors. **Lett. Drug Des. Discovery** 2 (2005): 118-123.
- [105] Urbani, A., Bianchi, E., Narjes, F., Tramontano, A., De Francesco, R., Steinkühler, C. and Pessi, A. Substrate specificity of the hepatitis C virus serine protease NS3. **J. Biol. Chem.** 272 (1997): 9204-9209.
- [106] Yao, N., Reichert, P., Taremi, S.S., Prosser, W.W. and Weber, P.C. Molecular views of viral polyprotein processing revealed by the crystal structure of the hepatitis C virus bifunctional protease-helicase. **Structure** 7 (1999): 1353-1363.
- [107] Pan, D., Xue, W., Zhang, W., Liu, H. and Yao, X. Understanding the drug resistance mechanism of hepatitis C virus NS3/4A to ITMN-191 due to R155K, A156V, D168A/E mutations: A computational study. **Biochim. Biophys. Acta.** 1820 (2012): 1526-1534.
- [108] Sheng, X.C., Casarez, A., Cai, R., Clarke, M.O., Chen, X., Cho, A., Delaney IV, W.E., Doerffler, E., Ji, M., Mertzman, M., Pakdaman, R., Pyun, H.-J., Rowe, T., Wu, Q., Xu, J. and Kim, C.U. Discovery of GS-9256: A novel phosphinic acid derived inhibitor of the hepatitis C virus NS3/4A protease with potent clinical activity. **Bioorg. Med. Chem. Lett.** 22 (2012): 1394-1396.

- [109] Zhu, J., Li, Y., Yu, H., Zhang, L., Mao, X. and Hou, T. Insight into the structural requirements of narlaprevir-type inhibitors of NS3/NS4A protease based on HQSAR and molecular field analyses. **Comb. Chem. High Throughput Screen.** 15 (2012): 439-450.
- [110] Barbato, G., Cicero, D.O., Cordier, F., Narjes, F., Gerlach, B., Sambucini, S., Grzesiek, S., Matassa, V.G., De Francesco, R. and Bazzo, R. Inhibitor binding induces active site stabilization of the HCV NS3 protein serine protease domain. **EMBO J.** 19 (2000): 1195-1206.
- [111] McCoy, M.A., Senior, M.M., Gesell, J.J., Ramanathan, L. and Wyss, D.F. Solution structure and dynamics of the single-chain hepatitis C virus NS3 protease NS4A cofactor complex. **J. Mol. Biol.** 305 (2001): 1099-1110.
- [112] Franciscus, A. Hepatitis C treatments in current clinical development. Hepatitis C Support Project, 2012.
- [113] Martinez, A. and Gish, R.G. **Future of allopathic hepatitis C treatment.** In: Hepatitis C choice, Tina M. St. John, M., Sandt, L. Eds., Caring Ambassadors Program, Inc., 2008, pp. 150.
- [114] Laohpongspaisan, C., Rungrotmongkol, T., Intharathep, P., Malaisree, M., Decha, P., Aruksakunwong, O., Sompornpisut, P. and Hannongbua, S. Why amantadine loses its function in influenza m2 mutants: MD simulations. **J. Chem. Inf. Model.** 49 (2009): 847-852.
- [115] Rungrotmongkol, T., Frecer, V., De-Eknamkul, W., Hannongbua, S. and Miertus, S. Design of oseltamivir analogs inhibiting neuraminidase of avian influenza virus H5N1. **Antiviral Res.** 82 (2009): 51-58.
- [116] Rungrotmongkol, T., Udommaneethanakit, T., Frecer, V. and Miertus, S. Combinatorial design of avian influenza neuraminidase inhibitors containing pyrrolidine core with a reduced susceptibility to viral drug resistance. **Comb. Chem. High Throughput Screen** 13 (2010): 268-277.
- [117] Lee, V.S., Nimmanpipug, P., Aruksakunwong, O., Promsri, S., Sompornpisut, P. and Hannongbua, S. Structural analysis of lead fullerene-based inhibitor bound to human immunodeficiency virus type 1 protease in solution from molecular dynamics simulations. **J. Mol. Graph. Model.** 26 (2007): 558-570.
- [118] Punkvang, A., Saparpakorn, P., Hannongbua, S., Wolschann, P., Beyer, A. and Pungpo, P. Investigating the structural basis of arylamides to improve potency against M. tuberculosis strain through molecular dynamics simulations. **Eur. J. Med. Chem.** 45 (2010): 5585-5593.

- [119] Arasappan, A., Bennett, F., Bogen, S.L., Venkatraman, S., Blackman, M., Chen, K.X., Hendrata, S., Huang, Y., Huelgas, R.M., Nair, L., Padilla, A.I., Pan, W., Pike, R., Pinto, P., Ruan, S., Sannigrahi, M., Velazquez, F., Vibulbhan, B., Wu, W., Yang, W., Saksena, A.K., Girijavallabhan, V., Shih, N.-Y., Kong, J., Meng, T., Jin, Y., Wong, J., McNamara, P., Prongay, A., Madison, V., Piwinski, J.J., Cheng, K.-C., Morrison, R., Malcolm, B., Tong, X., Ralston, R. and Njoroge, F.G. Discovery of narlaprevir (SCH 900518): A potent, second generation HCV NS3 serine protease inhibitor. **ACS Med. Chem. Lett.** 1 (2010): 64-69.
- [120] Bogen, S.L., Arasappan, A., Bennett, F., Chen, K., Jao, E., Liu, Y.-T., Lovey, R.G., Venkatraman, S., Pan, W., Parekh, T., Pike, R.E., Ruan, S., Liu, R., Baroudy, B., Agrawal, S., Chase, R., Ingravallo, P., Pichardo, J., Prongay, A., Brisson, J.-M., Hsieh, T.Y., Cheng, K.-C., Kemp, S.J., Levy, O.E., Lim-Wilby, M., Tamura, S.Y., Saksena, A.K., Girijavallabhan, V. and Njoroge, F.G. Discovery of SCH446211 (SCH6): A new ketoamide inhibitor of the HCV NS3 serine protease and HCV subgenomic RNA replication. **J. Med. Chem.** 49 (2006): 2750-2757.
- [121] Han, W., Hu, Z., Jiang, X. and Decicco, C.P. α -Ketoamides, α -ketoesters and α -diketones as HCV NS3 protease inhibitors. **Bioorg. Med. Chem. Lett.** 10 (2000): 711-713.
- [122] Yip, Y., Victor, F., Lamar, J., Johnson, R., Wang, Q.M., Barket, D., Glass, J., Jin, L., Liu, L., Venable, D., Wakulchik, M., Xie, C., Heinz, B., Villarreal, E., Colacino, J., Yumibe, N., Tebbe, M., Munroe, J. and Chen, S.-H. Discovery of a novel bicycloproline P2 bearing peptidyl α -ketoamide LY514962 as HCV protease inhibitor. **Bioorg. Med. Chem. Lett.** 14 (2004): 251-256.
- [123] Bogen, S.L., Arasappan, A., Velazquez, F., Blackman, M., Huelgas, R., Pan, W., Siegel, E., Nair, L.G., Venkatraman, S., Guo, Z., Doll, R., Shih, N.-Y. and George Njoroge, F. Discovery of potent sulfonamide P4-capped ketoamide second generation inhibitors of hepatitis C virus NS3 serine protease with favorable pharmacokinetic profiles in preclinical species. **Bioorg. Med. Chem.** 18 (2010): 1854-1865.
- [124] Chen, K.X., Nair, L., Vibulbhan, B., Yang, W., Arasappan, A., Bogen, S.L., Venkatraman, S., Bennett, F., Pan, W., Blackman, M.L., Padilla, A.I., Prongay, A., Cheng, K.C., Tong, X., Shih, N.Y. and Njoroge, F.G. Second-generation highly potent and selective inhibitors of the hepatitis C virus NS3 serine protease. **J. Med. Chem.** 52 (2009): 1370-1379.
- [125] Nair, L.G., Bogen, S., Ruan, S., Pan, W., Pike, R., Tong, X., Cheng, K.-C., Guo, Z., Doll, R.J. and Njoroge, F.G. Towards the second generation of boceprevir: Dithianes as an alternative P2 substituent for 2,2-dimethyl cyclopropyl proline in HCV NS3 protease inhibitors. **Bioorg. Med. Chem. Lett.** 20 (2010): 1689-1692.

- [126] Nair, L.G., Sannigrahi, M., Bogen, S., Pinto, P., Chen, K.X., Prongay, A., Tong, X., Cheng, K.C., Girijavallabhan, V. and George Njoroge, F. P4 capped amides and lactams as HCV NS3 protease inhibitors with improved potency and DMPK profile. **Bioorg. Med. Chem. Lett.** 20 (2010): 567-570.
- [127] Velázquez, F., Sannigrahi, M., Bennett, F., Lovey, R.G., Arasappan, A., Bogen, S.p., Nair, L., Venkatraman, S., Blackman, M., Hendrata, S., Huang, Y., Huelgas, R., Pinto, P., Cheng, K.-C., Tong, X., McPhail, A.T. and Njoroge, F.G. Cyclic sulfones as novel P3-caps for hepatitis C virus NS3/4A (HCV NS3/4A) protease inhibitors: Synthesis and evaluation of inhibitors with improved potency and pharmacokinetic profiles. **J. Med. Chem.** 53 (2010): 3075-3085.
- [128] Venkatraman, S., Blackman, M., Wu, W., Nair, L., Arasappan, A., Padilla, A., Bogen, S., Bennett, F., Chen, K., Pichardo, J., Tong, X., Prongay, A., Cheng, K.-C., Girijavallabhan, V. and George Njoroge, F. Discovery of novel P3 sulfonamide-capped inhibitors of HCV NS3 protease. Inhibitors with improved cellular potencies. **Bioorg. Med. Chem.** 17 (2009): 4486-4495.
- [129] Venkatraman, S., Velazquez, F., Wu, W., Blackman, M., Madison, V. and Njoroge, F.G. Potent ketoamide inhibitors of HCV NS3 protease derived from quaternized P1 groups. **Bioorg. Med. Chem. Lett.** 20 (2010): 2151-2155.
- [130] Plewczynski, D., Łaźniewski, M., Augustyniak, R. and Ginalski, K. Can we trust docking results? Evaluation of seven commonly used programs on PDBbind database. **J. Comput. Chem.** 32 (2011): 742-755.
- [131] Wang, R., Lu, Y., Fang, X. and Wang, S. An extensive test of 14 scoring functions using the PDBbind refined set of 800 protein–ligand complexes. **J. Chem. Inf. Comput. Sci.** 44 (2004): 2114-2125.
- [132] Ismail, N.S., El Dine, R.S., Hattori, M., Takahashi, K. and Ihara, M. Computer based design, synthesis and biological evaluation of novel indole derivatives as HCV NS3-4A serine protease inhibitors. **Bioorg. Med. Chem.** 16 (2008): 7877-7887.
- [133] Takaya, D., Yamashita, A., Kamijo, K., Gomi, J., Ito, M., Maekawa, S., Enomoto, N., Sakamoto, N., Watanabe, Y., Arai, R., Umeyama, H., Honma, T., Matsumoto, T. and Yokoyama, S. A new method for induced fit docking (GENIUS) and its application to virtual screening of novel HCV NS3-4A protease inhibitors. **Bioorg. Med. Chem.** 19 (2011): 6892-6905.
- [134] Arad-Haase, G., Chuartzman, S.G., Dagan, S., Nevo, R., Kouza, M., Mai, B.K., Nguyen, H.T., Li, M.S. and Reich, Z. Mechanical unfolding of acylphosphatase studied by single-molecule force spectroscopy and MD simulations. **Biophys. J.** 99 (2010): 238-247.

- [135] Arsawang, U., Saengsawang, O., Rungrotmongkol, T., Sornmee, P., Wittayanarakul, K., Remsungnen, T. and Hannongbua, S. How do carbon nanotubes serve as carriers for gemcitabine transport in a drug delivery system? **J. Mol. Graphics Modell.** 29 (2011): 591-596.
- [136] Mai, B.K., Viet, M.H. and Li, M.S. Top leads for swine influenza A/H1N1 virus revealed by steered molecular dynamics approach. **J. Chem. Inf. Model.** 50 (2010): 2236-2247.
- [137] Shen, Z., Cheng, F., Xu, Y., Fu, J., Xiao, W., Shen, J., Liu, G., Li, W. and Tang, Y. Investigation of indazole unbinding pathways in CYP2E1 by molecular dynamics simulations. **PLoS One** 7 (2012): e33500.
- [138] Rungrotmongkol, T., Udommaneethanakit, T., Malaisree, M., Nunthaboot, N., Intharathep, P., Sompornpisut, P. and Hannongbua, S. How does each substituent functional group of oseltamivir lose its activity against virulent H5N1 influenza mutants? **Biophys. Chem.** 145 (2009): 29-36.
- [139] Sornmee, P., Rungrotmongkol, T., Saengsawang, O., Arsawang, U., Remsungnen, T. and Hannongbua, S. Understanding the molecular properties of doxorubicin filling inside and wrapping outside single-walled carbon nanotubes. **J. Comput. Theor. Nanos.** 8 (2011): 1385-1391.
- [140] Case, D.A., Darden, T.A., Cheatham III, T.E., Simmerling, C.L., Wang, J., Duke, R.E., Luo, R., Crowley, M., Walker, R.C., Zhang, W., Merz, K.M., Wang, B., Hayik, S., Roitberg, A., Seabra, G., Kolossváry, I., Wong, K.F., Paesani, F., Vanicek, J., Wu, X., Brozell, S.R., Steinbrecher, T., Gohlke, H., Yang, L., Tan, C., Mongan, J., Hornak, V., Cui, G., Mathews, D.H., Seetin, M.G., Sagui, C., Babin, V. and Kollman, P.A. AMBER 10. University of California, San Francisco, 2008.
- [141] Sousa da Silva, A.W. and Vranken, W.F. ACPYPE - AnteChamber PYthon Parser interface. **BMC Res. Notes** 5 (2012): 367.
- [142] Irwin, J.J. and Shoichet, B.K. ZINC – A free database of commercially available compounds for virtual screening. **J. Chem. Inf. Model.** 45 (2004): 177-182.
- [143] Korb, O., Stützel, T. and Exner, T.E. Empirical scoring functions for advanced protein–ligand docking with PLANTS. **J. Chem. Inf. Model.** 49 (2009): 84-96.
- [144] Hess, B., Kutzner, C., van der Spoel, D. and Lindahl, E. GROMACS 4: Algorithms for highly efficient, load-balanced, and scalable molecular simulation. **J. Chem. Theory Comput.** 4 (2008): 435-447.
- [145] Van Der Spoel, D., Lindahl, E., Hess, B., Groenhof, G., Mark, A.E. and Berendsen, H.J. GROMACS: Fast, flexible, and free. **J. Comput. Chem.** 26 (2005): 1701-1718.

- [146] Hess, B., Bekker, H., Berendsen, H.J.C. and Fraaije, J.G.E.M. LINCS: A linear constraint solver for molecular simulations. **J. Comput. Chem.** 18 (1997): 1463-1472.
- [147] Darden, T., York, D. and Pedersen, L. Particle mesh ewald: An $N \cdot \log(N)$ method for ewald sums in large systems. **J. Chem. Phys.** 98 (1993): 10089-10092.
- [148] Essmann, U., Perera, L., Berkowitz, M.L., Darden, T., Lee, H. and Pedersen, L.G. A smooth particle mesh ewald method. **J. Chem. Phys.** 103 (1995): 8577-8593.
- [149] Chovancova, E., Pavelka, A., Benes, P., Strnad, O., Brezovsky, J., Kozlikova, B., Gora, A., Sustr, V., Klvana, M., Medek, P., Biedermannova, L., Sochor, J. and Damborsky, J. CAVER 3.0: A tool for the analysis of transport pathways in dynamic protein structures. **PLoS Comput. Biol.** 8 (2012): e1002708.
- [150] Petrek, M., Otyepka, M., Banas, P., Kosinova, P., Koca, J. and Damborsky, J. CAVER: A new tool to explore routes from protein clefts, pockets and cavities. **BMC Bioinformatics** 7 (2006): 316.
- [151] Kumar, S. and Li, M.S. Biomolecules under mechanical force. **Phys. Rep.** 486 (2010): 1-74.
- [152] Carrion-Vazquez, M., Li, H., Lu, H., Marszalek, P.E., Oberhauser, A.F. and Fernandez, J.M. The mechanical stability of ubiquitin is linkage dependent. **Nat. Struct. Biol.** 10 (2003): 738-743.
- [153] Kitchen, D.B., Decornez, H., Furr, J.R. and Bajorath, J. Docking and scoring in virtual screening for drug discovery: Methods and applications. **Nat. Rev. Drug Discov.** 3 (2004): 935-949.
- [154] Kwong, A.D., Kim, J.L., Rao, G., Lipovsek, D. and Raybuck, S.A. Hepatitis C virus NS3/4A protease. **Antiviral Res.** 40 (1998): 1-18.
- [155] Stempniak, M., Hostomska, Z., Nodes, B.R. and Hostomsky, Z. The NS3 proteinase domain of hepatitis C virus is a zinc-containing enzyme. **Journal of Virology** 71 (1997): 2881-2886.
- [156] Oliva, C., Rodriguez, A., Gonzalez, M. and Yang, W. A quantum mechanics/molecular mechanics study of the reaction mechanism of the hepatitis C virus NS3 protease with the NS5A/5B substrate. **Proteins** 66 (2007): 444-455.
- [157] Cassidy, C.S., Lin, J. and Frey, P.A. A new concept for the mechanism of action of chymotrypsin: the role of the low-barrier hydrogen bond. **Biochemistry** 36 (1997): 4576-4584.
- [158] Topf, M., Várnai, P. and Richards, W.G. Ab Initio QM/MM Dynamics Simulation of the Tetrahedral Intermediate of Serine Proteases: Insights into the Active Site Hydrogen-Bonding Network. **J. Am. Chem. Soc.** 124 (2002): 14780-14788.

- [159] Rodriguez, A., Oliva, C. and Gonzalez, M. A comparative QM/MM study of the reaction mechanism of the Hepatitis C virus NS3/NS4A protease with the three main natural substrates NS5A/5B, NS4B/5A and NS4A/4B. **Phys. Chem. Chem. Phys.** 12 (2010): 8001-8015.
- [160] Pang, Y.P., Xu, K., Yazal, J.E. and Prendergas, F.G. Successful molecular dynamics simulation of the zinc-bound farnesyltransferase using the cationic dummy atom approach. **Protein Sci.** 9 (2000): 1857-1865.
- [161] AmberTools12 Reference Manual.
- [162] D.A. Case, T.A. Darden, T.E. Cheatham, I., C.L. Simmerling, J. Wang, R.E. Duke, R. Luo, R.C. Walker, W. Zhang, K.M. Merz, B. Roberts, S. Hayik, A. Roitberg, G. Seabra, J. Swails, A.W. Goetz, I. Kolossváry, K.F. Wong, F. Paesani, J. Vanicek, R.M. Wolf, J. Liu, X. Wu, S.R. Brozell, T. Steinbrecher, H. Gohlke, Q. Cai, X. Ye, J. Wang, M.-J. Hsieh, G. Cui, D.R. Roe, D.H. Mathews, M.G. Seetin, R. Salomon-Ferrer, C. Sagui, V. Babin, T. Luchko, S. Gusarov, A. Kovalenko and Kollman, P.A. AMBER 12. University of California, San Francisco, 2012.
- [163] Rungrotmongkol, T., Decha, P., Sompornpisut, P., Malaisree, M., Intharathep, P., Nunthaboot, N., Udommaneethanakit, T., Aruksakunwong, O. and Hannongbua, S. Combined QM/MM mechanistic study of the acylation process in furin complexed with the H5N1 avian influenza virus hemagglutinin's cleavage site. **Proteins** 76 (2009): 62-71.
- [164] Senn, H.M. and Thiel, W. QM/MM methods for biomolecular systems. **Angew. Chem. Int. Ed.** 48 (2009): 1198-1229.
- [165] van der Kamp, M.W. and Mulholland, A.J. Combined quantum mechanics/molecular mechanics (QM/MM) methods in computational enzymology. **Biochemistry** 52 (2013): 2708-2728.
- [166] Seabra, G.d.M., Walker, R.C., Elstner, M., Case, D.A. and Roitberg, A.E. Implementation of the SCC-DFTB Method for Hybrid QM/MM Simulations within the Amber Molecular Dynamics Package†. **The Journal of Physical Chemistry A** 111 (2007): 5655-5664.
- [167] Walker, R.C., Crowley, M.F. and Case, D.A. The implementation of a fast and accurate QM/MM potential method in Amber. **Journal of Computational Chemistry** 29 (2008): 1019-1031.
- [168] Kumar, S., Rosenberg, J.M., Bouzida, D., Swendsen, R.H. and Kollman, P.A. THE weighted histogram analysis method for free-energy calculations on biomolecules. I. The method. **Journal of Computational Chemistry** 13 (1992): 1011-1021.

- [169] Roux, B. The calculation of the potential of mean force using computer simulations. **Computer Physics Communications** 91 (1995): 275-282.
- [170] Zhang, R. and Windsor, W.T. In vitro kinetic profiling of hepatitis C virus NS3 protease inhibitors by progress curve analysis. **Methods Mol. Biol.** 1030 (2013): 59-79.
- [171] Collins, P.J., Haire, L.F., Lin, Y.P., Liu, J., Russell, R.J., Walker, P.A., Skehel, J.J., Martin, S.R., Hay, A.J. and Gamblin, S.J. Crystal structures of oseltamivir-resistant influenza virus neuraminidase mutants. **Nature** 453 (2008): 1258-1261.
- [172] Sugaya, N. and Ohashi, Y. Long-acting neuraminidase inhibitor laninamivir octanoate (CS-8958) versus oseltamivir as treatment for children with influenza virus infection. **Antimicrob. Agents Chemother.** 54 (2010): 2575-2582.
- [173] Vavricka, C.J., Li, Q., Wu, Y., Qi, J., Wang, M., Liu, Y., Gao, F., Liu, J., Feng, E., He, J., Wang, J., Liu, H., Jiang, H. and Gao, G.F. Structural and functional analysis of laninamivir and its octanoate prodrug reveals group specific mechanisms for influenza NA inhibition. **PLoS Pathog.** 7 (2011): e1002249.
- [174] Rungrotmongkol, T., Yotmanee, P., Nunthaboot, N. and Hannongbua, S. Computational studies of influenza A virus at three important targets: hemagglutinin, neuraminidase and M2 protein. **Curr. Pharm. Des.** 17 (2011): 1720-1739.
- [175] Birnkrant, D. and Cox, E. The emergency use authorization of peramivir for treatment of 2009 H1N1 influenza. **N. Engl. J. Med.** 361 (2009): 2204-2207.
- [176] Makoto, Y. R-118958, a unique anti-influenza agent showing high efficacy for both prophylaxis and treatment after a single administration: from the in vitro stage to phase I study. **Int. Congr. Ser.** 1263 (2004): 38-42.
- [177] Nguyen, H.T., Sheu, T.G., Mishin, V.P., Klimov, A.I. and Gubareva, L.V. Assessment of pandemic and seasonal influenza A (H1N1) virus susceptibility to neuraminidase inhibitors in three enzyme activity inhibition assays. **Antimicrob. Agents Chemother.** 54 (2010): 3671-3677.
- [178] Yamashita, M. Laninamivir and its prodrug, CS-8958: long-acting neuraminidase inhibitors for the treatment of influenza. **Antivir. Chem. Chemother.** 21 (2010): 71-84.
- [179] Mai, B.K. and Li, M.S. Neuraminidase inhibitor R-125489 - a promising drug for treating influenza virus: steered molecular dynamics approach. **Biochem. Biophys. Res. Commun.** 410 (2011): 688-691.
- [180] Malaisree, M., Rungrotmongkol, T., Decha, P., Intharathep, P., Aruksakunwong, O. and Hannongbua, S. Understanding of known drug-target interactions in the catalytic pocket of neuraminidase subtype N1. **Proteins: Struct., Funct., Bioinf.** 71 (2008): 1908-1918.

- [181] Udommaneethanakit, T., Rungrotmongkol, T., Bren, U., Frecer, V. and Stanislav, M. Dynamic behavior of avian influenza A virus neuraminidase subtype H5N1 in complex with oseltamivir, zanamivir, peramivir, and their phosphonate analogues. **J. Chem. Inf. Model.** 49 (2009): 2323-2332.
- [182] Pan, D., Sun, H., Bai, C., Shen, Y., Jin, N., Liu, H. and Yao, X. Prediction of zanamivir efficiency over the possible 2009 influenza A (H1N1) mutants by multiple molecular dynamics simulations and free energy calculations. **J. Mol. Model.** 17 (2011): 2465-2473.
- [183] Rungrotmongkol, T., Intharathep, P., Malaisree, M., Nunthaboot, N., Kaiyawet, N., Sompornpisut, P., Payungporn, S., Poovorawan, Y. and Hannongbua, S. Susceptibility of antiviral drugs against 2009 influenza A (H1N1) virus. **Biochem. Biophys. Res. Commun.** 385 (2009): 390-394.
- [184] Bonnet, P. and Bryce, R.A. Molecular dynamics and free energy analysis of neuraminidase-ligand interactions. **Protein Sci.** 13 (2004): 946-957.
- [185] Le, L., Lee, E., Schulten, K. and Truong, T.N. Molecular modeling of swine influenza A/H1N1, Spanish H1N1, and avian H5N1 flu N1 neuraminidases bound to tamiflu and relenza. **PLoS Curr.** 1 (2009): RRN1015.
- [186] Wei, D.-Q., Du, Q.-S., Sun, H. and Chou, K.-C. Insights from modeling the 3D structure of H5N1 influenza virus neuraminidase and its binding interactions with ligands. **Biochem. Biophys. Res. Commun.** 344 (2006): 1048-1055.
- [187] Le, L., Lee, E.H., Hardy, D.J., Truong, T.N. and Schulten, K. Molecular dynamics simulations suggest that electrostatic funnel directs binding of tamiflu to influenza N1 neuraminidases. **PLoS Comput. Biol.** 6 (2010): e1000939.
- [188] Malaisree, M., Rungrotmongkol, T., Nunthaboot, N., Aruksakunwong, O., Intharathep, P., Decha, P., Sompornpisut, P. and Hannongbua, S. Source of oseltamivir resistance in avian influenza H5N1 virus with the H274Y mutation. **Amino Acids** 37 (2009): 725-732.
- [189] Oakley, A.J., Barrett, S., Peat, T.S., Newman, J., Streltsov, V.A., Waddington, L., Saito, T., Tashiro, M. and McKimm-Breschkin, J.L. Structural and functional basis of resistance to neuraminidase inhibitors of influenza B viruses. **J. Med. Chem.** 53 (2010): 6421-6431.
- [190] Varghese, J.N., Smith, P.W., Sollis, S.L., Blick, T.J., Sahasrabudhe, A., McKimm-Breschkin, J.L. and Colman, P.M. Drug design against a shifting target: a structural basis for resistance to inhibitors in a variant of influenza virus neuraminidase. **Structure** 6 (1998): 735-746.

- [191] Rungrotmongkol, T., Malaisree, M., Nunthaboot, N., Sompornpisut, P. and Hannongbua, S. Molecular prediction of oseltamivir efficiency against probable influenza A (H1N1-2009) mutants: molecular modeling approach. **Amino Acids** 39 (2010): 393-398.
- [192] Shie, J.J., Fang, J.M., Wang, S.Y., Tsai, K.C., Cheng, Y.S., Yang, A.S., Hsiao, S.C., Su, C.Y. and Wong, C.H. Synthesis of tamiflu and its phosphonate congeners possessing potent anti-influenza activity. **J. Am. Chem. Soc.** 129 (2007): 11892-11893.
- [193] Gohlke, H., Kiel, C. and Case, D.A. Insights into protein-protein binding by binding free energy calculation and free energy decomposition for the Ras-Raf and Ras-RalGDS complexes. **J. Mol. Biol.** 330 (2003): 891-913.
- [194] Zoete, V., Meuwly, M. and Karplus, M. Study of the insulin dimerization: Binding free energy calculations and per-residue free energy decomposition. **Proteins: Struct., Funct., Bioinf.** 61 (2005): 79-93.
- [195] Liu, H., Yao, X., Wang, C. and Han, J. In silico identification of the potential drug resistance sites over 2009 influenza A (H1N1) virus neuraminidase. **Mol. Pharm.** 7 (2010): 894-904.



APPENDIX

จุฬาลงกรณ์มหาวิทยาลัย
CHULALONGKORN UNIVERSITY

SUPPLEMENTAL INFORMATION

CHAPTER 3

In Silico Screening for Potent Inhibitors against the NS3/4A Protease of
Hepatitis C Virus

This article has been accepted in journal: Current Pharmaceutical Design Year:
2013.

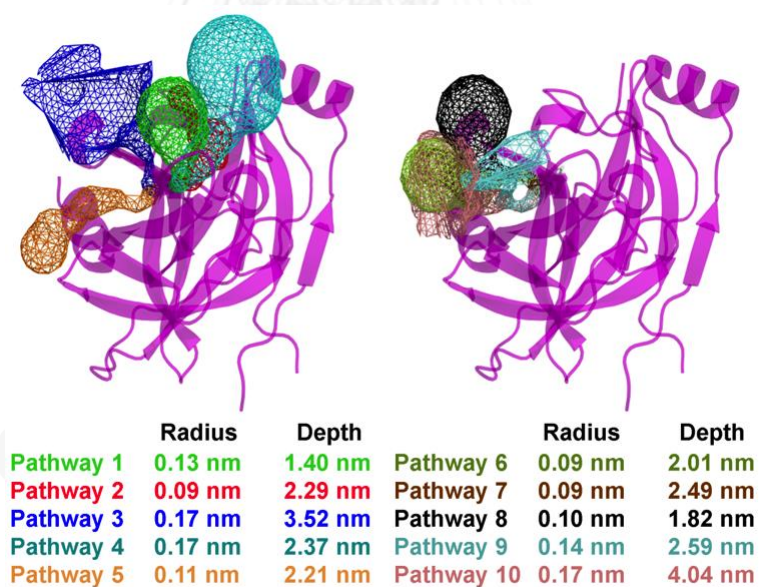


Figure S1. The ten possible pathways with their average radius and depth

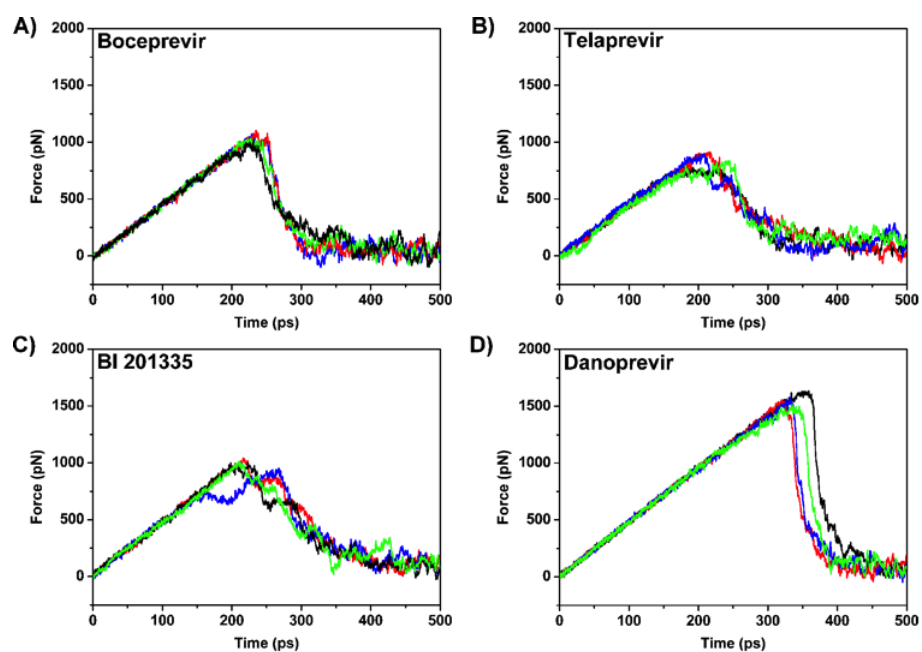


Figure S2. Time dependencies of the force along the SMD time

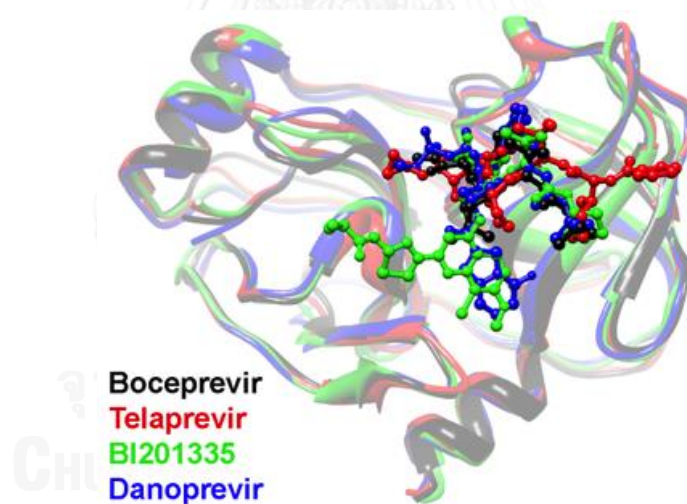


Figure S3. Superimposition of the last snapshots of the NS3/4A complex bound with boceprevir, telaprevir, BI201335 and danoprevir.

Table S1. Rupture force obtained by AMBER ff03 force field for 44 ligands

Rank	ZINC ID	Rupture force (pN)	CHEMPLP Score	Rank (docking)
1	Danoprevir	1572.40 ± 46.89	-896.68	1
2	59500093	1222.64 ± 107.88	-960.82	44
3	59784724	1137.59 ± 117.11	-937.24	24
4	Boceprevir	1058.25 ± 39.32	-953.22	42
5	BI201335	1000.87 ± 38.27	-904.11	2
6	13527817	951.65 ± 31.14	-943.41	34
7	26660256	912.26 ± 24.17	-932.25	14
8	Telaprevir	859.04 ± 58.10	-943.33	33
9	29482733	810.97 ± 71.19	-921.29	3
10	25977181	800.06 ± 79.19	-924.53	6
11	28005928	779.60 ± 71.84	-935.97	22
12	13527826	767.04 ± 54.90	-940.76	29
13	13471529	763.17 ± 81.03	-946.99	39
14	72112491	729.22 ± 12.33	-946.24	36
15	3966122	707.77 ± 42.16	-934.40	18
16	49756462	690.48 ± 96.17	-934.69	19
17	1895578	684.96 ± 38.90	-931.97	13
18	22342	679.38 ± 65.38	-932.88	16
19	1903930	649.94 ± 97.43	-930.03	10
20	23547	611.64 ± 54.82	-930.63	11
21	3925317	601.30 ± 6.15	-938.06	26
22	25977172	594.61 ± 48.14	-933.69	17
23	2005813	593.81 ± 82.85	-931.41	12
24	72181357	587.06 ± 50.96	-940.29	28
25	1894693	579.37 ± 15.41	-928.81	7
26	13527821	565.10 ± 59.03	-938.71	27
27	3925316	547.57 ± 61.01	-934.80	20
28	3966114	529.68 ± 66.69	-932.57	15
29	26658166	521.57 ± 84.34	-929.83	9
30	43178451	521.43 ± 48.59	-922.39	5
31	29482733	521.01 ± 66.44	-921.29	4
32	1903942	515.77 ± 25.40	-941.28	30

33	1903936	508.34 ± 48.86	-937.61	25
34	59782084	496.28 ± 57.14	-946.47	38
35	13589564	490.45 ± 58.39	-949.71	40
36	13527802	480.58 ± 56.93	-944.54	35
37	13527806	472.03 ± 119.13	-943.18	32
38	49756827	450.79 ± 44.51	-929.65	8
39	22341	414.49 ± 97.25	-935.51	21
40	3596259	412.72 ± 56.80	-942.17	31
41	27518377	350.58 ± 67.04	-936.31	23
42	7518	335.15 ± 54.72	-946.32	37
43	143992	321.18 ± 36.15	-950.28	41
44	164954	309.71 ± 82.12	-959.60	43

VITA

PERSONAL DATA

Name Arhitaya Meeprasert
 Nationality Thai
 Date of Birth 15 December 1985
 E-mail Address A.meeprasert@gmail.com

EDUCATION

2004 – 2007 B.Sc. in Chemistry (1st honor)
 Department of Chemistry, Faculty of Sciences,
 King Mongkut's University of Technology Thonburi, Bangkok,
 Thailand
 2008 – 2013 Ph.D. in Physical Chemistry
 Department of Chemistry, Faculty of Sciences,
 Chulalongkorn University, Bangkok, Thailand

SCHOLARSHIP AND AWARDS

2008 - 2013 (Ph.D. scholarship) The Royal Golden Jubilee Ph.D. Scholarship, by Chulalongkorn University and Thailand Research Fund
 2004 - 2007 (B.Sc. scholarship) Pechprachormkiao scholarship by King Mongkut's University of Technology Thonburi
 2009 (December) Sokendai Asian Winter School 2009, organized by Institute for Molecular Science, Japan
 2011 (August) – 2011 (October) JENESYS Program by Japan Student Service Association (JASSO), Institute for Molecular Science, Japan

PUBLICATIONS

1. Meeprasert, A., Khuntawee, W., Kamlungsua, K., Nunthaboot, N., Rungrotmongkol, T. and Hannongbua, S. Binding pattern of the long acting neuraminidase inhibitor laninamivir towards influenza A subtypes H5N1 and pandemic H1N1. *J. Mol. Graph. Model.* 38 (2012): 148-154.
2. Meeprasert, A., Rungrotmongkol, T., Li, M.S. and Hannongbua, S. In Silico Screening for Potent Inhibitors against the NS3/4A Protease of Hepatitis C Virus. *Curr. Pharm. Des.* (2013). (accepted)
3. Meeprasert, A., Hannongbua, S. and Rungrotmongkol, T. Key Binding and Susceptibility of NS3/4A Serine Protease Inhibitors against Hepatitis C Virus. *J. Chem. Inf. Model.* (2014). (accepted)